FINAL TECHNICAL REPORT

on

NASA GRANT NSG - 7159

for

"Crustal Deformation and Seismic Measurements in the Region of McDonald Observatory, West Texas"

by

Dr. H. James Dorman *
The University of Texas at Austin
Institute for Geophysics

Research period
8 September 1975 - 30 June 1981

Total Funding
$ 349,056.00

(NASA-CR-164964) CRUSTAL DEFORMATION AND SEISMIC MEASUREMENTS IN THE REGION OF MCDONALD OBSERVATORY, WEST TEXAS Final Technical Report (Texas Univ. at Arlington.) 134 p HC A07/MF A01 CSCL 08K G3/46 N82-11695 Unclas 08299

* Dr. Dorman is now with Exxon Corp., Houston, Tx.

LIST OF PUBLICATIONS

Chan, K.N. (1977), Modeling of West Texas Crustal Structure from Earthquake Data, MS Thesis, The University of Texas, 38 p.

Dumas, D. B., H. J. Dorman, and G. V. Latham. A reevaluation of the August 16, 1931 Texas Earthquake, Bull. Seism. Soc. Am. 70-4, 1171-1180.

Dumas, D. Seismicity in the Basin and Range Privince of Texas and Northeastern Chihuahua, Mexico. New Mexico Geological Society Guidebook, Trans-Pecos Region, 1980.

Dumas, D. (1981), Seismicity of West Texas, Ph.D. Dissertation, The University of Texas, 91 p.

Attachment I

SUMMARY OF LOCAL AND REGIONAL EARTHQUAKES (S-P<30 SEC) RECORDED AT THE UNIVERSITY OF TEXAS/ NATIONAL AERONAUTICS AND SPACE ADMINISTRATION (UT/NASA) SEISMIC ARRAY

by

David Dumas

The University of Texas
Marine Science Institute
Contribution No. 465
Galveston Geophysics Laboratory

Table of Contents

Introduction

This report is a summary of the arrival times of regional and local earthquakes and located earthquakes in the Basin and Range province and the adjacent areas of Chihuahua, Mexico from January-1976 to August 1980 at the UT/NASA seismic array. The seismicity of the area and details of the UT/NASA array have been previously described by Dumas (to be published in 1981). Therefore the reader should refer to these for details of the array and the methods used in the hypocenter locations. Also, a listing of all published works derived from the UT/NASA array data is given in Appendix I.

References

Dumas, D.B. (to be published). A recent seismic study in west Texas.

Dumas, D.B. (1980). Seismicity in the Basin and Range province of Texas and Northern Chihuahua, Mexico. New Mexico Geological Society Guidebook 31st Field Conference, Trans-Pecos Region, 77-81.

Lee, W.H.K. and J.C. Lahr (1975). HYPO-71 (revised) a computer program for determining hypocenters, magnitudes, and first motion patterns of local earthquakes, U. S. Geol. Surv., Open File Rept., 75-311.

Muehlberger. W. (1978). The areal extent of Cenozoic faulting in Trans-Pecos Texas, Bureau of Economic Geology, Guidebook 19, A. Walter and C. Henry, Editors, 19-21.

Table 1. Station names, coordinates, elevation, and station corrections.

	Station	Lat.	Long.	Elev.(m)
MOT	McDonald Observatory	30.68N	104.01W	2080
BP	Boracho Peak	30.93N	104.39W	1720
EM	Eagle Mountain	30.90N	105.08W	2088
MR	Miller Ranch	30.53N	104.67W	1584
BR	Brite Ranch	30.27N	104.58W	1584
CLN	Carlsbad	32.04N	103.73W	1094
KTX	Kermit	31.53N	103.29W	847
KT4	Kermit	31.91W	103.32W	948

Appendix I

Listing of all published works from the UT/NASA array

Dumas, D.B. (1978). Seismicity in and around west Texas, Bureau of Economic Geology Guidebook 19, A. Walton and C. Henry, Editors, 22-27.

Dumas, D.B. (1979). Active seismic focus near Snyder, Texas, Bull. Seis. Soc. Am., 69, 1295-1299.

Dumas, D.B., H.J. Dorman, and G.V. Latham (1980). A reevaluation of the August 16, 1931 Texas earthquake, Bull. Seis. Soc. Am., 70, 1171-1180.

Dumas, D.B. (1980). Seismicity in the Basin and Range province of Texas and Northeastern Chihuahua, Mexico, New Mexico Geological Society 31st Field Conference, Trans-Pécos Region, 77-81.

Dumas, D.B. (to be publish). A recent seismic study in west Texas.

Figure 1. Seismicity map of the Basin and Range province and the adjacent area of Mexico. The stations are indicated by triangles (Δ) and locations and abbreviations are given in Table 1. Crosses (+) indicate epicenters located (Appendix III) by the five-station seismic array. Epicenters located by the USGS are indicated by solid squares (■) and open circles (o) indicate epicenters located by the ISC. Abbreviations for structural features are: BG-Black Gap Area, DM-Davis Mountains, DP-Diablo Plateau, MB-Marfa Basin, RR-Rim Rock Fault, SB-Salt Basin Graben, and WM-Wylie Mountains. The dashed line marks Muehlberger's (1979) proposed eastern boundary of Basin and Range faulting. Earthquakes with the same epicenter are indicated by (M). The town of Valentine (V) is indicated by the small open square (□).

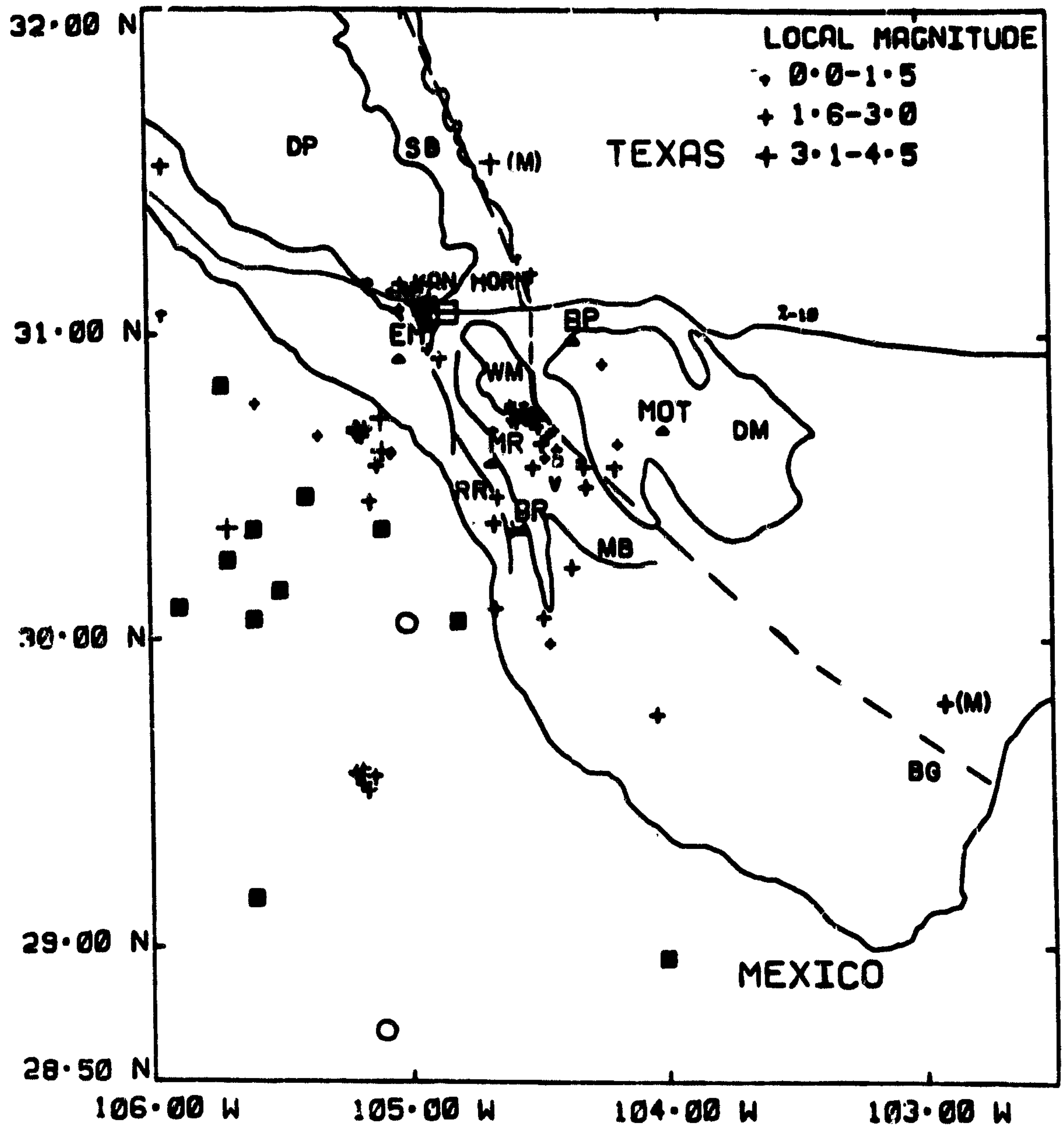

LOCAL MAGNITUDE
0.0-1.5
1.6-3.0
3.1-4.5
TEXAS
MEXICO
DP
SB
(M)
VAN HORN
EM
BP
I-10
WM
MOT
DM
MR
RR
BR
MB
BG
32.00 N
31.00 N
30.00 N
29.00 N
28.50 N
106.00 W
105.00 W
104.00 W
103.00 W

Appendix II

Arrival times for local and regional earthquakes (S-P<30 sec) recorded at station MOT from January 1976 to August 1980.

STATION: MCDONALD OBS., TEXAS CODE MOT LAT.30.68N LONG. 104.887W

YR/MO/DA	PHASE	TIME(UT)	PHASE	TIME(UT)	MAG(LOCAL)
76 1 7	EP	333 17.0	S	333 39.0	2.6
76 1 10	EP	150 26.0	S	150 46.0	3.1
76 1 15	EP	2044 23.0	S	2044 46.7	2.6
76 1 21	EP	2311 44.4	S	2312 7.4	2.6
76 1 22	EP	722 23.6	S	722 44.1	2.9
76 1 22	EP	2049 59.0	S	2050 22.3	
76 1 23	IP	1313 44.0	S	1313 56.7	2.2
76 1 25	IP	448 54.1	S	449 14.9	3.9
76 1 28	P	208 30.0	S	208 49.7	2.4
76 2 6	P	19 37.0	S	19 40.5	3.9
76 2 9	P	240 51.0	S	240 59.0	2.2
76 2 14	IP	535 51.1	S	536 14.1	2.4
76 2 17	IP	11 36.3	S	12 1.6	2.7
76 2 18	IP	2333 47.2	S	2334 13.4	2.5
76 2 20	IP	2143 24.3	S	2143 49.6	2.5
76 2 24	IP	2330 45.1	S	2330 10.0	2.5
76 2 29	EP	1914 16.4	S	1914 17.3	
76 3 1	EP	848 31.0			2.5
76 3 8	IP	216 51.7	S	216 54.0	1.9
76 3 9	P	650 6.5			3.5
76 3 12	P	1240 15.3			3.1
76 3 18	EP	1959 43.4	S	2000 2.5	2.6
76 3 18	EP	2253 44.1	S	2254 10.9	3.0
76 3 18	EP	2307 38.1	S	2308 2.5	
76 3 19	EP	350 56.8	S	351 24.4	2.2
76 3 20	EP	1242 39.2	S	1242 49.5	1.9
76 3 27	IP	2240 52.9	S	2241 16.9	2.8
76 3 30	EP	2356 53.6	S	2357 2.2	2.2
76 4 3	EP	2041 8.5	S	2041 19.9	2.8
76 4 9	IP	203 20.7	S	203 22.9	
76 4 12	EP	803 6.5	S	803 30.0	2.3
76 4 21	EP	840 39.1	S	841 3.1	2.4
76 4 23	EP	34 29.8	S	34 54.8	2.4
76 4 23	EP	2327 10.0	S	2327 32.2	2.3
76 4 28	EP	2214 28.8	S	2214 53.7	1.9
76 4 30	EP	1929 1.3	S	1929 21.9	2.5
76 5 3	EP	653 38.1	S	654 9.4	3.0
76 5 3	P	801 6.9	S	801 27.6	1.9
76 5 3	P	1128 8.1	S	1128 29.0	2.0
76 5 5	EP	1549 37.0	S	1549 57.0	2.2
76 5 6	EP	1718 50.0	S	1719 11.0	2.1
76 5 8	EP	1147 8.5	S	1147 29.4	1.8
76 5 11	EP	2305 13.8	S	2305 35.9	2.9
76 5 17	IP	1239 39.8	S	1239 46.2	
76 5 20	EP	2247 26.0	S	2247 35.6	

STATION: MCDONALD OBS., TEXAS CODE MOT LAT.30.68N LONG. 104.007W

YR/MO/DA	PHASE	TIME(UT)	PHASE	TIME(UT)	MAG(LOCAL)
76 5 21	EP	1310 0.6	S	1310 20.9	2.7
76 5 23	P	926 34.0	S	926 53.9	
76 5 23	P	1327 42.7	S	1327 57.5	
76 5 26	P	1153 4.5	S	1153 36.2	
76 6 4	P	2040 5.0	S	2040 31.5	2.0
76 6 7	P	2140 37.2	S	2141 0.1	
76 6 13	P	2205 22.2	S	2205 33.0	1.9
76 6 14	P	2004 36.7	S	2204 59.0	
76 6 14	P	2330 26.0	S	2330 40.2	1.9
76 6 15	P	220 20.1	S	220 49.0	2.0
76 6 15	P	333 17.3	S	333 40.7	
76 6 15	EP	850 49.4	S	851 11.3	2.6
76 6 15	P	1405 47.0	S	1406 9.3	
76 6 29	P	501 16.0	S	501 19.1	
76 6 30	P	2312 20.1	S	2312 59.0	
76 6 15	P	333 17.3	S	333 40.7	
76 7 11	P	1053 31.9	S	1053 38.4	
76 7 14	P	2037 21.7	S	2037 46.1	1.0
76 8 2	P	813 20.7	S	813 50.9	
76 8 5	P	2224 4.5	S	2224 30.6	2.6
76 8 6	P	2100 54.0	S	2101 5.7	
76 8 6	P	2113 9.0	S	2113 32.0	2.5
76 8 10	P	903 46.5	S	904 9.4	2.4
76 8 10	P	913 0.2	S	913 22.0	2.0
76 8 10	P	1015 49.0	S	1015 11.6	2.4
76 8 15	IP	1524 22.0	S	1524 47.0	
76 8 15	IP	1912 25.7	S	1912 43.2	2.0
76 8 16	EP	2101 31.4	S	2101 54.0	
76 8 25	EP	106 0.4	S	106 31.5	
76 8 25	P	115 37.0	S	115 52.0	
76 8 25	P	121 46.0	S	122 9.5	2.2
76 8 25	P	120 17.0	S	120 29.0	2.0
76 8 26	IP	1522 40.3	S	1523 9.6	2.5
76 8 29	IP	1949 45.1	S	1950 3.6	2.4
76 8 30	EP	1151 52.3	S	1152 16.0	1.9
76 8 30	EP	2245 45.0	S	2246 10.5	0.0
76 8 31	IP	1246 46.0	S	1247 9.0	2.4
76 9 3	EP	2325 9.0	S	2325 34.0	
76 9 5	EP	1040 20.0	S	1040 45.0	1.0
76 9 6	EP	652 32.4	S	652 56.0	1.9
76 9 6	P	1232 21.2	S	1232 43.2	
76 9 8	IP	43 23.7	S	43 30.2	1.5
76 9 8	P	57 2.1	S	57 8.0	0.4
76 9 8	IP	118 34.7	S	118 41.2	1.2
76 9 8	P	123 35.6	S	123 42.0	0.6

STATION: MCDONALD OBS., TEXAS CODE MDT LAT.30.68N LONG. 104.007W

YR/MO/DA	PHASE	TIME(UT)	PHASE	TIME(UT)	MAG(LOCAL)
76 9 9	EP	259 52.0	S	300 20.0	
76 9 9	EP	1029 0.2			
76 9 10	EP	2310 24.1	S	2310 50.0	1.9
76 9 17	IP	248 17.9	S	248 40.5	3.0
76 9 17	EP	356 55.9	S	357 16.9	2.0
76 9 17	EP	1536 10.0	S	1536 42.0	1.5
76 9 17	EP	2207 44.0	S	2208 7.9	1.0
76 9 18	EP	2341 23.6	S	2341 40.1	1.4
76 9 19	EP	1023 53.4	S	1024 13.0	1.2
76 9 19	IP	1040 54.3			3.1
76 9 19	IP	1045 2.5	S	1045 8.6	0.9
76 9 30	EP	2228 19.0	S	2228 44.0	1.5
76 10 2	IP	957 1.0	S	957 7.9	1.0
76 10 3	IP	2306 52.7			2.3
76 10 8	EP	1340 47.0	S	1341 10.5	2.0
76 10 9	EP	111 51.9	S	112 13.9	2.2
76 10 12	EP	322 27.5	S	322 34.0	1.0
76 10 13	EP	1326 28.7			
76 10 14	EP	225 24.6			
76 10 14	EP	1103 32.3	S	1103 55.5	2.3
76 10 18	EP	622 46.0	S	622 52.0	1.9
76 10 22	IP	506 44.3	S	507 8.0	3.4
76 10 23	EP	1252 7.5	S	1252 29.0	2.3
76 10 25	EP	27 34.0	S	27 56.7	3.0
76 10 25	EP	1053 1.1	S	1053 23.9	2.1
76 10 26	EP	1045 1.2	S	1045 10.1	2.0
76 11 4	EP	1756 5.1	S	1756 38.5	2.5
76 11 8	EP	2324 39.4	S	2325 5.4	2.5
76 11 5	EP	1805 9.0	S	1805 32.0	2.3
76 11 6	EP	2251 31.0	S	2251 56.7	2.5
76 11 17	EP	2316 20.6	S	2317 5.3	2.5
76 11 25	EP	2225 1.4	S	2225 27.0	2.5
76 11 27	EP	510 26.7	S	510 46.6	2.0
76 12 12	EP	2300 42.1	S	2301 3.0	2.6
76 12 12	EP	2326 24.8	S	2326 47.6	1.9
76 12 15	EP	852 10.0			
76 12 16	EP	2325 23.0	S	2325 49.9	2.3
76 12 17	EP	2133 26.0	S	2133 50.0	
76 12 19	EP	2126 45.0	S	2127 10.1	2.1
76 12 19	EP	2354 54.3	S	2355 17.5	2.4
76 12 19	EP	2357 19.0	S	2357 43.5	2.6
76 12 22	EP	2320 5.0	S	2320 31.3	2.5
76 12 31	EP	2247 16.1	S	2247 41.5	2.5
77 1 6	EP	1459 21.0	S	1459 32.1	2.5

STATION: MCDONALD OBS., TEXAS CODE MOT LAT.30.68N LONG. 104.007W

YR/MO/DA	PHASE	TIME(UT)	PHASE	TIME(UT)	MAG(LOCAL)
77 1 7	EP	1920 48.0	S	1921 16.8	2.1
77 1 29	IP	940 52.7	S	940 59.0	2.5
77 2 2	EP	618 42.4	S	618 53.0	2.0
77 2 4	IP	748 26.3	S	748 32.7	2.6
77 2 4	IP	1622 40.4	S	1622 45.6	2.0
77 2 10	EP	233 21.2	S	233 45.0	2.2
77 2 11	EP	2223 2.0	S	2223 22.4	2.2
77 3 1[illegible]	IP	2321 40.6	S	2322 4.3	2.5
77 3 17	EP	514 44.0	S	515 7.0	2.0
77 3 19	EP	2128 11.5	S	2128 30.0	2.1
77 3 20	EP	754 40.0	S	755 2.1	2.6
77 3 21	IP	1645 18.2	S	1645 25.7	2.2
77 3 21	IP	1906 28.7	S	1906 [illegible]2.1	
77 3 23	EP	1103 23.9	S	1103 44.9	2.2
77 3 23	EP	2324 54.1	S	2325 18.2	2.4
77 3 25	IP	2 15.0	S	2 44.6	2.2
77 3 31	IP	516 53.0	S	516 13.8	2.3
77 3 31	IP	546 11.2	S	546 34.1	
77 4 7	IP	546 11.3	S	546 33.0	3.0
77 4 12	EP	2135 57.8			1.8
77 4 12	EP	2318 51.0			2.6
77 4 16	EP	644 43.0	S	644 58.0	2.0
77 4 16	EP	1726 6.9	S	1727 27.6	2.3
77 4 17	EP	2147 41.0	S	2148 0.5	2.3
77 4 18	EP	1823 45.0			2.3
77 4 20	EP	1012 54.0	S	1013 10.0	1.9
77 4 23	EP	151 26.6	S	151 46.4	2.1
77 4 24	IP	915 44.0	S	916 10.0	2.2
77 4 25	IP	1013 23.0	S	1013 46.8	2.4
77 4 26	IP	903 33.5	S	903 41.6	3.2
77 4 28	EP	1106 34.1	S	1106 57.0	
77 4 28	EP	1255 9.1	S	1255 31.0	2.4
77 4 28	EP	1256 11.0	S	1256 33.1	2.7
77 4 28	EP	1256 50.9	S	1257 14.0	2.2
77 4 28	EP	1523 7.0	S	1523 29.8	2.6
77 4 29	EP	310 11.7	S	310 33.4	
77 5 3	IP	2317 27.0	S	2317 38.6	1.7
77 5 5	IP	2115 44.0	S	2116 13.3	2.2
77 5 6	IP	2012 46.0	S	2013 15.0	2.4
77 5 7	IP	2056 56.7	S	2057 2.5	2.0
77 5 9	IP	452 15.2	S	452 19.2	1.5
77 5 19	EP	1056 47.0	S	1056 58.8	2.0
77 5 22	EP	1630 46.0	S	1636 56.5	1.9

STATION: MCDONALD OBS., TEXAS CODE MOT LAT.30.68N LONG. 104.007W

YR/MO/DA	PHASE	TIME(UT)	PHASE	TIME(UT)	MAG(LOCAL)
77 6 6	EP	2324 5.6	S	2324 35.1	
77 6 8	EP	1054 30.0	S	1054 51.0	
77 7 8	EP	1606 0.0			2.5
77 7 9	EP	1607 15.0	S	1607 25.0	1.9
77 7 11	IP	1232 23.9	S	1232 45.7	
77 7 11	IP	1330 18.0	S	1330 40.0	
77 7 11	EP	1719 55.2	S	1720 14.2	2.0
77 7 11	EP	2015 40.9			1.4
77 7 12	EP	1914 44.1			1.5
77 7 14	EP	221 22.0			
77 7 16	P	1719 55.2	S	1720 14.0	2.0
77 7 16	P	1740 2.0			1.9
77 7 19	P	2377 14.5			
77 7 20	EP	342 36.1			1.8
77 7 21	P	2304 30.0			
77 7 28	EP	1217 37.0			1.8
77 7 28	EP	2335 1.0			1.5
77 7 30	EP	1617 35.0			1.7
77 7 30	EP	2315 0.0			2.3
77 8 1	EP	1644 9.7			1.8
77 8 3	EP	1622 5.0			1.2
77 8 4	EP	1928 8.0			1.7
77 8 6	EP	2044 19.4			2.0
77 8 9	P	1607 15.0			1.9
77 8 21	EP	301 13.0			3.3
77 8 22	EP	1229 0.0			2.2
77 8 20	EP	229 1.4			2.6
77 10 3	EP	2152 23.0	S	2152 50.0	2.2
77 10 4	EP	435 2.1	S	435 19.2	1.7
77 10 4	EP	630 37.0			1.9
77 10 12	EP	2207 7.0			1.8
77 10 14	EP	1709 47.6	S	1710 14.3	2.3
77 10 16	IP	2125 12.4	S	2125 35.3	2.5
77 10 18	IP	648 33.6	S	648 44.6	2.0
77 10 19	EP	2107 41.0			2.0
77 10 20	EP	639 44.3	S	640 5.7	2.4
77 10 20	EP	1102 23.0	S	1102 46.5	2.0
77 10 20	IP	2058 13.0	S	2058 40.1	2.3
77 10 21	EP	1505 51.8	S	1506 12.1	2.7
77 10 22	EP	2228 53.1	S	2228 57.0	2.6
77 10 24	IP	2250 33.5	S	2250 52.0	2.3
77 10 25	EP	103 0.8	S	103 23.0	2.0
77 10 26	EP	2105 10.0	S	2105 34.0	
77 10 27	EP	1016 44.5	S	1017 16.2	2.7
77 10 27	EP	1024 51.0	S	1025 14.2	2.4

STATION: MCDONALD OBS., TEXAS CODE MDT LAT.30.68N LONG. 104.007W

YR/MO/DA	PHASE	TIME(UT)	PHASE	TIME(UT)	MAG(LOCAL)
77 10 27	EP	1036 13.8	S	1036 27.0	2.4
77 10 27	EP	2150 17.7			
77 10 27	IP	2243 4.0	S	2243 31.4	2.3
77 10 28	EP	2241 24.1	S	2241 41.4	2.1
77 10 29	IP	49 17.8			1.9
77 10 29	EP	219 9.0	S	219 31.5	2.5
77 10 29	EP	1946 0.0			
77 10 31	EP	2312 13.4	S	2312 36.7	2.5
77 11 1	EP	708 28.1	S	708 50.7	1.9
77 11 1	EP	716 35.0	S	716 57.2	2.0
77 11 1	EP	2244 34.4	S	2245 1.4	2.2
77 11 2	IP	2206 13.0			1.8
77 11 3	EP	638 14.3	S	638 38.0	2.2
77 11 3	EP	1000 42.3	S	1001 4.1	2.2
77 11 3	EP	1511 8.8	S	1511 31.2	1.9
77 11 3	EP	2323 10.5	S	2323 35.2	2.2
77 11 4	EP	147 48.3			
77 11 4	EP	149 6.0			2.2
77 11 5	EP	1228 14.1			1.9
77 11 7	EP	2024 15.3	S	2024 38.5	1.9
77 11 11	EP	2315 5.4	S	2315 32.0	2.2
77 11 13	EP	1830 28.2			
77 11 14	IP	721 33.8	S	721 50.9	2.0
77 11 14	IP	726 48.7			3.1
77 11 14	IP	746 16.0	S	746 32.4	2.1
77 11 14	EP	2334 1.5			
77 11 15	EP	1224 53.6			2.6
77 11 15	EP	2324 44.5			2.2
77 11 16	EP	1325 39.3			2.1
77 11 16	EP	2330 20.4	S	2330 32.8	1.7
77 11 17	EP	753 0.5	S	753 23.1	1.9
77 11 18	EP	2253 55.0			2.2
77 11 22	EP	2202 7.0			2.0
77 11 22	EP	2325 57.7	S	2326 25.0	
77 11 23	EP	652 55.8	S	653 19.4	1.8
77 11 23	EP	1514 54.8	S	1515 3.4	
77 11 23	EP	1924 8.7	S	1924 31.8	2.6
77 11 23	EP	2133 6.8	S	2133 33.7	2.1
77 11 25	EP	1754 39.9			1.8
77 11 28	IP	141 47.3			3.3
77 11 28	IP	301 7.4	S	301 23.3	1.9
77 11 30	EP	1032 20.0	S	1032 31.1	1.8
77 12 5	EP	2340 41.8			2.2
77 12 6	EP	828 18.0	S	828 40.0	1.9

STATION: MCDONALD OBS., TEXAS CODE MDT LAT.30.68N .ONG. 104.007W

YR/MO/DA	PHASE	TIME(UT)	PHASE	TIME(UT)	MAG(LOCAL)
77 12 6	EP	1015 53.0	S	1016 15.4	1.8
77 12 7	EP	1755 9.7	S	1755 32.0	2.0
77 12 12	EP	1346 0.3	S	1346 7.1	1.9
77 12 12	EP	1603 31.0	S	1603 54.0	1.4
77 12 13	EP	2347 18.2	S	2347 43.0	1.9
78 1 14	EP	844 4.0	S	844 20.0	1.8
78 1 15	EP	2224 3.5			2.8
78 1 15	EP	2239 15.2			2.5
78 1 15	EP	2315 34.9	S	2315 57.5	2.3
78 1 16	EP	258 54.6	S	259 16.6	1.9
78 1 17	EP	123 13.4	S	123 28.8	1.8
78 1 17	EP	2017 50.2			2.1
78 1 18	EP	853 40.5	S	853 56.2	2.1
78 1 19	EP	343 10.9	S	343 36.8	2.2
78 1 21	IP	117 13.0			3.2
78 1 21	EP	121 10.0	S	121 19.0	1.5
78 1 21	EP	606 33.2	S	606 56.0	2.0
78 1 24	EP	1426 33.1			2.1
78 1 27	EP	1933 58.1			
78 1 28	IP	117 23.2			3.2
78 2 1	EP	36 1.5			1.5
78 2 1	EP	1917 20.0			1.8
78 2 1	EP	2344 18.1	S	2344 31.5	2.0
78 2 2	EP	230 1.2	S	230 22.7	2.2
78 2 3	EP	2324 53.1	S	1802 7.8	2.0
78 2 4	EP	1551 9.6	S	1551 25.4	1.7
78 2 5	EP	1046 46.2			1.7
78 2 5	IP	1420 9.0			2.7
78 2 14	P	1756 1.5			2.6
78 2 14	EP	1950 27.0			1.7
78 2 14	P	2103 58.7			2.7
78 2 16	EP	131 27.0			2.0
78 2 18	P	1422 29.6			3.6
78 2 18	P	1429 41.9			2.5
78 2 18	EP	1504 36.0			2.0
78 2 18	EP	1529 58.9			1.8
78 2 18	EP	1620 59.1			1.8
78 2 18	EP	1644 26.6			1.8
78 2 18	P	1730 30.1			2.9
78 2 18	EP	1754 32.2			2.3
78 2 18	EP	1845 37.7			2.1
78 2 18	EP	1858 59.5	S	1859 3.2	1.5
78 2 18	P	2159 58.2			2.5
78 2 19	EP	120 35.6	S	120 42.9	1.5

STATION: MCDONALD OBS., TEXAS CODE MOT LAT.30.68N LONG. 104.007W

YR/MO/DA	PHASE	TIME(UT)	PHASE	TIME(UT)	MAG(LOCAL)
78 2 19	EP	145 18.0	S	145 34.6	1.5
78 2 19	EP	253 18.3			1.9
77 2 19	EP	704 40.8			1.9
78 2 19	EP	253 18.3			1.9
78 2 19	P	1212 21.6			2.9
78 2 19	EP	1222 36.1			1.7
78 2 19	EP	1531 54.4	S	1532 0.5	1.7
78 2 19	EP	1816 10.0	S	1016 34.5	2.1
78 2 19	EP	1818 19.4	S	1818 42.0	2.4
78 2 19	EP	2216 52.0			1.5
78 2 20	EP	253 18.3			1.9
78 2 20	P	2050 52.7			2.5
78 2 21	P	2257 0.7			
78 3 2	EP	858 22.2			2.5
78 3 4	EP	1938 28.0			1.9
78 3 5	EP	1248 49.9			1.5
78 3 5	EP	1420 29.6	S	1420 56.3	2.3
78 3 6	EP	16 41.8			1.4
78 3 6	EP	2347 17.8			2.3
78 3 8	EP	1355 47.2			2.5
78 3 8	EP	2130 33.0			
78 3 9	EP	536 48.5			1.5
78 3 9	EP	2301 32.8			2.4
78 3 12	EP	7 59.2			2.6
78 3 13	EP	2301 59.0			2.4
78 3 14	EP	301 2.0			2.3
78 3 14	EP	1520 56.0			2.4
78 3 14	EP	1739 34.3			1.7
78 3 16	EP	1751 59.9			2.4
78 3 16	EP	1844 8.9			1.5
78 3 16	EP	1935 45.8			2.7
78 3 14	EP	306 46.6			2.5
78 3 17	EP	2116 29.0			2.2
78 3 19	EP	1049 17.1			2.5
78 3 20	EP	14 19.6			1.7
78 3 22	EP	2003 49.0	S	2004 17.1	2.5
78 3 25	EP	755 19.2			2.2
78 3 31	EP	5 57.5			1.9
78 3 31	EP	2101 53.0			1.8
78 3 31	EP	2355 23.5			2.0
78 3 31	EP	2222 18.5			
78 4 1	EP	2335 10.5	S	2335 29.2	1.8
78 4 4	EP	424 2.9	S	424 30.0	2.3

STATION: MCDONALD OBS., TEXAS CODE MDT LAT.30.68N LONG. 104.007W

YR/MO/DA	PHASE	TIME(UT)	PHASE	TIME(UT)	MAG(LOCAL)
78 4 4	EP	1335 51.0	S	1336 12.0	1.9
78 4 4	EP	2313 1.5	S	2313 21.0	1.8
78 4 6	EP	913 43.9	S	913 55.9	2.0
78 4 6	EP	1959 26.0	S	1959 46.0	1.9
78 4 7	P	58 18.1	S	58 48.0	2.6
78 4 7	EP	1250 15.1	S	1205 35.1	2.2
78 4 12	EP	2305 10.0			1.9
78 4 13	EP	820 29.0	S	820 31.9	1.0
78 4 16	EP	1101 3.6	S	1101 25.8	2.2
78 4 16	IP	1534 26.2	S	1534 29.5	1.4
78 4 26	EP	1158 20.0	S	1158 42.0	2.2
78 5 1	EP	1007 7.1	S	1007 25.6	1.8
78 5 3	P	2336 30.1			3.9
78 5 5	EP	1812 3.0	S	1812 23.0	2.1
78 5 8	IP	2125 22.6	S	2125 49.9	2.5
78 5 9	EP	2121 15.1	S	2121 43.5	2.3
78 5 11	IP	2214 21.0	S	2214 49.9	2.5
78 5 17	EP	1837 59.0			3.0
78 5 17	EP	2304 52.0	S	2305 15.0	2.5
78 5 18	EP	2110 33.3	S	2110 51.0	1.9
78 5 24	EP	523 34.2	S	523 46.0	1.8
78 5 25	IP	1929 34.0	S	1930 3.0	2.3
78 5 25	EP	2359 58.8	S	2359 11.3	1.8
78 5 27	EP	2008 20.6			1.4
78 5 28	EP	446 33.0			1.4
78 5 28	EP	1237 9.0			2.0
78 5 28	EP	1253 28.0			2.2
78 5 29	EP	1908 35.5	S	1908 56.2	2.0
78 5 30	EP	1150 22.4			1.5
78 5 30	EP	1319 0.0			2.2
78 6 3	IP	1140 32.1			2.4
78 6 6	EP	1459 56.3	S	1500 17.9	2.2
78 6 6	EP	2050 12.4			2.2
78 6 7	EP	154 54.4	S	155 15.2	2.5
78 6 7	EP	653 14.3	S	653 36.4	2.2
78 6 9	EP	454 28.0			1.9
78 6 9	EP	459 29.9			1.9
78 6 13	EP	347 6.2	S	347 27.1	2.0
78 6 14	EP	1905 40.8	S	1906 1.0	2.7
78 6 19	EP	1441 38.8			1.8
78 6 22	EP	955 36.8	S	955 58.2	1.8
78 6 27	EP	2317 27.1			2.4
78 6 28	IP	403 45.1			2.6

/MO/DA

STATION: MCDONALD OBS., TEXAS CODE MDT LAT.30.68N LONG. 104.007W

YR/MO/DA	PHASE	TIME(UT)	PHASE	TIME(UT)	MAG(LOCAL)
78 6 28	EP	2046 30.0			1.7
78 6 29	EP	2059 17.0	S	2059 30.0	2.9
78 6 30	EP	1759 4.4	S	1759 33.4	2.3
78 7 5	EP	112 20.1	S	112 50.9	1.5
78 7 5	EP	245 36.8	S	245 58.9	2.0
78 7 5	EP	1041 1.1	S	1041 23.5	2.0
78 7 5	EP	2300 13.6	S	2300 41.0	2.0
78 7 6	EP	1109 20.0	S	1109 43.0	1.8
78 7 6	EP	1753 46.0	S	1754 15.5	2.3
78 7 9	EP	2115 14.0	S	2115 35.5	1.8
78 7 10	IP	1554 4.9	S	1554 20.2	2.1
78 7 10	EP	1735 1.5	S	1735 25.8	2.6
78 7 13	EP	430 20.0			0.8
78 7 13	IP	952 40.4	S	952 54.1	1.7
78 7 13	IP	959 12.6	S	959 18.2	1.2
78 7 13	IP	1025 34.0	S	1025 39.5	2.0
78 7 13	EP	1135 55.4	S	1135 50.0	0.4
78 7 13	IP	1210 51.0	S	1210 57.2	1.3
78 7 13	EP	1212 41.0	S	1212 46.2	0.8
78 7 13	IP	1223 59.8	S	1224 4.9	1.3
78 7 13	EP	1328 40.0	S	1328 44.0	0.7
78 7 13	EP	2027 10.1	S	2027 10.2	1.1
78 7 13	EP	2238 31.4			1.8
78 7 14	IP	944 20.0	S	944 25.5	0.3
78 7 14	IP	1006 1.0	S	1006 6.2	0.8
78 7 14	IP	1553 10.0	S	1553 15.0	0.5
78 7 14	EP	1420 34.0	S	1420 39.0	1.6
78 7 17	IP	2215 39.5			1.7
78 7 17	IP	2230 37.5	S	2230 43.0	1.6
78 7 17	EP	2250 43.0	S	2251 11.0	2.2
78 7 17	EP	2256 51.0	S	2256 57.0	1.4
78 7 18	IP	149 32.2	S	149 37.5	2.1
78 7 18	IP	454 3.9	S	454 8.6	1.4
78 7 18	IP	454 43.0	S	454 47.0	0.7
78 7 18	IP	807 49.9	S	807 54.9	1.2
78 7 18	IP	1207 40.2	S	1207 45.7	2.6
78 7 24	EP	2212 44.3	S	2213 3.0	2.0
78 7 25	EP	2357 50.0			1.8
78 7 26	EP	1826 6.8	S	1826 9.0	1.2
78 7 26	EP	1851 14.1	S	1851 34.2	2.0
78 7 26	EP	2033 15.4	S	2033 32.0	2.0
78 7 27	EP	1157 29.7			
78 7 27	EP	1441 43.4	S	1442 2.9	2.0
78 7 28	EP	1801 43.6	S	1802 5.7	2.0
78 7 28	EP	2010 40.8	S	2011 11.8	2.2
78 7 28	EP	2015 9.0	S	2015 37.6	2.0

STATION: MCDONALD OBS., TEXAS CODE MDT LAT.30.68N LONG. 104.007W

YR/MO/DA	PHASE	TIME(UT)	PHASE	TIME(UT)	MAG(LOCAL)
78 7 28	EP	2223 15.8	S	2223 40.3	2.3
78 7 29	EP	1050 43.1	S	1050 52.8	1.8
78 7 29	EP	2054 41.6	S	2055 1.5	2.0
78 8 1	EP	1736 19.2	S	1736 46.5	2.2
78 8 1	EP	2332 40.0	S	2332 6.0	1.8
78 8 2	EP	2234 24.7	S	2234 30.0	2.1
78 8 4	EP	1937 20.0	S	1937 47.0	2.4
78 8 7	EP	2305 5.5			2.0
78 8 8	EP	1221 22.1	S	1221 48.9	2.2
78 8 9	IP	2010 23.8	S	2010 50.8	2.5
78 8 9	IP	2228 3.9	S	2228 31.0	2.4
78 8 10	EP	1218 27.1			1.4
78 8 11	IP	1927 28.9	S	1928 6.5	2.3
78 8 13	EP	914 41.3	S	915 3.8	1.8
78 8 13	EP	927 58.0			1.6
78 8 13	EP	933 0.5	S	933 22.0	2.0
78 8 14	EP	506 9.5	S	506 30.0	2.0
78 8 14	EP	1330 12.1	S	1330 32.2	2.9
78 8 14	EP	2022 3.8	S	2022 31.0	2.5
78 8 14	EP	557 10.0			2.9
78 8 15	EP	1447 10.0	S	1447 30.1	2.7
78 8 21	EP	1030 12.2	S	1030 33.0	1.8
78 8 21	EP	2040 27.2			1.8
78 8 21	IP	2221 6.0	S	2221 33.0	2.5
78 8 21	EP	2339 0.5	S	2339 27.8	2.0
78 8 22	EP	18 4.5	S	18 22.0	2.4
78 8 23	EP	1423 24.1	S	1423 40.8	2.0
78 8 25	EP	2051 46.6			1.7
78 8 28	EP	2033 55.9			1.7
78 8 28	EP	2314 18.7	S	2314 45.2	2.0
78 8 31	EP	1819 47.6			1.7
78 9 2	EP	716 55.4			1.2
78 9 2	EP	2053 25.0			2.0
78 9 4	EP	207 5.5			0.6
78 9 11	EP	924 17.0	S	924 40.0	2.2
78 9 12	EP	1909 45.5	S	1910 25.7	2.5
78 9 13	EP	1833 53.7			1.7
78 9 16	EP	1410 10.0	S	1410 30.9	2.0
78 9 17	EP	1146 44.2	S	1147 4.2	2.0
78 9 17	EP	1149 42.1	S	1150 4.5	2.0
78 9 18	IP	239 30.9	S	239 51.0	1.4
78 9 29	EP	2008 11.1	S	2008 31.0	2.9
78 9 29	EP	2254 56.8	S	2255 16.5	2.0
78 9 30	EP	752 44.8	S	752 48.2	1.1
78 9 30	EP	2332 13.0	S	2332 32.8	2.2

STATION: MCDONALD OBS., TEXAS CODE MOT LAT.30.68N LONG. 104.007W

YR/MO/DA	PHASE	TIME(UT)	PHASE	TIME(UT)	MAG(LOCAL)
78 10 2	EP	935 35.0	S	935 55.2	2.3
78 10 2	EP	959 1.4	S	959 22.0	2.1
78 9 18	EP	1008 54.7			0.5
78 9 18	EP	1011 2.0			0.4
78 9 18	EP	1012 6.0			0.6
78 9 18	IP	1156 58.4			0.7
78 9 18	IP	2017 7.9	S	2017 34.7	2.2
78 9 18	IP	2136 35.3	S	2136 48.0	2.2
78 9 19	EP	1849 37.0			1.7
78 9 19	IP	1935 22.7	S	1935 35.0	2.3
78 9 19	EP	1940 6.9	S	1940 35.7	2.0
78 9 22	EP	15 30.5			0.9
78 9 22	EP	819 46.8	S	820 9.9	2.0
78 9 22	EP	1806 32.1	S	1806 53.0	1.7
78 9 28	IP	1121 25.5	S	1121 27.5	0.4
78 9 29	EP	1759 50.6			2.2
78 9 29	EP	2002 26.0	S	2002 48.0	1.8
78 10 2	EP	1125 37.3	S	1125 57.0	2.9
78 10 2	EP	2236 24.0			1.8
78 10 3	EP	612 44.6	S	613 4.5	2.0
78 10 6	EP	1524 17.1	S	1524 37.0	2.8
78 10 10	EP	951 45.1			
78 10 10	EP	1444 19.0	S	1444 28.6	2.4
78 10 11	EP	2218 16.8	S	2218 44.4	2.0
78 10 17	IP	831 40.0	S	831 42.9	0.7
78 10 20	IP	307 57.3	S	308 18.0	2.5
78 10 20	EP	742 45.0	S	743 7.0	2.0
78 10 20	IP	2153 15.9	S	2153 45.8	2.2
78 10 20	EP	2220 19.2			1.5
78 10 23	EP	2046 44.0	S	2047 6.0	2.4
78 10 26	IP	412 58.9	S	413 21.4	1.8
78 10 26	EP	1758 8.0	S	1758 36.5	2.3
78 10 29	EP	700 12.0	S	700 30.0	1.7
78 10 30	EP	1721 4.9	S	1721 34.0	2.1
78 10 31	EP	2150 18.2	S	2150 41.7	2.0
78 10 31	EP	2243 21.0			1.7
78 11 3	EP	4 38.2	S	5 6.0	1.8
78 11 7	EP	2346 44.5	S	2347 11.4	1.8
78 11 13	EP	2357 29.1	S	2357 53.8	2.0
78 11 15	EP	1502 28.8			0.9
78 11 15	IP	2007 4.0	S	2007 24.0	1.3
78 11 16	EP	346 7.8	S	346 17.0	1.3
78 11 16	EP	2040 0.0	S	2040 20.0	2.0
78 11 18	EP	2128 7.8	S	2128 34.0	1.8
78 11 19	EP	328 7.1	S	328 24.5	1.6

STATION: MCDONALD OBS., TEXAS CODE MOT LAT.30.68N LONG. 104.007W

YR/MO/DA	PHASE	TIME(UT)	PHASE	TIME(UT)	MAG(LOCAL)
78 11 19	EP	1106 14.5	S	1106 37.7	1.8
78 11 21	IP	2105 47.9			2.8
78 11 22	EP	234 15.2	S	234 27.4	1.7
78 11 22	IP	1438 34.5	S	1439 1.8	2.0
78 11 26	EP	1239 40.6			1.7
78 12 1	EP	744 25.6			2.2
78 12 1	EP	836 30.5			2.1
78 12 4	EP	210 35.1			2.2
78 12 10	EP	132 41.5			2.0
78 12 12	EP	1755 34.5	S	1756 2.0	2.0
78 12 15	EP	2209 7.5	S	2209 32.9	2.0
78 12 17	EP	2349 43.6			1.6
78 12 18	IP	1243 2.4			1.4
78 12 18	IP	1932 43.7	S	1933 11.0	2.0
78 12 18	IP	2110 54.1	S	2111 21.4	2.0
78 12 20	IP	131 32.0			1.1
78 12 31	EP	1712 15.6			1.5
78 12 31	EP	1714 11.5			1.7
79 1 1	EP	952 18.0	S	952 37.0	1.7
79 1 1	EP	956 12.0	S	956 30.0	2.0
79 1 3	IP	2244 28.0	S	2244 31.0	0.6
79 1 3	IP	2256 54.2	S	2256 56.0	0.6
79 1 4	IP	303 30.5	S	303 32.4	0.6
79 1 4	EP	1720 25.9	S	1720 53.5	2.0
79 1 5	EP	2108 12.8	S	2108 40.0	1.9
79 1 6	IP	39 42.2	S	39 45.0	0.8
79 1 8	EP	855 27.0	S	855 42.1	1.8
79 1 9	EP	12 11.6	S	12 26.5	1.8
79 1 11	P	348 49.0	S	348 54.5	1.0
79 1 15	P	36 36.9	S	32 54.1	1.5
79 1 19	IP	908 15.3	S	908 31.2	1.8
79 1 26	EP	2110 1.8	S	2110 28.2	2.1
79 1 27	IP	2137 40.0	S	2138 6.5	1.8
79 1 27	EP	2234 53.0	S	2235 7.7	1.6
79 2 1	EP	2110 19.9	S	2110 41.8	2.0
79 2 1	IP	2156 20.6	S	2156 24.1	1.2
79 2 1	IP	927 13.0	S	927 33.4	2.0
79 2 4	EP	1758 46.0			1.6
79 2 8	IP	2222 25.4	S	2222 42.0	
79 2 5	IP	18 12.6	S	18 14.0	2.5
79 2 9	IP	1751 35.5	S	1752 3.9	2.0
79 2 9	EP	2212 48.2	S	2213 7.2	2.1
79 2 10	IP	52 21.4			0.4
79 2 13	IP	1902 27.0	S	1902 36.0	2.0
79 2 13	EP	2232 0.5	S	2232 18.5	1.7

STATION: MCDONALD OBS., TEXAS CODE MDT LAT.30.60N LONG. 104.007W

YR/MO/DA	PHASE	TIME(UT)	PHASE	TIME(UT)	MAG(LOCAL)
77 8 4	P	2131 10.0			1.0
79 2 15	EP	2240 0.0	S	2240 17.0	2.0
79 2 16	P	2350 49.8	S	2351 3.1	2.0
79 2 18	IP	1017 17.4	S	1017 32.7	2.0
79 2 19	IP	2153 46.8	S	2154 14.0	2.0
79 2 20	EP	2125 35.8	S	2125 44.6	1.5
79 2 21	IP	2249 33.2			2.0
79 2 23	IP	517 25.7	S	517 30.0	0.9
79 2 27	IP	501 57.8	S	501 17.0	2.4
79 3 1	IP	516 20.0	S	516 34.2	1.8
79 3 1	EP	549 18.4			0.4
79 3 1	IP	2216 0.9	S	2216 29.0	2.2
79 3 3	EP	2103 39.9	S	2103 48.0	1.8
79 3 11	2P	1250 59.7	S	1251 4.5	1.8
79 3 11	IP	1937 38.4	S	1937 43.0	1.5
79 3 15	EP	4 2.0			1.8
79 3 15	EP	1247 10.0	S	1247 18.0	1.4
79 3 16	IP	1956 57.0	S	1957 24.5	2.3
79 3 17	P	1949 13.6			1.1
79 3 23	EP	2140 22.6	S	2140 30.5	1.8
79 3 24	P	1455 44.7	S	1455 49.5	1.1
79 3 27	EP	1753 23.4	S	1753 51.0	2.2
79 3 28	IP	551 56.8	S	552 11.0	1.9
79 3 28	EP	1457 28.5			1.2
79 3 28	EP	1505 25.4			2.6
79 3 29	EP	936 7.2			2.5
79 3 29	EP	1352 39.8			1.4
79 3 29	EP	1953 37.2	S	1954 3.5	2.2
79 3 30	EP	341 32.0			0.6
79 3 31	IP	1446 53.8	S	1446 56.2	0.4
79 4 1	EP	1336 58.9	S	1340 1.0	0.7
79 4 1	EP	2025 36.7	S	2025 44.4	2.0
79 4 4	IP	2135 40.0	S	2136 8.0	2.2
79 4 5	EP	1921 23.4	S	1921 52.0	2.2
79 4 8	IP	156 15.9	S	156 29.0	1.9
79 4 10	EP	539 29.1			1.6
79 4 16	IP	2349 57.8	S	2350 26.0	2.1
79 4 17	IP	40 44.9	S	40 53.0	1.8
79 4 18	EP	43 46.0	S	44 9.2	1.8
79 4 18	EP	58 15.9	S	58 43.0	1.8
79 4 24	IP	640 56.2			0.4
79 4 25	IP	20 5.2	S	20 32.3	1.8
79 4 25	IP	1858 15.7			0.5
79 4 28	IP	101 49.9			3.6

STATION: MCDONALD OBS., TEXAS CODE MOT LAT.30.68N LONG. 104.007W

YR/MO/DA	PHASE	TIME(UT)	PHASE	TIME(UT)	MAG(LOCAL)
79 4 28	EP	155 14.6			1.2
79 4 28	IP	1755 25.6	S	1536 45.4	1.6
79 4 28	IP	1814 28.0	S	1814 37.0	1.3
79 4 29	EP	1536 35.2	S	1536 45.4	1.6
79 4 30	IP	2246 4.0	S	2246 8.3	1.3
79 5 2	IP	2333 44.6	S	2334 11.7	1.8
79 5 15	EP	2306 22.1	S	2306 46.0	1.9
79 5 22	EP	21 56.0			1.7
79 5 25	IP	2312 14.6	S	2312 22.3	1.5
79 5 30	EP	0 35.0	S	0 58.9	2.0
79 6 8	EP	5 45.5	S	6 9.0	1.8
79 6 9	EP	129 9.0	S	129 15.3	1.9
79 6 9	IP	1706 28.9	S	1706 30.5	1.3
79 6 10	IP	1047 57.5			1.7
79 6 12	IP	743 29.9	S	743 53.0	2.0
79 6 14	EP	1455 28.3			2.2
79 6 16	EP	2119 53.2	S	2120 16.2	1.8
79 6 17	IP	1626 17.5	S	1626 19.0	0.8
79 6 17	IP	1736 40.2	S	1736 47.1	1.7
79 6 20	IP	1202 10.0	S	1202 11.2	0.6
79 6 21	IP	1032 13.3	S	1032 19.6	1.2
79 6 22	IP	558 26.3	S	558 32.5	1.8
79 6 23	EP	2225 30.6	2	2225 32.2	0.2
79 6 25	IP	1723 41.7	S	1723 44.2	1.1
79 6 28	IP	337 23.7	S	337 34.2	1.5
77 6 28	P	1923 6.4			1.9
79 6 28	IP	2101 14.5	S	2101 32.0	2.1
79 6 30	IP	718 56.0	S	719 18.0	2.0
79 7 1	IP	732 27.0	S	732 51.0	1.6
79 7 10	EP	2132 37.0	S	2132 43.5	0.9
79 7 10	EP	2146 25.5	S	2146 31.8	0.9
79 7 10	EP	2200 32.5	S	2200 38.8	0.9
79 7 10	EP	2209 24.8	S	2209 30.8	0.9
79 7 12	EP	334 57.0	S	335 5.8	0.7
79 7 14	EP	20 57.2	S	21 0.1	0.6
79 7 18	IP	1059 30.5			0.6
79 7 22	EP	27 49.0			0.5
79 7 22	IP	1450 28.5			0.7
79 7 23	IP	2042 0.0			0.7
79 7 24	IP	307 6.2	S	307 12.9	1.7
79 7 25	EP	2106 7.0	S	2106 30.5	1.8
79 7 26	EP	25 52.7	S	26 1.0	1.7
79 7 27	EP	1236 5.6			0.4
79 7 27	EP	1237 47.9			0.6

STATION: MCDONALD OBS., TEXAS CODE MOT LAT.30.68N LONG. 104.007W

YR/MO/DA	PHASE	TIME(UT)	PHASE	TIME(UT)	MAG(LOCAL)
79 7 27	EP	1256 0.0			1.2
79 7 28	IP	1424 25.2			0.5
79 7 30	IP	1202 32.0	S	1202 44.0	1.2
79 7 31	IP	1741 50.0	S	1741 9.9	2.0
79 8 4	IP	2131 10.0			1.0
79 8 7	EP	1109 26.0	S	1109 28.0	0.6
79 8 9	EP	1258 13.0			1.2
79 8 9	EP	1443 58.6			1.4
79 8 11	EP	2238 6.3	S	2238 17.0	1.3
79 8 14	EP	2022 55.5			1.5
79 8 14	EP	2331 34.0			2.0
79 8 15	EP	2146 37.5	S	2146 58.0	1.7
79 8 16	EP	2256 54.0	S	2257 14.5	1.7
79 8 24	IP	2302 46.7	S	2303 1.7	2.0
79 8 25	IP	122 48.0	S	122 59.5	2.1
79 8 27	EP	1008 9.8	S	1008 25.5	1.5
79 8 27	EP	1118 6.5	S	1118 22.0	1.5
79 8 27	EP	1837 17.1	S	1837 32.2	1.6
79 8 27	EP	2119 5.9	S	2119 13.2	1.4
79 8 28	EP	2346 44.4			1.0
79 9 1	EP	120 41.0			1.9
79 9 2	EP	401 22.1			1.6
79 9 4	EP	1921 51.9	S	1921 59.4	1.4
79 9 5	EP	819 22.0	S	819 44.1	1.8
79 9 6	EP	1206 49.0	S	1207 11.0	2.1
79 9 7	EP	2254 51.0	S	2255 1.0	1.7
79 9 8	EP	2338 11.0	S	2338 17.2	1.3
79 9 11	EP	645 59.0	S	646 21.0	1.9
79 9 11	EP	1141 13.8	S	1141 36.0	1.9
79 9 11	EP	1205 22.8	S	1205 43.5	2.1
79 9 15	EP	215 37.5	S	216 0.5	2.3
79 9 16	EP	1246 22.0			1.2
79 9 19	EP	2259 36.1			1.7
79 9 22	EP	613 57.0	S	614 27.0	2.6
79 9 22	EP	1647 14.9	S	1647 24.1	1.6
79 9 28	EP	2022 51.5	S	2023 8.0	1.4
79 10 4	EP	113 34.0	S	113 47.0	1.6
79 10 7	EP	2142 42.5	S	2142 51.2	1.8
79 10 9	IP	124 51.2			
79 10 16	EP	1701 56.1			
79 10 25	EP	1333 1.1	S	1333 10.5	1.7
79 10 29	IP	1925 10.0			
79 10 30	EP	2306 26.5			1.6
79 10 31	EP	2054 29.5			1.5
79 11 2	EP	1116 22.8			1.5

STATION: MCDONALD OBS., TEXAS CODE MOT LAT.30.60N LONG. 104.007W

YR/MO/DA	PHASE	TIME(UT)	PHASE	TIME(UT)	MAG(LOCAL)
79 11 28	EP	301 41.0	S	302 1.0	2.0
79 12 5	IP	313 52.0	S	313 54.0	0.5
79 12 10	EP	2245 54.0	S	2246 10.5	2.0
79 12 10	IP	2346 28.4	S	2346 37.1	1.8
79 12 13	IP	437 0.1			1.2
79 12 14	EP	1758 17.7	S	1758 36.2	1.9
79 12 21	EP	2338 23.0	S	2338 28.5	1.4
79 12 21	EP	2350 30.0	S	2350 46.0	2.0
79 12 22	IP	615 42.3	S	615 44.2	2.3
79 12 23	EP	1635 54.5	S	1636 0.4	1.5
79 12 31	IP	1205 9.5			2.2
80 1 7	IP	1102 32.2	S	1102 51.0	2.3
80 1 7	IP	1214 51.0	S	1214 20.5	2.2
80 1 7	EP	2003 28.0	S	2003 48.0	2.1
80 1 7	IP	2259 57.0	S	2300 16.5	2.2
80 1 8	EP	2230 6.0			1.6
80 1 9	EP	535 37.0	S	536 5.5	2.9
80 1 9	IP	1241 3.0	S	1241 6.0	1.8
80 1 11	EP	2142 49.0			0.9
80 1 12	IP	38 24.3	S	38 29.2	0.6
80 1 12	IP	1732 59.5			
80 1 13	IP	302 5.0			
80 1 15	EP	1803 7.5			
80 1 21	EP	2331 31.0	S	2331 37.8	1.8
80 1 22	IP	1508 22.0			3.6
80 1 22	IP	2337 18.1	S	2337 39.0	2.9
80 3 7	EP	1357 52.0	S	1358 2.1	1.8
80 3 8	EP	723 49.0	S	724 10.0	1.9
80 3 10	EP	9 28.2	S	9 53.0	2.1
80 3 11	EP	1753 32.4	S	1754 1.0	
80 3 21	EP	835 53.1	S	836 15.0	2.4
80 3 26	IP	330 5.8	S	330 11.1	1.8
80 3 29	EP	2 0.5	S	2 24.6	1.9
80 4 1	EP	1021 31.0	S	1021 50.0	1.7
80 4 6	EP	248 22.6	S	248 41.5	2.9
80 4 6	EP	305 25.4	S	305 44.6	1.7
80 4 6	EP	547 8.9	S	547 26.0	1.6
80 4 6	EP	701 33.1	S	701 52.1	2.5
80 4 8	EP	1521 7.7	S	1521 22.5	1.8
80 4 23	EP	1326 29.2	S	1326 56.5	2.0
80 4 28	EP	445 11.0	S	445 29.0	1.7
80 4 28	EP	1055 27.6	S	1055 49.5	1.9
80 4 28	EP	1105 45.0	S	1106 7.0	1.8
80 4 28	EP	1252 22.0	S	1252 44.0	1.6
80 4 29	IP	155 30.0	S	155 52.0	2.5

STATION: MCDONALD OBS., TEXAS CODE MDT LAT.30.68N LONG. 104.007W

YR/MO/DA	PHASE	TIME(UT)	PHASE	TIME(UT)	MAG(LOCAL)
80 5 25	IP	1143 4.7	S	1143 11.0	1.0
80 5 28	EP	1705 42.0	S	1706 1.0	2.2
80 6 6	EP	2307 35.8	S	2307 48.0	2.0
80 6 16	EP	2351 37.5			
80 6 21	EP	1341 17.0	S	1341 39.0	1.8
80 6 21	EP	2008 22.0	S	2208 44.0	1.7
80 6 22	EP	302 38.3	S	303 0.8	1.9
80 6 22	EP	1210 44.7	S	1211 6.0	1.9
80 6 22	EP	1410 22.5	S	1410 25.0	0.1
80 6 22	EP	2130 23.3	S	2130 45.6	2.5
80 6 23	EP	1109 46.7	S	1110 9.0	1.6
80 6 24	EP	1146 48.0			1.7
80 6 24	EP	2323 30.5			2.0
80 6 25	EP	829 47.4	S	830 9.1	2.0
80 6 27	EP	722 56.1	S	723 18.2	2.4
80 6 27	EP	1140 39.0	S	1140 59.0	3.1
80 6 27	EP	1151 4.5	S	1151 11.2	1.2
80 6 27	EP	1159 51.6			0.7
80 6 27	EP	1204 47.6	S	1204 54.3	1.3
80 6 27	EP	1228 3.6	S	1228 10.0	0.7
80 7 3	EP	353 50.2			0.4
80 7 3	EP	1943 12.4	S	1943 31.3	2.0
80 7 8	EP	2308 18.4	S	2308 38.0	2.0
80 7 8	EP	2329 50.0	S	2330 1.0	1.8
80 7 10	EP	923 21.4	S	923 41.5	2.7
80 7 17	IP	342 1.2			3.8
80 7 17	EP	729 49.0	S	730 10.2	1.7
80 7 17	EP	807 31.1	S	807 51.2	2.6
80 7 17	EP	847 57.8	S	848 20.0	1.7
80 7 17	EP	1524 26.1	S	1524 46.2	1.8
80 7 18	EP	2104 42.4	S	2105 4.5	2.2
80 7 21	EP	941 1.5	S	941 19.0	1.8
80 7 28	IP	1639 26.0	S	1639 31.0	1.6
80 7 29	IP	1211 49.8	S	1212 5.0	1.7
80 7 30	EP	0 39.7	S	0 47.7	0.7
80 8 5	EP	354 12.0	S	354 34.0	2.0

Appendix III

Instrumental locations for earthquakes in the Basin and Range province of Texas and the adjacent area of Mexico. Locations were determined by the use of HYPO-71 (Lee and Lahr, 1975). The column headings are as follows:

Date - Year/month/day

Origin Time - This is universal time (UT) and is given to the nearest tenth of a second.

Lat N - Latitude (North) given to the nearest hundredth of a minute.

Long W - Longitude (West) given to the nearest hundredth of a minute.

Depth - Depth is given in km. (*) indicates depth is constrained to 4 km.

Mag - The magnitudes listed are local magnitudes determined from signal durations and are obtained from the following formula (Dumas, In preparation)

$$m_1 = 2.1 \log t - 2.51$$

MOT, BP, EM, MR, and BR - These are the UT/NASA stations used in the location scheme. The numbers in the columns indicate the number of readings used to locate each event per station. One (1) indicates P-wave arrival only and two (2) indicate both P and S wave arrivals were used.

Dmin - Distance to nearest station in km.

Gap - Largest azimuthal separation in degrees between stations.

RMS - Root mean square error of time residuals in sec.

ERH - Estimated standard error of the epicenter in km. If ERH is blank this means ERH cannot be computed because of insufficient data.

ERZ - Estimated standard error of the focal depth. If ERZ is blank this means that ERZ cannot be computed because either the focal depth was fixed in the solution or because of insufficient data.

Q - Quality of the hypocenter solution. This measure is intended to indicate the general reliability of the solution (Lee and Lahr, 1975).

Comments - The three (3) letter code indicate additional station(s) used in the epicenter locations.

DATE	ORIGIN TIME	LAT N	LONG W	DEPTH	MAG	MOT	BP	EM	MR	BR	DMIN	GAP	RMS	ERH	ERZ	Q	COMMENTS
77/ 7/11	1719 37.6	30-58.80	104-53.80	4.00*	2.0	1	2	2	2	1	20	213	0.37	13.7	15.2	D	
77/ 7/11	2015 20.5	31- 4.22	105- 0.64	3.64	1.3	2	1	2	1	1	20	265	0.73	14.9	10.9	D	
77/ 7/12	1914 24.1	31- 1.00	105- 1.00	20.45	1.5	2	2	1	0	0	14	254	0.22	7.0	5.3	D	
77/ 7/16	1747 31.3	29-44.74	105-33.70	1.44	1.9	2	2	2	1	2	110	321	0.91	14.2	9.7	D	
77/ 7/28	1217 17.8	31- 6.00	105- 1.00	4.00*	1.9	2	1	2	1	2	23	274	0.94	21.2	14.3	D	
77/ 7/28	2335 43.1	31- 0.27	104-54.55	4.00*	1.8	1	2	2	1	1	20	225	0.21	19.5	19.6	D	
77/ 7/30	1617 16.0	31- 1.00	104-54.80	2.00	1.5	2	2	2	1	1	21	230	1.28	70.3	72.6	D	
77/ 8/ 1	1644 51.1	30-58.00	104-55.09	4.00*	1.8	0	2	1	2	2	17	210	1.23	44.0	50.2	D	
77/ 8/ 3	1622 47.2	30-53.00	104-54.91	4.00*	1.6	2	2	2	1	1	16	167	1.57	26.2	41.9	D	
77/ 8/ 6	2043 59.7	31- 2.15	104-57.85	9.75	2.0	2	2	2	2	1	19	246	0.60	13.6	8.7	D	
77/ 8/ 7	1928 48.0	31- 4.58	105- 3.00	13.00	1.5	1	1	2	2	1	20	276	0.51	6.5	19.2	D	
77/ 8/ 9	1607 0.3	31- 2.52	104-39.12	4.00*	1.9	2	0	0	2	2	57	301	0.19	12.0	11.5	D	
77/ 8/21	301 8.2	30-33.07	105- 5.67	21.56	3.3	1	1	0	1	1	41	270	0.99	24.7	11.2	D	KTX,KT4,CLN
77/10/29	49 11.6	30-30.00	104-11.26	4.00*	1.9	2	2	2	2	2	27	195	0.77	8.8	9.8	D	
77/11/ 5	1228 53.7	31- 5.09	104-58.15	6.28	1.9	1	1	1	1	1	23	260	0.75			D	
73/ 1/21	117 2.4	31-30.06	104-39.15	2.46	3.2	1	1	1	0	0	68	190	0.03			C	CLN
78/ 1/24	1426 22.4	30-41.06	104-35.14	14.98	1.9	2	2	2	2	0	19	115	0.63	4.0	15.1	C	
78/ 2/ 5	1419 55.8	31-30.41	104-39.15		2.7												MOT,BP,CLN
78/ 2/18	1422 8.0	30-37.15	105-11.66	2.00	2.0	1	1	2	2	0	33	278	0.32	3.4	3.0	D	
78/ 2/18	1422 22.1	30-39.43	105- 6.00	1.12	3.6	1	1	1	1	0	27	255	0.04			C	
78/ 2/18	1429 20.3	30-37.35	105- 9.72	2.52	2.5	2	2	2	2	0	32	272	0.28	3.0	1.4	D	
78/ 2/18	1529 37.0	30-36.00	105-10.82	2.00	1.9	1	1	2	2	0	35	277	0.37	6.7	5.5	D	
78/ 2/18	1644 4.7	30-36.85	105-11.46	2.00	1.8	1	1	2	2	0	33	278	0.30	5.8	4.9	D	
78/ 2/18	1730 9.5	30-36.84	105-11.49	0.40	2.9	2	2	2	2	0	33	278	0.31	3.2	1.6	D	
78/ 2/18	1754 9.8	30-36.74	105-11.45	0.32	2.3	2	2	2	2	0	34	278	0.28	2.9	1.4	D	
78/ 2/18	1845 16.5	30-37.45	105-11.92	2.00	2.1	2	2	2	2	0	33	279	0.34	6.8	5.4	D	
78/ 2/19	705 18.7	30-36.89	105-11.00	2.00	1.9	2	1	2	2	0	33	277	0.32	10.2	8.9	D	
78/ 2/19	1212 0.0	30-36.85	105-11.58	0.69	2.9	2	2	2	2	0	34	279	0.35	3.6	1.7	D	
78/ 2/20	252 55.4	30-37.33	105-11.89	2.00	1.9	2	2	2	2	0	33	279	0.32	5.9	4.9	D	
78/ 3/20	14 10.6	30-26.00	104-10.00	2.00	1.7	2	1	0	2	0	37	241	0.45	0.2	0.1	D	
78/ 4/ 6	913 27.4	30-51.68	104-51.75	4.00*	2.0	2	2	0	2	0	41	287	0.15	7.1	5.3	D	
78/ 4/12	2305 0.0	30-39.52	104-29.07	2.27	1.9	1	2	0	2	0	23	145	0.55	0.3	4.8	D	
78/ 5/30	1319 31.7	30-39.14	104-33.77	10.70	2.2	2	0	2	2	2	35	117	0.69	3.8		D	
78/ 6/ 3	1140 18.2	30-24.23	104-38.63	2.73	2.4	1	1	1	0	1	16	165	0.22	4.0	5.3	C	CLN
78/ 6/ 6	2005 0.1	30-18.00	104-35.00	18.94	2.2	1	1	1	0	1	3	150	1.02			D	
78/ 7/18		30-39.00	104-33.00		2.6	1											
78/ 8/28	2033 38.3	31- 1.81	104-56.74	9.26	1.7	1	2	2	1	1	19	240	0.38	11.7	7.4	D	
78/ 9/ 2	716 45.3	30-40.46	104-31.85	12.52	1.2	2	2	1	2	1	21	97	0.60	3.6	27.8	C	
78/ 9/29	1759 41.4	30-19.10	104-39.41	2.00	2.2	1	1	0	1	1	9	231	0.95			D	
78/12/20	131 21.8	30-37.97	104-28.69	6.35	1.0	2	2	0	2	0	22	155	0.52	6.8	6.6	D	
79/ 1/11	349 9.9	30-30.44	104-24.62	5.87	1.0	2	2	0	2	0	25	192	0.29	1.9	2.4	C	
79/ 1/15	36 35.8	30-35.81	105-21.04	8.26	1.5	2	2	2	2	1	42	282	0.31	9.9	11.3	D	
79/ 1/19	907 55.1	30-30.00	105- 7.14	2.40	1.8	2	1	1	2	2	43	249	0.29	3.2	1.8	D	
79/ 2/13	1902 13.4	30-10.29	104-21.47	1.80	1.8	2	2	0	2	0	50	292	0.61	7.4	7.2	D	
79/ 2/16	2350 32.5	31- 1.96	104-54.00	7.77	2.0	2	2	0	2	0	50	305	0.16	17.4	16.5	D	
79/ 3/17	1949 2.4	30-39.54	104-35.02	16.53	1.1	1	1	0	2	2	17	182	0.52	9.5	16.8	D	
79/ 3/24	1455 36.5	30-31.07	104-19.92	8.40	1.1	1	2	0	2	2	32	161	0.48	0.9	1.7	C	
79/ 3/28	551 35.4	29-41.64	104- 2.21	2.00	1.8	2	2	0	2	1	83	319	0.15	19.5	20.3	D	
79/ 3/28	1457 18.5	30-38.76	104-30.22	8.64	1.3	2	2	0	2	2	20	148	0.59	4.2	3.4	D	
79/ 3/29	935 40.9	29-35.47	102-55.05	4.00*	2.5	2	2	0	2	2	160	336	0.54			D	KTX,KT4
79/ 3/29	1352 29.2	30-40.84	104-32.26	9.03	1.3	2	2	0	2	2	21	170	0.54	4.8	3.5	D	
79/ 6/ 9	128 59.1	30-39.12	104-30.14	9.38	1.9	2	2	1	0	2	21	149	0.38	3.6	2.8	C	

79/ 6/10	1047	49.5	30-30.00	104-18.28	4.00*	1.7	2	2	0	2	2	35	171	0.64	3.7	4.4	D
79/ 6/17	1736	30.3	30-40.48	104-31.71	11.31	1.7	2	2	0	2	2	31	199	0.13	1.2	36.4	D
79/ 6/21	1032	3.5	30-36.06	104-26.68	0.40	1.2	2	2	0	2	2	23	121	0.62	1.1		D
79/ 6/22	558	16.0	30-34.56	104-28.06	5.43	1.7	2	2	0	1	2	20	122	0.35	2.6	3.8	C
79/ 6/25	1723	36.8	30-34.41	104-10.54	7.18	1.1	2	2	0	2	2	20	175	0.43	6.6	6.9	D
79/ 6/28	337	9.4	31-11.41	104-33.10	20.67	1.5	2	2	0	0	2	33	316	0.07	1.5	1.7	C
79/ 6/28	1923	45.4	30-23.06	105- 8.84	2.00	1.9	1	1	0	2	1	56	307	0.25	2.4		D
79/ 7/10	2132	27.2	30-40.40	104-29.53	10.99	0.9	2	2	0	0	2	30	188	0.25	2.4		D
79/ 7/10	2146	15.8	30-42.48	104-31.92	11.99	0.9	2	2	0	0	2	28	203	0.65	1.8	32.5	D
79/ 7/10	2202	22.4	30-40.10	104-29.83	8.03	0.9	2	2	0	0	2	31	189	0.53	0.5	0.8	D
79/ 7/10	2209	15.0	30-41.02	104-30.13	9.33	0.9	2	2	0	0	2	29	192	0.45	0.8	1.3	D
79/ 7/24	307	56.0	30-37.37	104-25.16	2.36	0.7	2	2	0	0	2	34	163	0.95	0.5	15.2	D
79/ 8/ 4	2131	8.2	30-50.13	104-13.91	4.00*	1.0	2	2	0	2	2	18	184	1.07	40.5	31.7	D
79/ 8/ 9	1257	55.2	31- 0.77	104-55.64	5.84	1.2	1	1	2	2	2	19	231	0.34	27.0	23.1	D
79/ 8/ 9	1443	40.3	30-32.71	105- 3.48	9.09	1.4	1	0	2	2	2	37	233	0.19	2.9	2.8	D
79/ 8/10	1804	42.5	31- 0.01	104-56.64	7.23	0.9	1	2	2	2	1	17	229	0.20	12.2	9.9	D
80/ 2/ 5	2356	54.7	29-55.46	104-26.50	3.20	1.2	2	2	0	2	2	41	304	0.42	3.0	1.4	D
80/ 6/22	302	8.2	29-29.89	105-11.79	2.00	1.9	2	0	2	2	2	104	323	0.36	31.5	26.6	D
80/ 6/22	1210	14.7	29-27.10	105- 9.38	6.01	1.9	2	1	2	2	2	106	323	0.27	8.8	7.7	D
80/ 6/22	2129	53.6	29-30.03	105-10.25	2.71	2.5	2	1	2	2	2	103	323	0.30	35.0	29.9	D
80/ 6/24	1146	18.4	29-29.98	105- 7.88	2.00	1.7	1	1	1	2	2	101	322	0.08	13.0	11.9	D
80/ 6/24	2323	0.6	29-28.28	105-10.63	4.00*	2.0	1	1	2	2	2	106	323	0.33	30.1	26.7	D
80/ 6/25	829	17.6	29-31.24	105-10.76	2.00	2.0	2	2	2	2	2	101	322	0.19	16.9	14.9	D
80/ 6/27	722	26.1	29-30.43	105-12.26	2.00	2.4	2	1	2	2	2	104	323	0.16	17.5	15.3	D
80/ 6/27	1159	41.9	30-37.16	104-39.64	19.82	0.7	1	1	1	2	2	10	123	0.72	3.6	7.3	C
80/ 6/27	1204	36.9	30-41.57	104-35.30	11.02	1.3	2	2	2	2	2	20	100	0.52	2.3		C
80/ 6/27	1227	52.6	30-42.42	104-35.17	7.81	0.7	1	1	1	2	2	21	103	0.47	3.3	2.3	C
80/ 7/ 3	353	38.8	30-42.17	104-35.54	6.20	0.4	1	1	1	2	2	21	102	0.41	2.9	2.1	C
80/ 7/30	0	29.3	30-31.72	104-27.28	1.00	0.7	2	2	1	2	2	20	134	0.42	1.1	2.4	C

SEISMICITY OF WEST TEXAS

by

DAVID BYRON DUMAS, BS, MA

DISSERTATION

Presented to the Faculty of

The University of Texas at Dallas

in Partial Fulfillment

of the Requirements

for the Degree of

DOCTOR OF PHILOSOPHY

THE UNIVERSITY OF TEXAS AT DALLAS

December 1981

Page intentionally left blank

ACKNOWLEDGMENTS

I thank Messrs. John Reynolds, Albert Fay, Clay Miller, and James E. White Jr., for permitting us to place our remote seismic stations on their ranches. The cooperation of Mr. Jess Sorrels, manager of the X Ranch, and Mr. John Herrin, manager of the Eagle Mountain Ranch, is also greatly appreciated. I thank Mr. Curtis Laughlin, superintendent of McDonald Observatory for his generous cooperation, and Mr. Robert Gonzales and Mr. Windell Williams for their invaluable help in operating and maintaining the central station equipment at McDonald Observatory. I would especially like to thank Mr. L. Pakiser and the U.S. Geological Survey for providing much of my personal financial support while undertaking this study. I thank C.A. Frohlich for providing am epicenter location program, along with the Herrin travel-time tables, also for critically reviewing the manuscript and for helpful comments. I am indebted to W.R. Muehlberger who pointed out that Sellards' intensity data are consistent with other information on the strike of the Valentine Fault and for other useful comments. A.R. Sanford and O. Nuttli gave helpful reviews of the paper (Dumas et al., 1980), upon which Part I is based. I also thank R. Buffler and D. McCowan for reviewing the manuscript and for their helpful comments. I thank Drs. B.A. Bolt and R. Uhrhammer for allowing us to examine Byerly's collection of seismograms of the Valentine earthquake. I also thank Drs. J. Dorman and G. Latham for their constant advice and guidance in writing this manuscript.

The West Texas network program was supported by the National Aeronautics and Space Administration Grant NSG-7159.

SEISMICITY OF WEST TEXAS

Publication No.

David Byron Dumas, Ph.D.
The University of Texas at Dallas, 1981

Supervising Professor: H. James Dorman

A four year seismic study has found the Basin and Range province of west Texas and the adjacent area of Mexico to be more seismically active than heretofore known. A University of Texas five station seismic array around the Marfa Basin has located or detected approximately 800 local and regional earthquakes with S-P times of less than 30 sec.

A crustal model for the Basin and Range is derived from natural and artifical sources and contains four layers having velocities of 3.60, 4.93, 6.11, and 6.60 km/sec, respectively, overlying a mantle of 8.37 km/sec. A moderate level of seismic activity has been detected near Van Horn, in the Marfa Basin (particular the eastern side), and along the Texas-Mexico border between latitudes 30° and 31°N. Five earthquake sequences were recorded, two near the Texas-Mexico border and three in the Marfa Basin. Four of these sequences showed quiescent periods in foreshock activity preceding the main shock. On the eastern side of the Marfa Basin a diffuse linear seismic zone may represent an unmapped fault, striking N 50°W that coincides with Muehlberger's proposed eastern boundary of Basin and Range faulting.

A new epicenter for the Valentine, Texas earthquake of August 16, 1931 has been relocated instrumentally at the northern end of this diffuse

zone. Regional and local teleseismic P-wave arrival time anomalies observed for the nearby Gnome underground nuclear explosion of 1961 are used to determine station corrections and thus to locate the new 1931 epicenter at 30.69°N, 104.57°W. Several estimates of magnitude (m_b) based on intensity data range from 5.6 to 6.4. Fault-plane and composite fault-plane solutions supports Muehlberger's hypothesis that the Basin and Range is undergoing extension in a SW-NE direction.

TABLE OF CONTENTS

PART I. A REEVALUATION OF THE AUGUST 16, 1931 TEXAS EARTHQUAKE

INTRODUCTION

On August 16, 1931, an earthquake occurred in far west Texas near Valentine, which shook most of Texas, New Mexico and the adjacent areas of Mexico. The main shock was preceded by several felt foreshocks and followed by several felt aftershocks which persisted for a period of at least 3 months (Sanford and Toppozada, 1974; Sellards, 1932). This event is said to have been the largest historic earthquake in Texas (von Hake, 1977).

Two instrumental locations and origin times have been published for this earthquake. The USCGS placed the epicenter at 29.90°N and 104.20°W, and the origin time at 11 hr 40 min 15 sec (UTC) (United States Earthquakes, 1931). Byerly (1934a and b) made a detailed investigation of the teleseismic travel times of this earthquake. By placing the arrival times of the nine nearest stations on a straight line, he found the epicenter to be 30.88°N and 104.18°W and the origin time to be 11 hr 40 min 21 sec. The problem posed by these contemporary reports is that both epicenters fall outside the area of maximum intensity (Figure 1). Since no surface breakage was reported from any area (Sellards, 1932), the active fault along which the earthquake occurred remained unidentified and the regional tectonic significance of the Valentine earthquake could not be satisfactorily assessed from the conflicting evidence.

This analysis was stimilated by the work of Herrin and Taggart (1962) who found the instrumentally located epicenter of the Gnome underground nuclear explosion, detonated near Carlsbad, New Mexico, on December 10, 1961, fell 16 km east of the explosion site. It was suggested (Herrin and Taggart, 1962) that this was caused by systematic differences between the velocities

Figure 1: Isoseismal (Rossi-Forel) map for the August 16, 1931 Texas earthquake (redrawn from Sellards, 1932). Byerly's epicenter location is indicated by * and the USCGS epicenter by ■ .

Figure 1

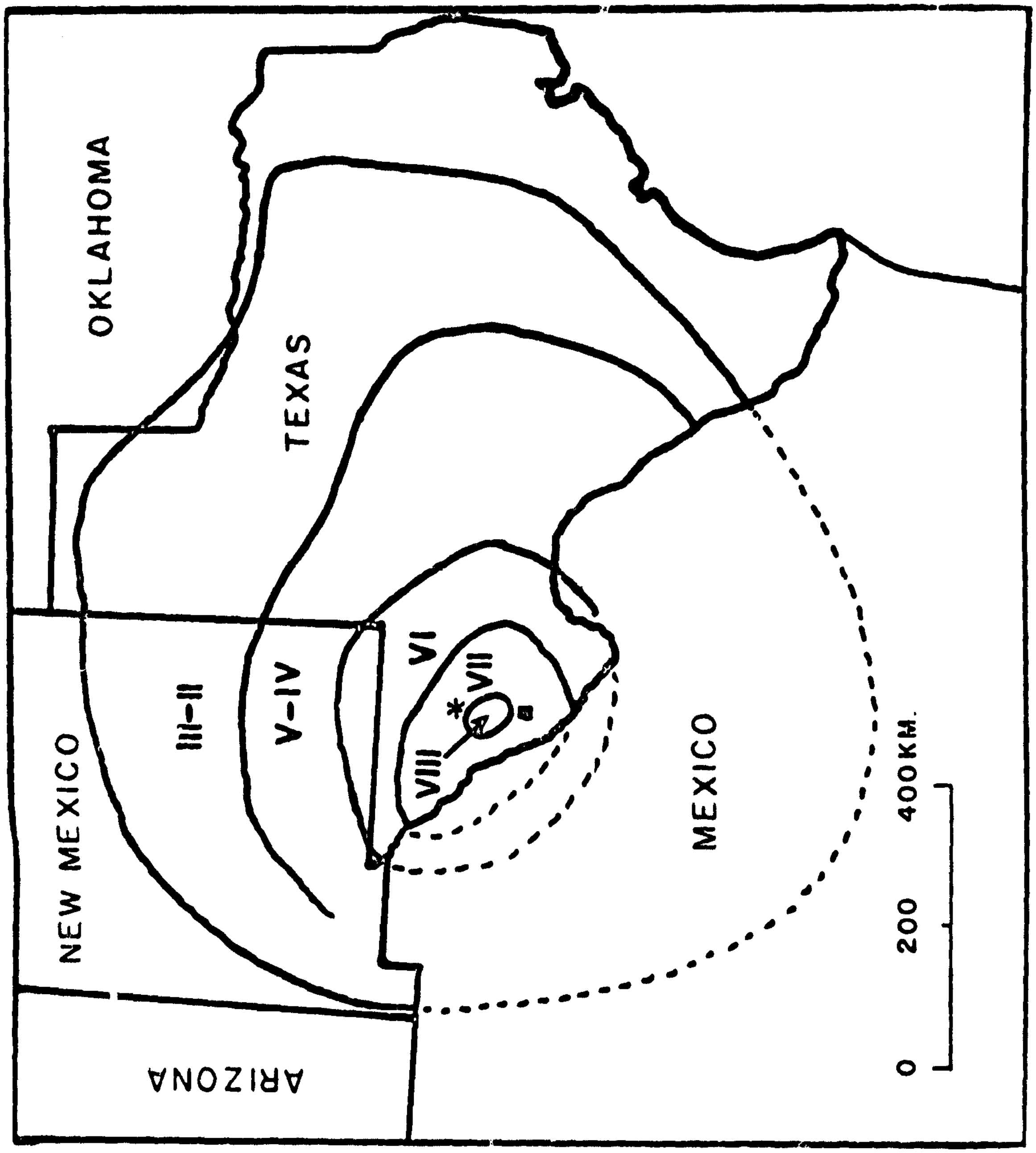
OKLAHOMA
TEXAS
NEW MEXICO
ARIZONA
MEXICO
III–II
V–IV
VI
VII
VIII
0
200
400KM.

of P_n in the eastern and western United States. A similar offset must be expected regarding Byerly's epicenter for the Texas earthquake since it lies only 160 km south of the Gnome site. This paper utilizes the observed residuals from the Gnome explosion to adjust station corrections and obtains a new epicenter based upon Byerly's arrival-time readings. This epicenter satisfies not only the travel-time data, but also coincides with the observed maximum isoseismal to the Texas earthquake and with the newly discovered active seismic trend near Valentine (See Part II). Thus, the new epicenter is consistent not only with the data of 1931, but also with relevant seismic data that have become available much more recently as well.

REVISED EPICENTER LOCATION

Local and regional P-wave arrival times listed in Table 1 (Byerly, 1934a) were used in a hypocenter location program. These 19 stations were chosen for the following reasons: (1) their Gnome travel-time residuals were available, and (2) the arrivals, as listed by Byerly, were of sufficient amplitude that they could be read with little uncertainity. Denton, Texas was not used in the hypocenter location program because the exact location of the 1931 seismic station could not be obtained. The program utilizes the Herrin earth model (Herrin et al., 1968) to determine hypocentral parameters by minimizing the observed minus the calculated travel-time residuals, in a weighted least-squares sense. The effect of local structure differing from the Herrin model was removed by subtracting from Byerly's readings the Gnome travel-time residuals (Herrin and Taggart, 1962) as listed in the corrections column of Table 1. Travel-time corrections for distant stations outside the conterminous 48 states were made by subtracting the mean travel-time residuals of station MOT (McDonald Observatory in far west Texas) for

TABLE 1

TELESEISMIC P-WAVE RESIDUALS FOR THE LOCATION OF THE 1931 EARTHQUAKE

Station	Delta (deg)	Az (deg)	Hr	Min	Sec	Residual (sec)	Weight	Corrections (sec)
TUC	5.55	286.86	11	41	48.5	-0.72	0.970	1
PAS	12.00	289.50	11	43	18.0	-1.11	0.963	3
TAC	12.24	155.69	11	43	20.0	-1.41	0.980	2
HAI	12.42	298.79	11	43	31.0	4.16	0.915	5
FLO	14.19	51.94	11	43	40.5	-3.12	0.894	-2
SLM	14.20	52.76	11	43	40.0	-3.73	0.809	2
BOZ	15.88	341.41	11	44	10.0	1.02	0.861	1
SCL	15.86	298.88	11	44	15.0	3.19	0.959	4
BRK	16.24	300.27	11	44	16.0	-0.69	0.970	4
CHI	17.57	46.67	11	44	24.0	-1.60	0.966	-4
CSC	20.15	74.84	11	45	01.0	3.60	0.908	-3
PIT	22.20	57.62	11	45	17.0	-1.67	0.965	-4
CTV	22.67	64.48	11	45	26.0	2.59	0.958	-4
VIC	22.87	326.23	11	45	28.0	-2.40	0.980	1
GEO	23.96	62.88	11	45	39.0	2.76	0.953	-4
OTT	26.87	49.03	11	46	07.0	3.71	0.898	-4
CAM	29.15	47.08	11	46	26.0	2.30	0.965	-4
SIT	33.92	329.83	11	46	04.0	-6.76	0.810	1
SJP	36.89	100.55	11	47	33.0	-1.67	0.965	1

earthquakes that are located in the vicinity of these distant stations. This procedure is valid for correcting the distant station data because of the near proximity of MOT and the new Valentine epicenter to the Gnome explosion. The residuals listed in Table 1 are those obtained with respect to the new epicentral solution.

Based on the data listed in Table 1, the new epicenter is 30.69° N±0.41, 104.57°W±0.30, the depth is 29.1±25 km, and the origin time is 11 hr 40 min 21.9±2.8 sec. The weighted standard error of the travel-time residuals is 2.85 sec. The standard error associated with the travel-time residuals is large and is typical of the formal uncertainities obtained with early data such as these (Gawthrop, 1978). This reflects the approximation in locations given for many of the older stations and also the less stringent standards of station time-keeping that prevailed in that era. Nevertheless, the revised epicenter location in the Marfa Basin, 42 km southwest of Byerly's epicenter, is closely consistent with the relationship noted between the instrumental and actual epicenters of the Gnome event. The displacement of the earlier epicenter and the azimuth of displacement is also different in the two cases because the azimuthal distributions of stations were different as well.

Examining the problem further, the numerical (least squares) equivalent to Byerly's graphical solution for the 1931 epicenter is calculated by fitting his nine closest data points to a single straight line. As expected, the results agrees precisely with Byerly's, since we merely solved the numerical version of Byerly's graphical problem. In this method, a uniform mantle to the east and to the west is implicit in the assumption of a single P_n line.

Gnome results and numerous refraction experiments in the west have shown a strong east-west gradient of mantle velocity across the eastern margin of the Rocky Mountain front and Rio Grande rift in New Mexico. This is reflected in the separation of the Gnome instrumental epicenter and the actual site of the explosion. Therefore, Byerly's closest readings of the Texas earthquake seismograms are compared directly with data of the Gnome explosion (Romney et al., 1962) which occurred at 32.264°N, 103.866°W, only 160 km to the north of Valentine. Byerly's closest observations of the Texas earthquake were TUC (Tucson Observatory), 650 km to the west, and Denton (in this paper Denton will be referred to as DTX), 700 km to the east, while during the Gnome experiment there were two recording points near Tucson, and there was a line of stations which passed near Denton, Texas. Byerly's 1931 readings are plotted as solid symbols in Figure 2 , while the Gnome P_n arrivals are plotted as open circles and squares. Clearly, Byerly's Tucson data point would agree better with the Gnome observations if his epicenter were moved 1 sec, or about 8 km, closer to Tucson.

Regarding the Denton data, Byerly's first arrival pick would be aligned with the Gnome-Denton line in Figure 2 if his epicenter were displaced by about an equal distance away from Denton. However, the true distance is probably four times as much, since three reasons are seen for questioning Byerly's (1934b) identification of the first arrival. First, he reported the earliest motion as a trace amplitude of 0.1 mm, while an arrival 3 sec later had an amplitude of 0.9 mm. He also reported 2 mm as the amplitude of first motion at Tucson. In the Gnome experiment, the stations around Denton recorded the largest ground amplitudes anywhere, about three times larger than those of the Tucson stations (Herrin and

Figure 2: Reduced travel-time data for the Gnome explosion of December 10, 1961 (Romney et al., 1962) and the Texas earthquake of August 16, 1931 (Byerly, 1934b) recorded near Denton, Texas and Tucson, Arizona. From left to right, the Gnome recording stations are Seymour, Mabelle, Nocomo, Ardmore, Tucson-T, Dallas, Tishomingo, and Volunteer Stations 17 and 42. The question mark identifies the first Denton arrival of 0.1 mm read by Byerly. The arrival 3 sec later was recorded as 0.9 mm in amplitude.

Figure 2

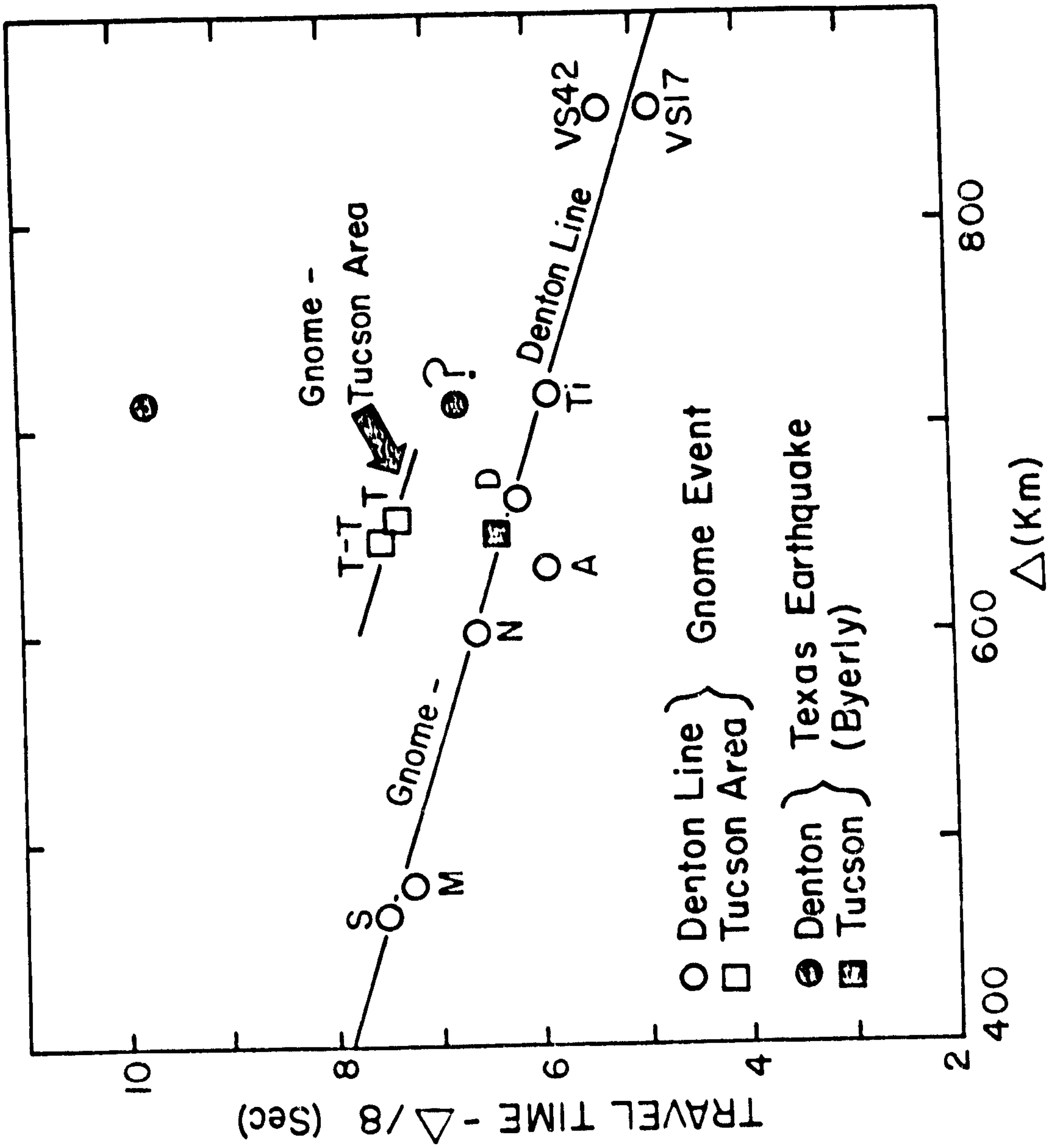

TRAVEL TIME - △/8 (Sec)
2
4
6
8
10
△(Km)
400
600
800
Gnome -
Tucson Area
T-T
T
Denton Line
VS42
VS17
?
D
N
A
Ti
S
M
Gnome -
Denton Line
Tucson Area
Gnome Event
Denton
Tucson
Texas Earthquake
(Byerly)

Taggart, 1962). While the magnification used at Denton and Tucson in 1931 is not known, it seems probable at this time that the first small motion at Denton might have been spurious noise. Having examined the original seismogram read by Byerly (his collected seismograms of this earthquake are stored at Berkeley), his pick seems credible, but it is nearly as small as any feature that could be seen on this seismogram. Thus, it can be regarded as doubtful. Second, the early pick at Denton leaves a very long $\bar{P} - P_n$ interval by comparison with Gnome observations at similar distances. Third, the polarity of the later and stronger arrival is in agreement with other points in the northeast quadrant of the fault-plane solution (Figure 3, DTX), while the earlier arrival is inconsistent on this score. Regarding $\bar{P}$, it is evident that the phase identified by Romney et al., (1962) on the Gnome records is not the same phase which Byerly called $\bar{P}$. The present interpretation has allowed for this fact.

Accepting the later pick for Denton, Byerly's epicenter of the Texas earthquake must be moved about 4 sec, or 32 km, away from Denton in order to place the Denton point on the Gnome-Denton line (Figure 2). This, combined with shifting the epicenter 8 km closer to Tucson, moves it southwestward about 35 km. This place the epicenter just north of Valentine, Texas and in the area of maximum seismal intensity (Sellards, 1932). This graphical solution is in excellent agreement with the solution obtained above by recomputation based on 19 first arrivals.

FAULT-PLANE SOLUTION

Using the first-motion readings reported by Byerly (1934a; the Denton, Texas polarity used is opposite that given by Byerly), a new fault-plane solution of the 1931 Texas earthquake was determined. Figure 3 shows

Figure 3: Fault-plane solution (equal area, lower hemisphere projection) for the 1931 earthquake. Closed circles indicate compression. Open circles indicate dilation. The direction of compression and tension axes are marked by P and T, respectively. The Denton, Texas arrival is indicated by the code DTX and the Tacubaya arrival by TAC. Polarities used in this solution are the readings of Byerly (1934a) except for DTX.

Figure 3

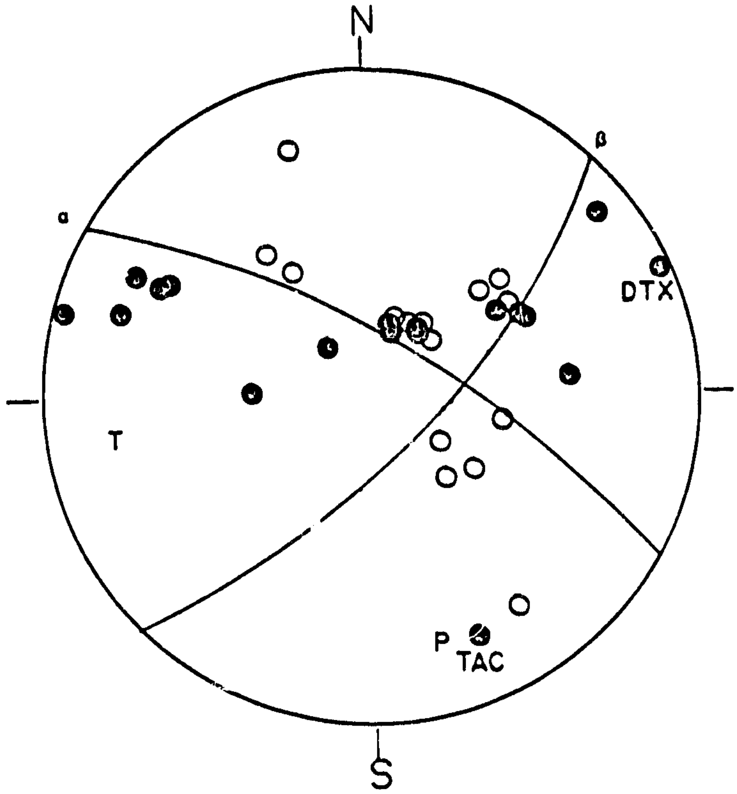

an equal area projection of the lower hemisphere of the focal sphere for all arrivals. The nodal planes are

	plane α	plane β
strike	N59°W	N36°E
dip	70°NE	70°SE

The strike of nodal plane β is approximately perpendicular to the trend of the Marfa Basin in which the epicenter falls. Therefore, it seems that nodal plane β is the auxiliary plane, and plane α is the fault plane. Thus, the solution indicates a strike-slip fault with right-lateral displacement. The tension and compression axes trend S74°W and S16°E, respectively. These directions indicate that elongation is occurring in the direction slightly south of west and north of east.

Using the polarity data of Byerly, Sanford and Toppozada (1974) obtained a solution indicating normal faulting striking N40°W, dipping 74°SW. Their solution, however, has more inconsistent points than the one represented in Figure 3. Figure 3 has only one gross inconsistency, a point in the southeast quadrant representing the first motion at Tacubaya (TAC). All other inconsistent points are near the the nodal planes.

MAGNITUDE

Several previous authors have estimated the magnitude of the 1931 Texas earthquake. Gutenberg and Richter (1949) gave a value of 6.4. The same value was obtained by Sanford and Toppozada (1974) using a method based on the size of the felt area. Nuttli (1976) obtained a magnitude (m_b) of 5.6 using the method of intensity gradient as described in detail by Nuttli (1973, 1976) and Nuttli et al., (1979). I reviewed the application of

Nuttli's method using the intensity data of Figure 1 which is plotted from Rossi-Forel intensities reported by Sellards (1932). Allowing for the difference between the Rossi-Forel and Modified Mercalli scales, one obtains agreement with Nuttli's result by using the spacing of isoseismals (Figure 1) normal to the trend of the valley, which is also normal to the direction of faulting (see fault-plane solution, Figure 3). Parallel to the valley, the spacing of isoseismals is greater, giving a magnitude of 5.9 (m_b) by the same method.

FORESHOCKS

Sellards (1932) mentioned that foreshocks of the 1931 earthquake were recorded at Denton, Texas and St. Louis, Missouri. Another reliable report of foreshocks was obtained from Mrs. York (personal communication) who lives on the western side of the Davis Mountains, about 25 km east of the new epicenter. She stated that she and her family had slept outside their ranch house during most of the preceding night because they felt several shocks hours before the main shock at 05:40 a.m. (local time).

CONCLUSION

A revised location of the Texas earthquake of 1931 places the epicenter at 30.69°N, 104.57°W, on a fault striking N 59°W and with a right lateral strike-slip mechanism. Discrepancies with other data are thereby resolved since the new location falls within the area of maximum seismic intenstites of the 1931 earthquake.

PART II. SEISMICITY AND CRUSTAL STRUCTURE OF THE BASIN AND RANGE PROVINCE OF WEST TEXAS

INTRODUCTION

In the summer of 1975 the University of Texas and the National Aeronautics and Space Administration (UT/NASA) began a long term geophysical program designed to support the geodetic laser ranging measurements from the McDonald Observatory located in the Davis Mountains of Texas. The purpose of the long term program is to maintain surveillance of the regional tectonic processes.

This paper describes the seismological results obtained during a four year period. Epicenters were calculated using a crustal model of the Basin and Range province obtained from natural and man-made seismic sources, including the 1960 Gnome underground nuclear explosion in southeastern New Mexico. When the data permitted, fault-plane and composite fault-plane solutions were also obtained. This study shows that the number of earthquakes recorded in Basin and Range province of west Texas and the adjacent area of Chihuahua, Mexico is greater than previously mentioned. None of the local or regional earthquakes detected or located during this study were located by the United States Geological Survey (USGS) or the International Seismological Centre (ISC).

GENERAL GEOLOGY AND PHYSIOGRAPHY

Trans-Pecos Texas (T-PT) is separated into two physiographic provinces, the Great Plains and Basin and Range provinces. Here the Great Plains province is characterized by a belt of plains and low plateaus, 80-100 km in width, with no major geologic changes within the province. West of the Great Plains in T-PT is a region of mountains and intermontane basins

(Basin and Range province, B&R). A geologic boundary between the northern and southern regions of the B&R is approximated by Interstate Highway 10. In the northern region, the rocks are mainly of Mesozoic and Paleozic ages, including extensive Permian limestones and dolomites, Cretaceous limestones and sandstones, and a few scattered outcrops of intrusive volcanics (Barker and Hodges, 1977). The region also contains one of the two exposures of Pre-Cambrian rocks in the state.

The most prominent structural feature of the northern region is the Salt Basin Graben (Figure 4). The graben is bounded on both sides by extensive Quaternary faults. Faults on the eastern side of the graben are short and widely dispersed; on the western side, the faults are more continuous (Muehlberger, 1978).

In the southern region, the rocks are composed mainly of Tertiary volcanic sequences. The Salt Basin Graben extends southward into the southern region where it is known as the Marfa Basin. The eastern side of the Marfa Basin exhibits very little surface evidence of faulting, but the western side is bounded by numerous normal faults, the most prominent being the Mayfield Fault. Most of the basin fill is composed of unconsolidated Quaternary sediments. Shurbet and Reeves (1977) estimated from gravity measurements basin fill to a depth of at least 2.4 km in the Marfa Basin.

West of the B&R is a narrow northwest-southeast trending structural depression known as the Chihuahua Trough. Sediments which accoumulated in the Chihuahua Trough during the late Jurassic and Cretaceous time underwent complex folding and eastward overthrusting with associated tear faults during the Laramide (Gries and Haenggi, 1970).

Figure 4: Geologic map showing major structural features of Trans-Pecos Texas. The dotted line indicates the boundary between the Basin and Range (southwest) and the Great Plains (northeast) provinces (Muehlberger, 1978). Station names and locations (▲) are identified in Table 2. Other abbreviations are: ct - Chihuahua Trough, I-10 - Interstate 10, mb - Marfa Basin, mf - Mayfield Fault, pr - Pecos River, sbg - Salt Basin Graben. (redrawn from the Geological Highway map of Texas).

Figure 4

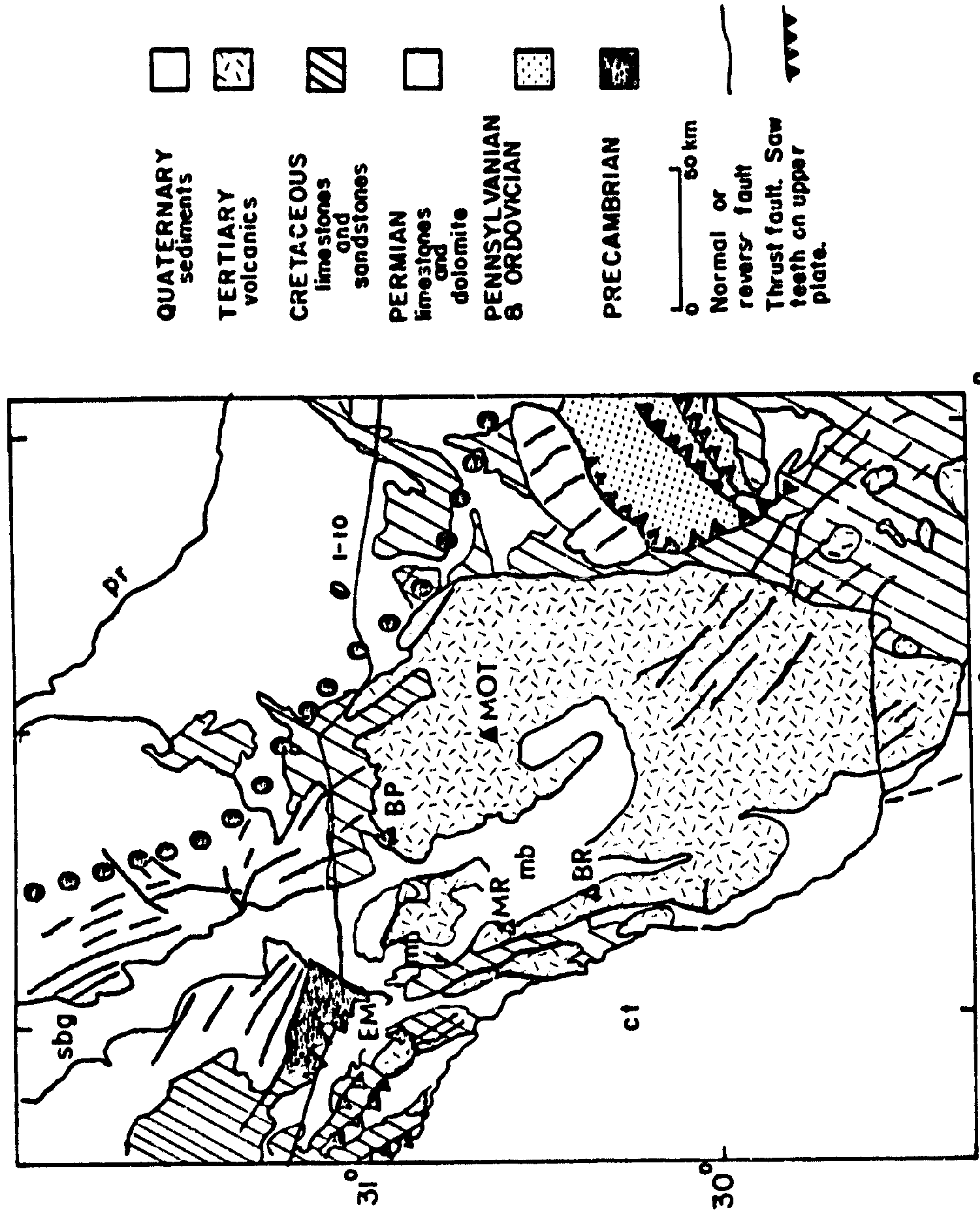
QUATERNARY sediments
TERTIARY volcanics
CRETACEOUS limestones and sandstones
PERMIAN limestones and dolomite
PENNSYLVANIAN & ORDOVICIAN
PRECAMBRIAN
0 50 km
Normal or reverse fault
Thrust fault. Saw teeth on upper plate.
pr
sbg
I-10
BP
MOT
mb
BR
MR
EM
ct
31°
30°
105°
104°
103°

HISTORICAL SEISMICITY OF WEST TEXAS AND CHIHUAHUA, MEXICO

Though there is evidence of minor seismicity in west Texas and Chihuahua, adequate historical information is lacking due to sparse population and poor instrumental coverage. The first documented earthquake in west Texas occurred near El Paso on March 7, 1923 (Sanford and Toppozada, 1974). Several events have since been located or felt in the El Paso area and other areas of T-PT (von Hake, 1977). The largest instrumentally located earthquake in Texas occurred on August 16, 1931 (Byerly, 1933a and Dumas et al., 1980) near the town of Valentine and aftershocks were felt for a period of three months (von Hake, 1977). The most recently felt earthquake in Valentine occurred on August 1, 1975.

Only recently have seismic studies begun to focus on the seismicity of west Texas. Chan (1977), in a three month study of the B&R, located 9 events across T-PT; of which three were located in the B&R. Dumas (1979) has noted an active seismic focus near Snyder, Texas. On June 16, 1978 a magnitude 4.6 earthquake occurred in the Snyder area and this earthquake is the largest event to occur in Texas since the 1931 event. Rogers (1979) suggests that local earthquakes recorded at the Kermit, Texas array in the Permian Basin may be associated with the secondary recovery of hydrocarbons.

In Chihuahua, the first earthquake located instrumentally occurred on September 10, 1963 (Earthquake File Tape, National Earthquake Information Service). Since then at least 15 earthquakes have been located (m_b>4.8) along a diffuse line striking northeasterly across northern Chihuahua.

SEISMIC ARRAY AND INSTRUMENTATION

The UT/NASA seismic array consists of five short-period remote stations (Table 2) located in the B&R of west Texas (Figure 4). The array

Table 2

Station Names, Corrdinates, Elevation, and Station Corr.

	Station	Lat.	Long.	Elev(m)	Corr.
MOT	McDonald Observatory	30.68N	104.01W	2080	0.10
BP	(MT1) Boracho Peak	30.93N	104.39W	1720	-0.03
EM	(MT2) Eagle Mountain	30.90N	105.08W	2088	0.10
MR	(MT3) Miller Ranch	30.53N	104.67W	1584	0.06
BR	(MT4) Brite Ranch	30.27N	104.58W	1584	-0.13

encloses an area of about 4000 km^2, the longest interstation distance is 105.5 km (stations EM and MOT).

Each station consists of a 1 hz vertical-component geophone (Geotech model 18300) situated on bedrock, a pre-amplifier (maximum gain of 104 db), a 5 hz low pass filter, a voltage controlled oscillator, and 0.25 watt radio transmitter. Each remote station is powered by a solar panel charging a 12 volt battery. The seismic signal is transmitted either directly or relayed to the central station at McDonald Observatory. At the central station the seismic signal from each station can be delayed 10, 20 or 40 sec in a digital memory. The selected delay time determines the sampling rate of the analog to digital converter and also determines the cutoff frequency for the low-pass antialiasing filter. For the west Texas network the 40 sec delay ensures the recording of the onsets of all local events for which late arriving phases "trigger" the array. The delayed signal is then recorded along with the WWV time code on an 8 channel Brush strip chart recorder. The recorder runs continuously at a chart speed of 0.01 mm/sec; however, the chart speed is automatically increased to 10 mm/sec when an event is detected at two, three, or more stations within a prescribed time window. Detection occurs when the instantaneous signal exceeds the average background signal by a selectable ratio. The average background signal is obtained by rectifying and smoothing (time constant 120 sec) the output of the seismometer. The system operates at a peak magnification of 250,000 (-12 db) at 6 hz (Figure 5). The output of the MOT seismometer, located 1 km from McDonald Observatory, is also recorded on a helicorder at a speed of 1 mm/sec, thereby ensuring a readable arrival time at MOT for events that are not recorded at 10 mm/sec. Because of the occasional high winds at EM and BP, peak magnification for these stations is limited to 125,000.

Figure 5: Magnification curves for the UT/NASA array and the Wood-Anderson torsion seismometer. The peak magnification of the UT/NASA system is 500,000 (at the -6db amplifier setting) at 6 hz.

Figure 6: Richter local magnitude versus signal duration curve for local events. Magnitudes were determined from equation 1. Signal duration is measured in seconds from the time of first break until the signal amplitude decays to twice the background noise.

Figure 5

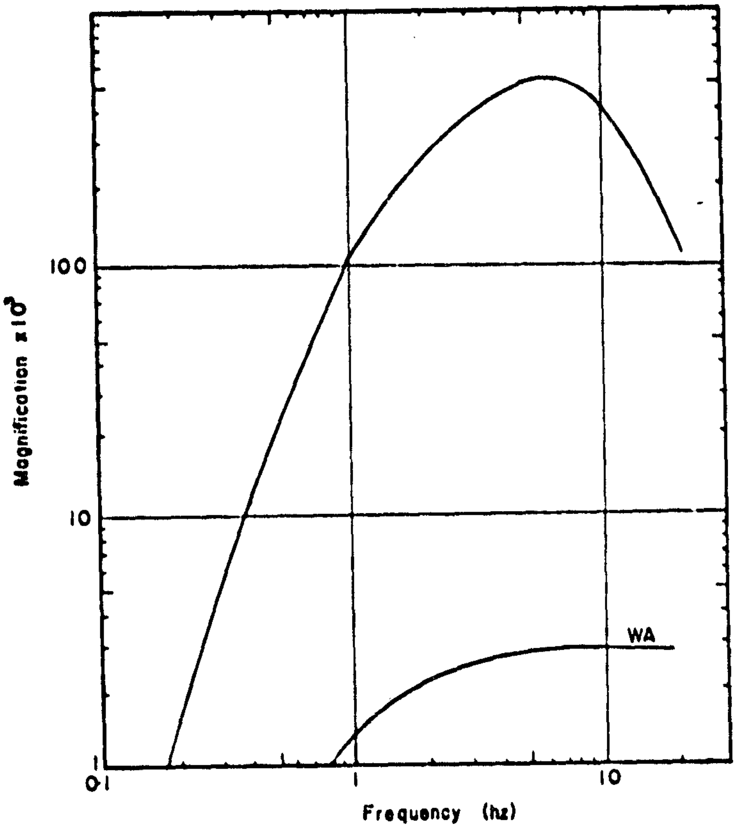

Figure 6

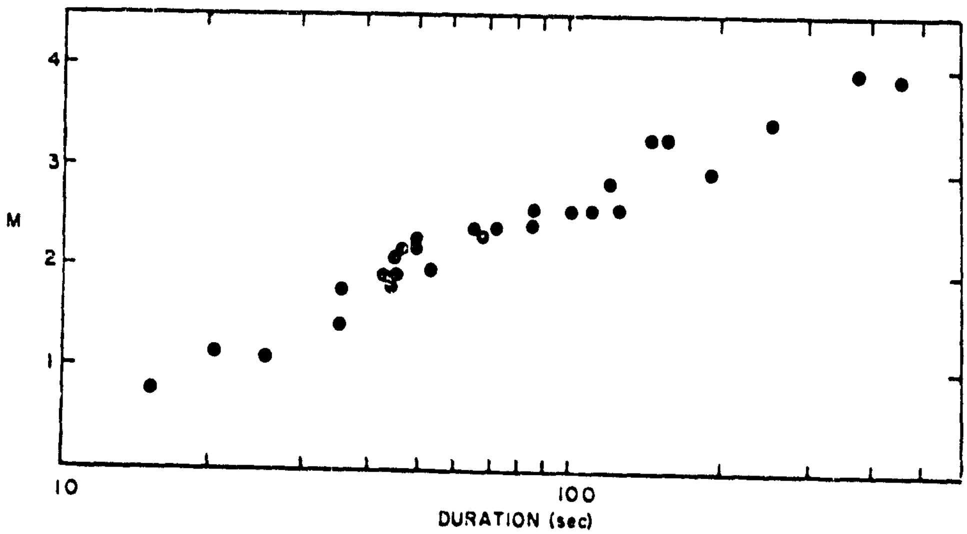

MAGNITUDE AND RECURRENCE TIME OF EARTHQUAKES

Local magnitudes (m_ℓ) listed in this paper were obtained by multiplying the trace amplitudes recorded at MOT by the ratio of the standard Wood-Anderson magnification curve to the MOT magnification curve. The definition of the local Richter magnitude then becomes:

$$m_\ell = \log A + \log (M_{wa}/M_{4-6}) - \log A_o \qquad (1)$$

where A is the peak recorded amplitude in millimeters at MOT, M_{wa} is the magnification of the Wood-Anderson torsion seismometer (2800), M_{4-6} is the mean magnification of the instrument at station MOT between 4 and 6 hz, and A_o is the amplitude of a magnitude zero earthquake in millimeters, recorded on a Wood-Anderson seismometer, as given by Richter (1958). The mean magnification between 4 and 6 hz (225,000) is used because the largest amplitudes in the seismic traces are in this frequency range. The 4 to 6 hz portion of the MOT magnification curve corresponds to the flat portion (2800) of the Wood-Anderson curve (Figure 5). The middle term on the right hand side of equation 1 is equal to -1.91 and varies by less than 0.1 unit of magnitude for the frequency range between 4 and 6 hz.

The magnitudes obtained from equation 1 are plotted against signal duration (Figure 6) for 28 events, located by this array and the Kermit array. Local magnitude can then be expressed in terms of duration as:

$$m_\ell = 2.10 \log \tau - 1.52 \qquad (0<\Delta<210 \text{ km}) \qquad (2)$$

$$m_\ell = 2.10 \log \tau - 1.52 + 0.0009\Delta \qquad (\Delta>210 \text{ km}) \qquad (3)$$

where Δ is the epicentral distance (km) to station MOT and τ is the signal duration measured from the time of the first break (P-wave arrival) to the time when the coda amplitude decays to twice the background noise. A reading error of ± 20% in signal duration corresponds to ± 0.2 magnitudes units. The inclusion of additional data in Figure 6 does not significantly alter equations 2 and 3. The distance correction in equation 3 was estimated by subtracting equation 2 from magnitudes listed for regional earthquakes (Earthquake Data Reports, USGS and Rogers, 1979) farther than 210 km from MOT.

The magnitude data used in the frequency-magnitude curve (Figure 7) were determined from equations 2 and 3. Artifical events near Van Horn (Seismicity Section) that may be included in the data have magnitudes less than 1.5. Since these events lie along the flat portion of the frequency-magnitude curve their effects on the slope of the curve is minimal. Rogers (1979), indicated that Kermit events with magnitudes greater than 1.9 may be related to hydro-carbon production and this would alter the slope of the frequency-magnitude curve in Figure 7. The 'b' values were computed by least-squares (LS) and maximum likelihood (ML) (Aki, 1965) methods and are given in equations 4 and 5, respectively:

$$\log N(m_\ell) = 4.85 - 1.17 \pm 0.03 m_\ell \quad (4)$$

$$\log N(m_\ell) = 4.51 - 1.04 \pm 0.11 m_\ell \quad (5)$$

where $N(m_\ell)$ is the cumulative number of earthquakes above magnitude 1.9. Both 'b' values are in agreement with Rogers (1979) 'b' values of 1.28 (LS) and 1.04 (ML) for events near Kermit.

Using equations 4 and 5, the probability that in the time interval, (0,T) at least one earthquake of magnitude m_ℓ should occur is given by

Figure 7: Cumulative number versus magnitude curve for all events recorded between January, 1976 and December, 1978 at station MOT (S-P<30 sec). Two 'b' values obtained for the portion of the curve greater than 1.9 are 1.17 and 1.04 by using the least-squares and maximum likelihood methods, respectively.

Figure 7

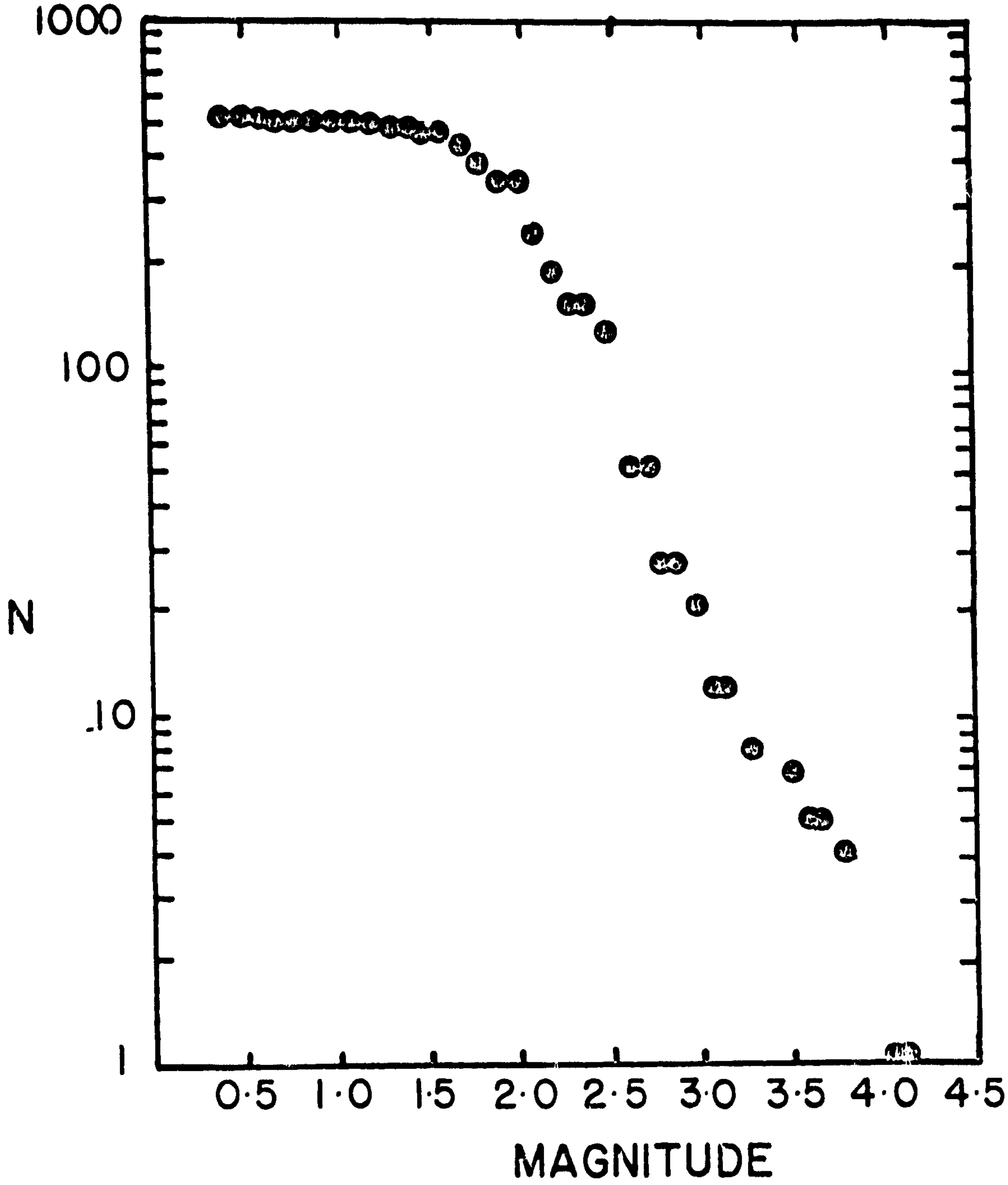

(Sacuiu and Zorilescu, 1970)

$$P(m_\ell,T) = 1-e^{-N(m_\ell)T/3.0} \qquad (6)$$

Since equations 4 and 5 were obtained over a 3.0 year period the exponent is divided by 3.0 to obtain the mean value for one year. Therefore, the mean recurrence period (in years) for an earthquake is

$$T_{mean} = \frac{3.0}{N(m_\ell)} \qquad (7)$$

The most destructive earthquake to occur in the area had a magnitude estimated to be between 5.6 and 6.4m_b (The 1931 earthquake). Extrapolating equations 4 and 5 beyond the given range of magnitudes shown in Figure 7 the estimated probability for magnitudes 5.6 and 6.4 earthquakes and their mean recurrence periods are given in Tables 3 and 4. The ML estimate of the mean recurrence based on equation 4 is 61 years for a magnitude 5.6 earthquake.

Although west Texas has been sparsely populated since the mid-19th century (and still is today), it is highly unlikely that a magnitude 5.6 earthquake would go undetected or unreported. The discrepancy between the theoretical recurrence period and the number of earthquakes (m_b = 5.6) actually occurring can be attributed to one or all of the following: (a) uncertainty in the 'b' value (ML), (b) differences between the local magnitude scale and body wave magnitudes, (c) temporal changes in seismicity, and (d) the 1931 earthquake was larger than 5.6. The other three mean recurrence periods based on the ML and LS methods for a 5.6 or 6.4 earthquake are large and cannot be verified on a historical basis.

Table 3

Earthquake Risk and Recurrence Rate

T^1	$P(5.6,T)^2_{LS}$	$T(5.6)^3_{LS}$	$P(5.6,T)^2_{ML}$	$T(5.6)^3_{ML}$
1	.007	151	.016	61
10	.064		.149	
25	.153		.333	
50	.282		.555	
100	.484		.802	

LS - Least squares estimate from equation 4.
ML - Maximum likelihood estimate from equation 5.
1 - (T) Time measured in years.
2 - {$P(m_\ell,T)$} Probability of a size m_ℓ earthquake occurring in T years (equation 6).
3 - mean recurrence rate

Table 4

Earthquake Risk and Recurrence Rate

T^1	$P(6.4,T)^2_{LS}$	$T(6.4)^3_{LS}$	$P(6.4,T)^2_{ML}$	$T(6.4)^3_{ML}$
1	.001	1303	.002	419
10	.008		.024	
25	.019		.058	
50	.038		.112	
100	.074		.212	

CRUSTAL MODELS

Crustal models (Figures 8a and b) for T-PT are derived from the data of untimed quarry blasts, the Gnome underground nuclear explosion, and located regicnal and local earthquakes. The B&R reduced travel-time curve obtained from a large untimed blast in a quarry west of Van Horn, Texas (VHB) is shown in Figure 9. Additional smaller blasts with waveforms and arrival time differences similar to those of the larger blast indicate all blasts are at the same location or within a few meters of each other (Nakamura, 1978). Therefore, data from several untimed blasts are used in this time distance plot. The first arrivals at all stations were impulsive and could be read to ± 0.05 sec. A later arrival that was consistently seen at stations EM and BP had an apparent velocity of 3.60 km/sec and is taken as the direct arrival. The ray path of the direct arrival at these two stations is mostly through sedimentary material. This phase could not be identified at the three remaining stations since the sedimentary layer is not continous from the shot point to these stations. The shot time of the large blast was estimated from the intercept of the direct arrival time curve extrapolated to the shot point. Using these data a model of the upper crust for the B&R consists of three layers 3.56, 2.39, and 12.59 km thick, with velocities of 3.60, 4.93 and 6.11 km/sec, respectively, overlying a 6.6 km/sec layer. The 4.93 km/sec layer probably represents a volcanic section and the 6.11 km/sec layer may be the first indication of basement depth beneath the B&R. Following the first arrival at station EM by 2.3 sec there is a third arrival that could not be identified at the other four stations. This arrival can be interpreted as the reflection from the base of the 6.11 km/sec layer because it's travel time agrees well with the calculated travel time for the model in Figure 8a. The reflected arrivals from the base of the 3.60 and

Figure 8: Summary of all crustal models mentioned in the text, (a) Van Horn Blast, Kermit and Snyder earthquakes, (b) Gnome and natural events around Kermit, (c) Chan, (1977), (d) Stewart and Pakiser, (1962). All models are described in the text. Dashed lines are inferred layer boundaries. (*) indicates a higher apparent velocity (see text for explanation).

Figure 8

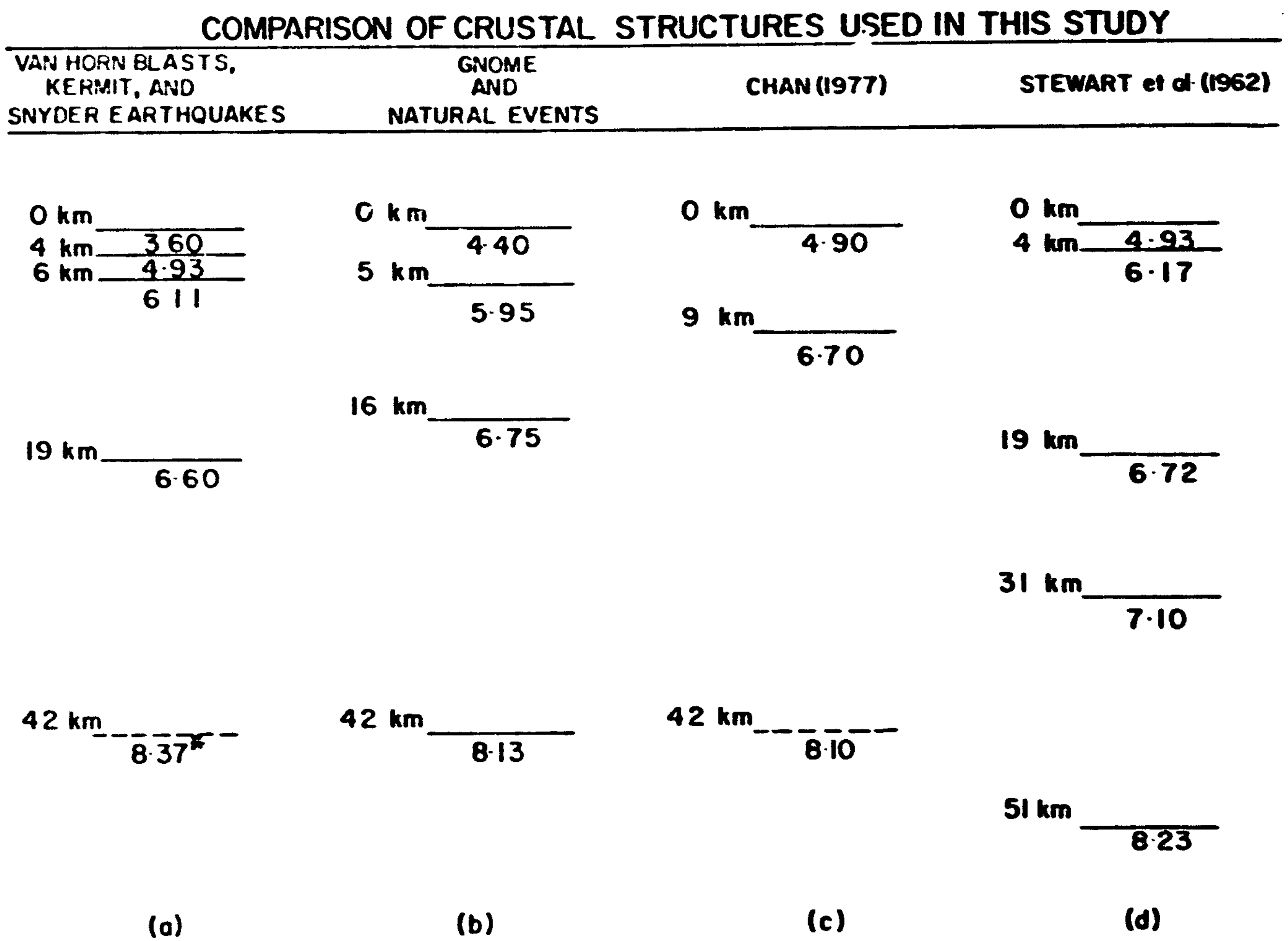
COMPARISON OF CRUSTAL STRUCTURES USED IN THIS STUDY
VAN HORN BLASTS, KERMIT, AND SNYDER EARTHQUAKES
GNOME AND NATURAL EVENTS
CHAN (1977)
STEWART et al (1962)
0 km
4 km
6 km
3.60
4.93
6.11
19 km
6.60
42 km
8.37*
0 km
4.40
5 km
5.95
16 km
6.75
42 km
8.13
0 km
4.90
9 km
6.70
42 km
8.10
0 km
4 km
4.93
6.17
19 km
6.72
31 km
7.10
51 km
8.23
(a)
(b)
(c)
(d)

Figure 9: Arrival time data used to derive the model in figure 8a recorded at stations MR, MOT, BP, and BR from a large explosion located at 104.959°W and 31.100°N. EM points were plotted on the same scale by using the time difference between EM and BP arrivals from smaller explosions at approximately the same source location.

Figure 9

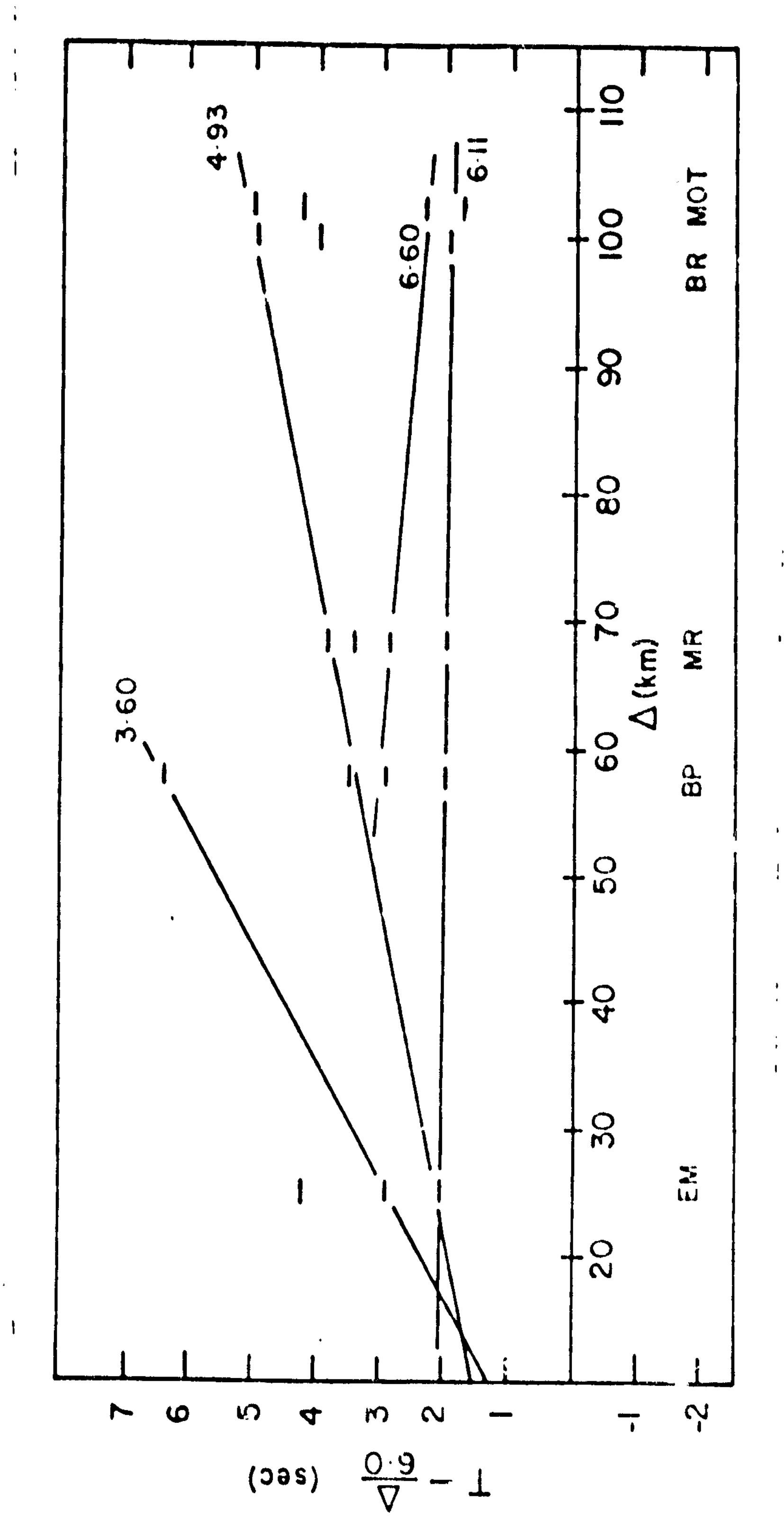
3·60
4·93
6·60
6·11
Δ (km)
EM
BP
MR
BR MOT
20
30
40
50
60
70
80
90
100
110
T − Δ/6·0 (sec)
7
6
5
4
3
2
1
-1
-2

4.93 km/sec layers at EM have approximately the same travel time as the first arrival from the respective layer, and therefore these phases could not be identified.

First arrivals from earthquakes about 190 km away near Kermit, Texas cross the UT/NASA array with an apparent velocity of 6.7 km/sec. The first arrival form the June 16, 1978 Snyder, Texas earthquake (Dumas, 1979) had an apparent velocity of 8.37 km/sec (epicentral distance ∿ 420 km) and a secondary arrival had an apparent velocity of 6.7 km/sec. The 6.7 km/sec arrivals from the Kermit and Snyder areas are compatiable with the 6.60 km/sec arrival from the VHB. Using the results from Figure 9 and the apparent velocities from the Kermit and Snyder earthquakes, we obtained a crustal model for the B&R that is summarized in Figure 8a. This model consists of four layers overlying a 8.37 km/sec mantle. The 8.37 km/sec velocity may be slightly higher than the actual mantle velocity beneath the B&R because at the epicentral distance of the Snyder earthquake the ray path pentrates deeper into the upper mantle thereby resulting in a higher apparent velocity. The data used to obtain this model were recorded entirely at the UT/NASA array.

To refine model 8a, an attempt was made to detect possible additional layers in the Marfa Basin using secondary arrivals observed from shallow earthquakes (<8 km). The epicentral distances for these events are between 20 and 56 km. The problem in using earthquakes is that they occur at various depths which will result in different travel times. However, we are interested only in the arrival time intervals between later arrivals in the seismic record and not the actual travel times. Since all the first arrivals were refracted from the 6.11 km/sec layer they were plotted on the same 6.11 km/sec curve regardless of depth. This has the effect of placing all foci on the same datum plane and, because the events were shallow, time corrections for a change in focal depth may be neglected. Thus, later arrivals from various earthquakes refracted from a given horizon fall roughly along the same time-distance curve. Layer thicknesses can be calculated from the difference between intercept times of the arrival refracted from the 6.11 km/sec layer and any later arrival. The interval between intercept times are insensitive to focal depth provided both ray paths in question are refracted arrivals. This produces a crustal model in which revised epicenters may be obtained. This procedure is repeated until the R.M.S. residuals of the earthquakes no longer decrease. Using this procedure a 6.11 km/sec half-space gave the smallest residuals. This may be understood by considering that the seismograph stations are located on hard rock (mountainous areas) which may have a velocity of nearly 6.11 km/sec. Later arrivals may nevertheless define shallower layering. Figure 10a is the reduced travel time curve based on epicenters located in a 6.11 km/sec half-space.

For the Marfa basin events, the 6.11 km/sec arrival and a later arrival representing a deeper layer could be seen at all stations. However, there was little correlation between later phases on seismograms from opposite sides of the array. The scatter of these data (Figure 10a) suggests lateral inhomogeneities and discontinuous layering above the 6.11 km/sec layer. Therefore, the time distance curves in Figure 10a were drawn for ray paths to the western and eastern sides of the array. The model for the western side of the array consists of two layers above the 6.11 km/sec layer with velocities of 3.56 and 4.26 km/sec. The 3.56 km/sec arrival identified at stations MR and BR represents the direct wave through sedimentary material and the 4.26 km/sec arrival as being refracted from a deeper layer. The time interval between the intercepts of the 3.56 and 4.26 km/sec curves is 0.1

Figure 10a. Reduced travel time curve using travel times for local earthquakes based on a 6.11 km/sec half-space. The first arrivals at each distance (not shown) were constrained to fall on the 6.11 km/sec line. Closed triangles and circles indicate arrival times to stations on the western and eastern sides of the array, respectively. Open symbols indicate S-wave arrivals (Δ - west, O - east). Numbers at the right are the velocities associated with the respective time distance curve.

Figure 10a

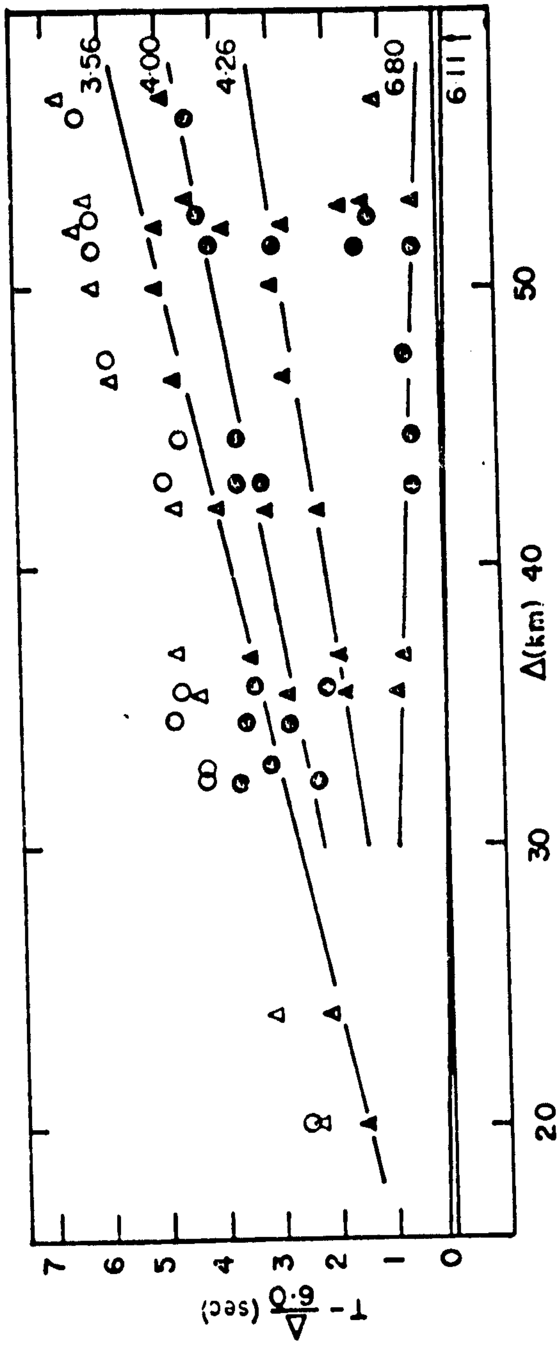

sec. Assuming a point source this would place the events in the sedimentary section just above the 4.26 km/sec layer. Considering the ray paths shown diagrammatically in Figure 10b and the time interval between the intercepts of the 4.26 and 6.11 km/sec, indicate that the 4.26 km/sec layer is 1.9 km thick.

On the eastern side of the array only a 4.00 km/sec arrival was detected above the 6.11 km/sec layer. The 4.00 km/sec velocity is an intermediate velocity between 3.56 and 4.26 km/sec velocities observed on the western side of the basin. A velocity between 3.56 and 4.26 km/sec would be expected of the direct arrival if the source is located in the second layer. Using the intercept times of the 4.00 and 6.11 km/sec curves the epicenters are located 1.2 km above the 6.11 km/sec layer. However, the total thickness of the shallower layers can not be determined. The complexities in the seismograms for the two stations located in the Davis Mountains (BP and MOT), made an unbiased selection of later arrivals difficult. This suggests that the Davis Mountains are very heterogenous.

The time interval between the intercepts of the 6.11 km/sec and 6.80 km/sec curves indicates the 6.11 km/sec layer is 10.2 km thick. This is in good agreement with the 12.6 km obtained from the VHB for the same layer considering the uncertainties associated with the use of earthquakes as a source for a refraction profile. If the differences between the two calculated depths are not due to observational errors then this suggest the Marfa Basin is dipping slightly (2.2°) towards the northwest. Figure 10b summarizes the crustal model for the Marfa Basin obtained from local earthquakes. Local events indicate non-homogenous and discontinuous layering above the 6.11 km/sec layer and that the eastern side of the Valentine Fault is structurally higher

Figure 10b. Schematic crustal model (not drawn to scale) for the Marfa Basin derived from Figure 10a. Number at the right in each layer is the layer velocity and to the left is the layer thickness. There is no basis for estimating thickness of shallow layering in the east model. Abbreviations are: DM - Davis Mountains, SV - Sierra Vieja Mountains, and VF - Valentine Fault zone (see Seismicity section). Asterisk indicates average focal depth of local events with respect to the 6.11 km/sec layer. Refracted ray paths are indicated by small arrows, inverted triangle is a seismic station in the mountainous area.

Figure 10b

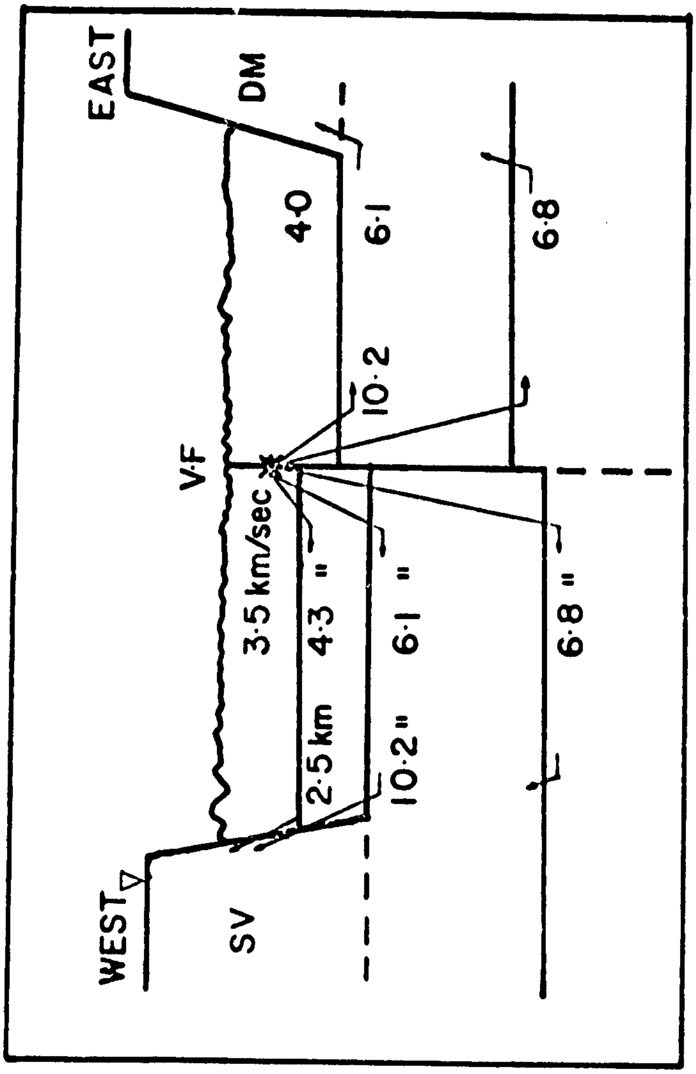

than the western side. Depth to each layer in Figure 10b is not given because the exact depth of the events are not known. However, layer thicknesses between refracting horizons are given along with velocities. Shurbet and Reeves (1977) estimated from gravity measurements that the sedimentary material in the Marfa Basin is at least 2.4 km thick.

In any case, we can obtain only limited information about such thin shallow layers using a large netweok and epicenters which are few and widely scattered. Thus, local earthquake data do not add sufficient information to refind the model of Figure 8a obtained from the VHB.

Travel-time data from the Gnome underground nuclear explosion (Romney et al., 1962) and well located natural events (GNE) recorded by many stations in the Great Plains and by two stations in the B&R, represent a regional travel-time curve (Figure 11) for west Texas. Interpreting these unreverse refraction data, we obtained a crustal model (Figure 8b) consisting of three layers totalling about 42 km, overlying an 8.13 km/sec mantle.

The B&R model in Figure 8a differs from the model derived by Chan (1977) (Figure 8c) from the Gnome underground nuclear explosion and local earthquakes (not located by the USGS). Chan's (1977) model consists of a layer 9 km thick with a velocity of 4.9 km/sec, overlying a 6.7 km/sec layer. The 6.0 km/sec layer was undetected by Chan, probably because of the smaller amount of data available to him. If he had been able to detect the 6.0 km/sec layer, then the calculated depth to his 6.7 km/sec layer would have been greater than shown in Figure 8c. Thus, the upper crust may be nearly the same in all models in Figure 8. This represents an almost uniform crustal

Figure 11: Travel-times for Gnome and natural events across west Texas. The Gnome data were recorded at temporary stations in west Texas (Romney et al. 1962) and the natural events were recorded at stations in the Kermit array (Keller, personal communications) and at the UT/NASA array. The travel-times indicate a three layer crust overlying a 8.13 km/sec half-space.

Figure 11

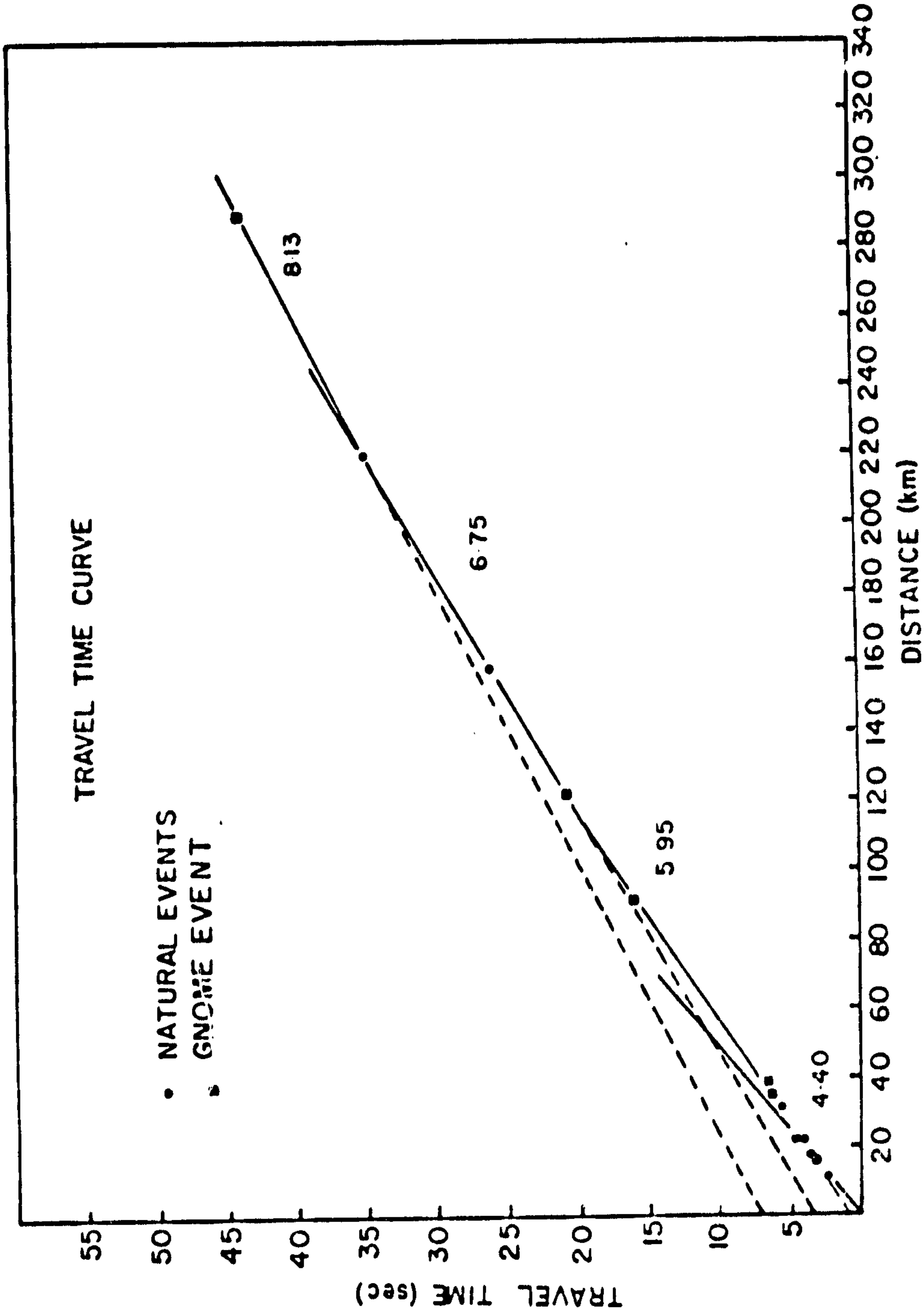
TRAVEL TIME CURVE
• NATURAL EVENTS
▪ GNOME EVENT
8.13
6.75
5.95
4.40
DISTANCE (km)
TRAVEL TIME (sec)
20 40 60 80 100 120 140 160 180 200 220 240 260 280 300 320 340
5 10 15 20 25 30 35 40 45 50 55

structure throughout T-PT.

Comparing the models shown in Figure 8, we find a 6.6 or 6.7 km/sec layer common to all models and a 6.0 km/sec layer common to three models. The west Texas models contrast notably with Stewart and Pakiser's New Mexico model by the absence of the 7.1 km/sec layer in the west Texas models. The addition of a 7.1 km/sec layer, which was unidentified in west Texas possibly because of sparse data would make those models nearly the same as the New Mexico model. On the other hand, west Texas models, as shown without the 7.1 km/sec layer in Figure 8 have shallower mantles than the New Mexico model. This alone could account for the differences in mantle depths between west Texas and New Mexico models.

SEISMICITY

Seismicity is low, yet detectable in the B&R and the northeastern part of Chihuahua, Mexico. Approximately 800 earthquakes with S-P intervals of less than 30 sec were detected and 10% of these were located. Hypocenter locations were obtained from P and S-wave arrivals, using the computer program HYPO 71 (Lee and Lahr, 1975) and the crustal model described in the previous section (Figure 8a). S-wave velocities were computed using a Poisson's ratio of 0.25. Station corrections (Table 2) were obtained by subtracting the theoretical arrival times of the large explosion (mentioned in the previous section) from the observed arrival times.

Whenever possible, arrival times from Carlsbad, New Mexico and/or the Kermit, Texas, network were also used in epicentral locations. Figure 12 shows that earthquakes in the B&R within 120 km of MOT and with magnitudes greater than 1.5 were within the locating capability of the UT/NASA network. Seismicity is best documented either inside or near the network in: 1) The area west to southwest of Van Horn; 2) The Marfa Basin (particular the eastern

Figure 12: Local magnitude vs. distance from MOT for small located events. Earthquakes with magnitudes of 1.5 could be located at least 120 km from MOT. The smallest event located by the network has a magnitude of 0.7.

Figure 12

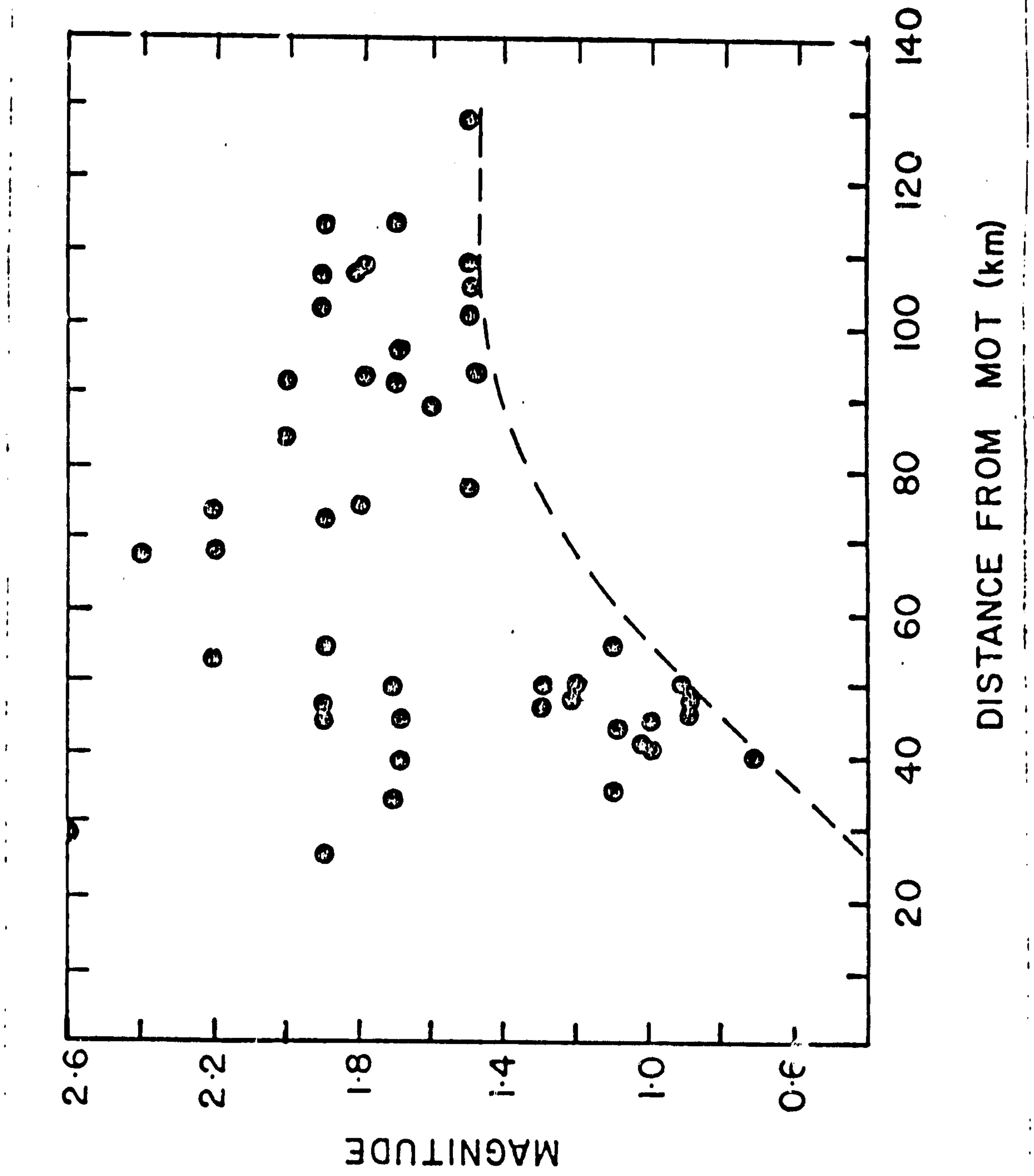
MAGNITUDE
2.6
2.2
1.8
1.4
1.0
0.6
DISTANCE FROM MOT (km)
20
40
60
80
100
120
140

Figure 13: Seismicity map of the B&R and the adjacent area of Mexico. The stations are indicated by triangles (▲). Crosses (+), solid squares (■), and open circles (◯) indicate epicenters located by this array, the USGS, and the ISC, respectively. Abbreviations for structural features are: BG - Black Gap, DM - Davis Mountains, DP - Diablo Plateau, MB - Marfa Basin, RR - Rim Rock Fault, SBG- Salt Basin Graben, SPP - Sierra Pilares and Pinosa Ranges, and WM - Wylie Mountains. The broken line marks Muehlberger's (1979) proposed eastern boundary of B&R faulting. Multiple earthquakes at the same epicenter are indicated by (M). The town of Valentine (V) is indicated by the small open square (□).

Figure 13

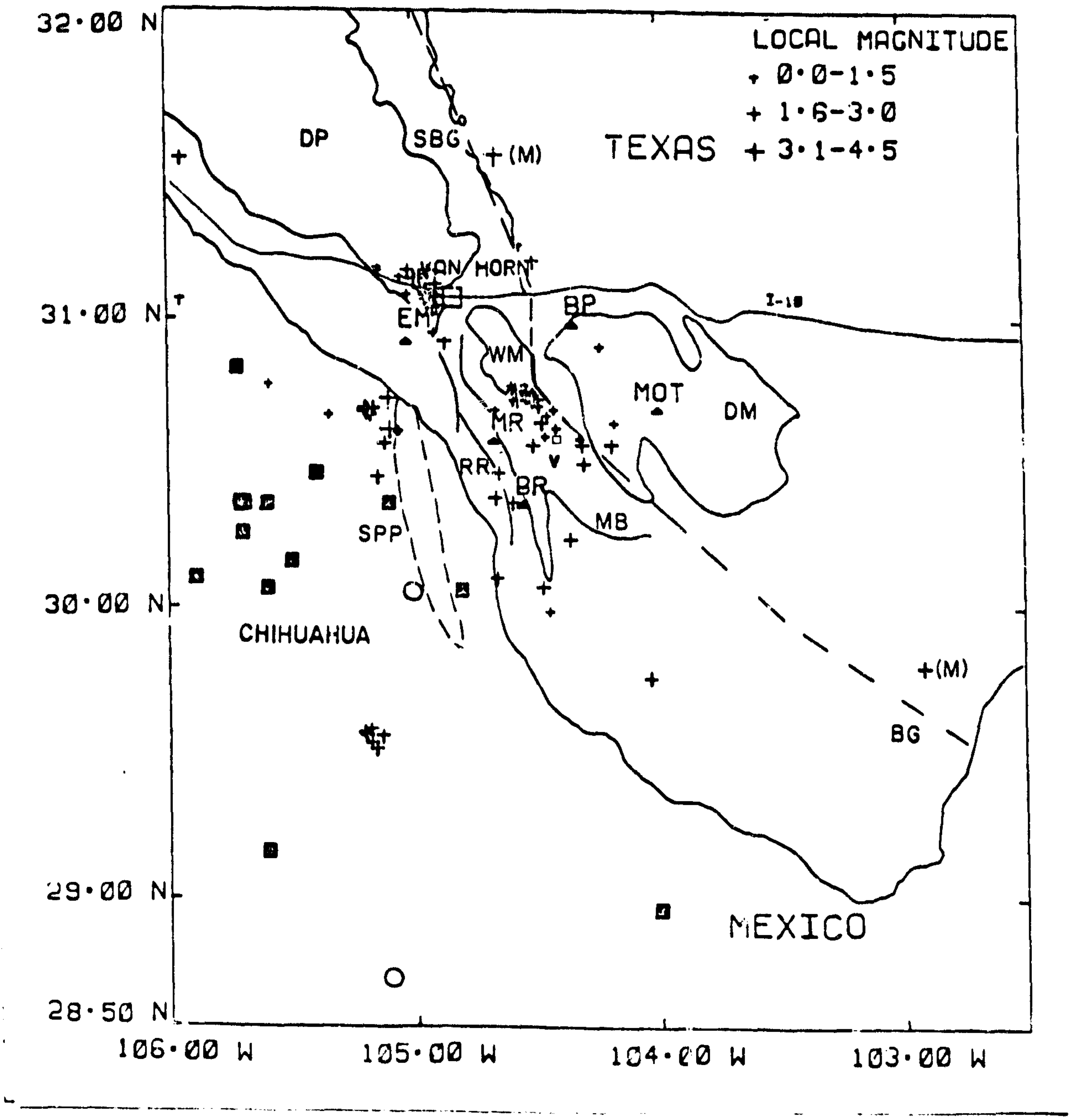
LOCAL MAGNITUDE
0·0-1·5
1·6-3·0
3·1-4·5
TEXAS
MEXICO
CHIHUAHUA
DP
SBG
(M)
VAN HORN
I-10
EM
BP
WM
MOT
DM
MR
RR
BR
MB
SPP
BG
32·00 N
31·00 N
30·00 N
29·00 N
28·50 N
106·00 W
105·00 W
104·00 W
103·00 W

side; and 3) The Texas-Mexico Border area. A few earthquakes have also been located in the Salt Basin Graben (SBG) and in the area north of the Black Gap.

Seismicity of Van Horn Area

The first instrumentally located earthquake (m_b = 3.5) in the Van Horn area occurred on March 6, 1962 at 31.2°N and 104.8°W (Sanford and Toppazada, 1974). Frequent quarry blasts west of Van Horn can be confused with natural seismicity. The quarries are located in an area characterized by numerous thrust, normal, and strike slip faults striking in a northwesterly direction (King, 1935). Since the dates and times of the blasts could not be obtained, all located events (natural and artifical) have been plotted in Figure   It is known that most of the blasts occur between 2130 and 2400 UT (1630-1900 local time). While the number of natural events is uncertain, events that occur outside of the 2130 to 2400 UT time interval are believed to be earthquakes. Whether these events were triggered by mining operations is still undetermined.

Southwest of Van Horn and east of station EM, a few events have been identified as earthquakes. These events may indicate an active northern branch of the Rim Rock Fault, which is locally the western boundary of the Marfa Basin.

Seismicity in the Marfa Basin

The area north of Valentine, Texas (Figure 13), has the greatest known seismic activity in the B&R. Here seismic activity is concentrated at the end of a northwesterly striking diffuse zone (Figure 13). This zone is thought to be an active fault or faults and is referred to as the Valentine Fault zone. Surface faulting has not been found; however, it is likely that the thick alluvium in the Marfa Basin covers the fault scarp. The revised epicenter of the 1931 Texas earthquake is located at 30.69°N and 104.57°W, at the northern end of this diffuse zone (Dumas et al., 1980).

One of the largest earthquakes in our list occurred on July 18, 1978 in the Valentine Fault zone. This earthquake was preceded by 18 foreshocks with magnitudes (m_ℓ) between 0.7 and 2.1. The 'b' (LS) value of 0.65 ±.48 for the frequency-magnitude curve (Figure 14) is less than the b value for the regional seismicity (equation 4). Foreshock activity began on July 13, 1978 with a 1.7 (m_ℓ) event and culminated on July 18, 1978 with the 2.6 (m_ℓ) main shock (Figures 15a and 15b), following which no aftershocks were detected. Though this sequence was recorded only on the 1 mm/sec helicorder at station MOT, epicenters for these events were estimated to be at or near 30.5°N and 104.5°W by comparing seismograms and S-P times for these events to those of located events in the Marfa Basin. This places the sequence along the newly found Valentine Fault zone. The first motion at MOT for each event in this sequence was compressional.

The July 18, 1978 sequence was one of three ($m_\ell > 2.5$) that occurred in the Marfa Basin. Figures 16A, B, and C illustrate the time history of these foreshock sequences. Evison (1977) described sequences terminating in large earthquakes ($m_b > 4.9$) which follow a pattern similar to those of the Marfa Basin sequences. He identified four successive stages of: a) normal seismicity; b) precursor swarm: c) precursor gap; and d) main event, which are illustrated in Figure 16. Sekiya (1977) and Kodama and Bufe (1979) described a similar pattern for earthquakes in Japan ($m_b > 4.1$) and Central California ($3.5 < m_b < 5.7$), respectively. Aggarwal et al. (1975) noted variations in V_p/V_s ratios preceding a 2.5 (m_b) event at Blue Mountain Lake in New York. However, they made no mention of the temporal variations in foreshock activity preceding the main shock. To the author's knowledge this is

Figure 14: a) Frequency-magnitude curve for the July 18, 1978 Marfa Basin sequence (Δ). The least-squares estimate of the 'b' value is 0.65 for magnitudes greater than 1.0. b) Frequency-magnitude curve for the February 18, 1978 Texas-Mexico sequence (●). The least-squares estimate of the 'b' value is 0.59.

Figure 15: a) Helicorder record from station MOT showing 5 foreshocks of the July 18, 1978 Marfa Basin Sequence which occurred 5 days before the main shock. b) Helicorder record of the magnitude 2.6 main event (*). Solid arrows point to fore-shocks and open arrows to time marks.

Figure 14

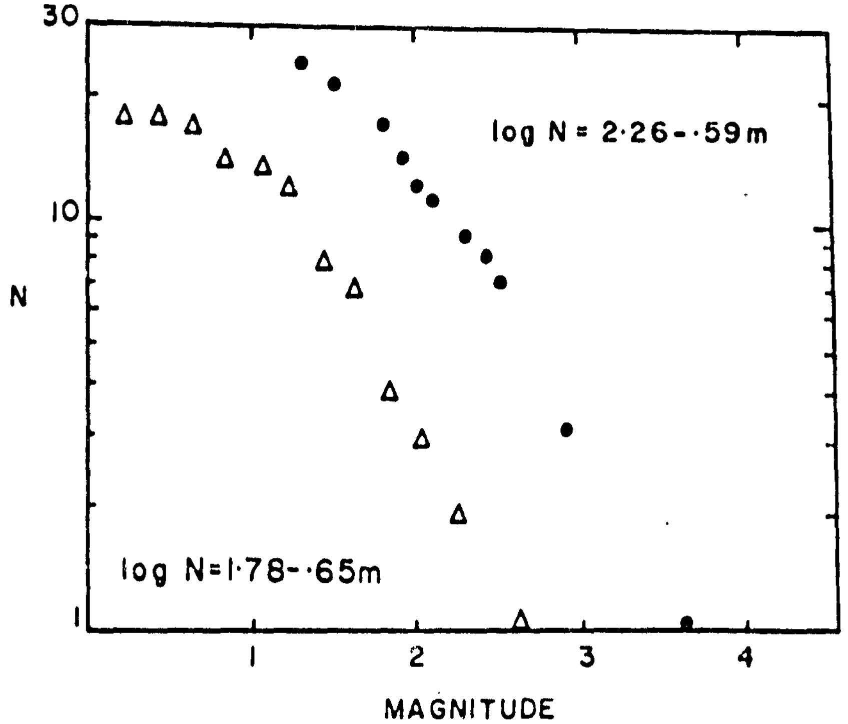

Figure 15

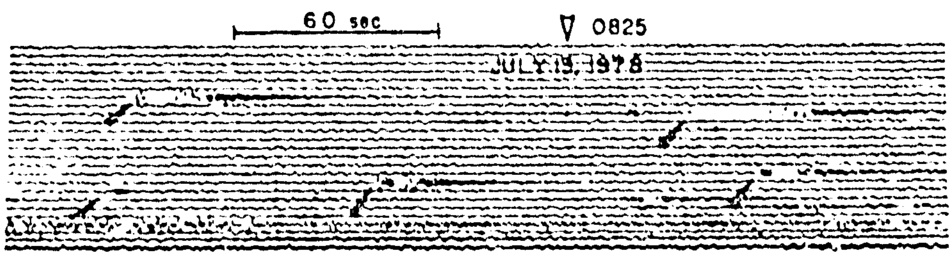

(a)

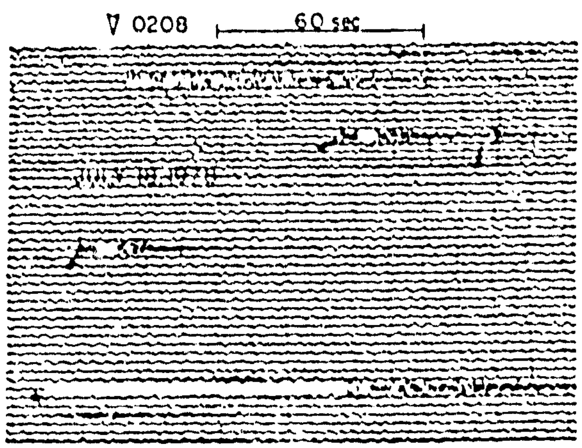

(b)

Figure 16: Temporal variation in seismicity preceding the main shocks (▽) of four sequences. Each sequence is characterized by: a) normal background seismicity; b) precursory swarm; c) precursor gap; and d) main shock. Sequences A, B, and C occurred in the Marfa Basin and D is the Chihuahua 1980 sequence.

Figure 16

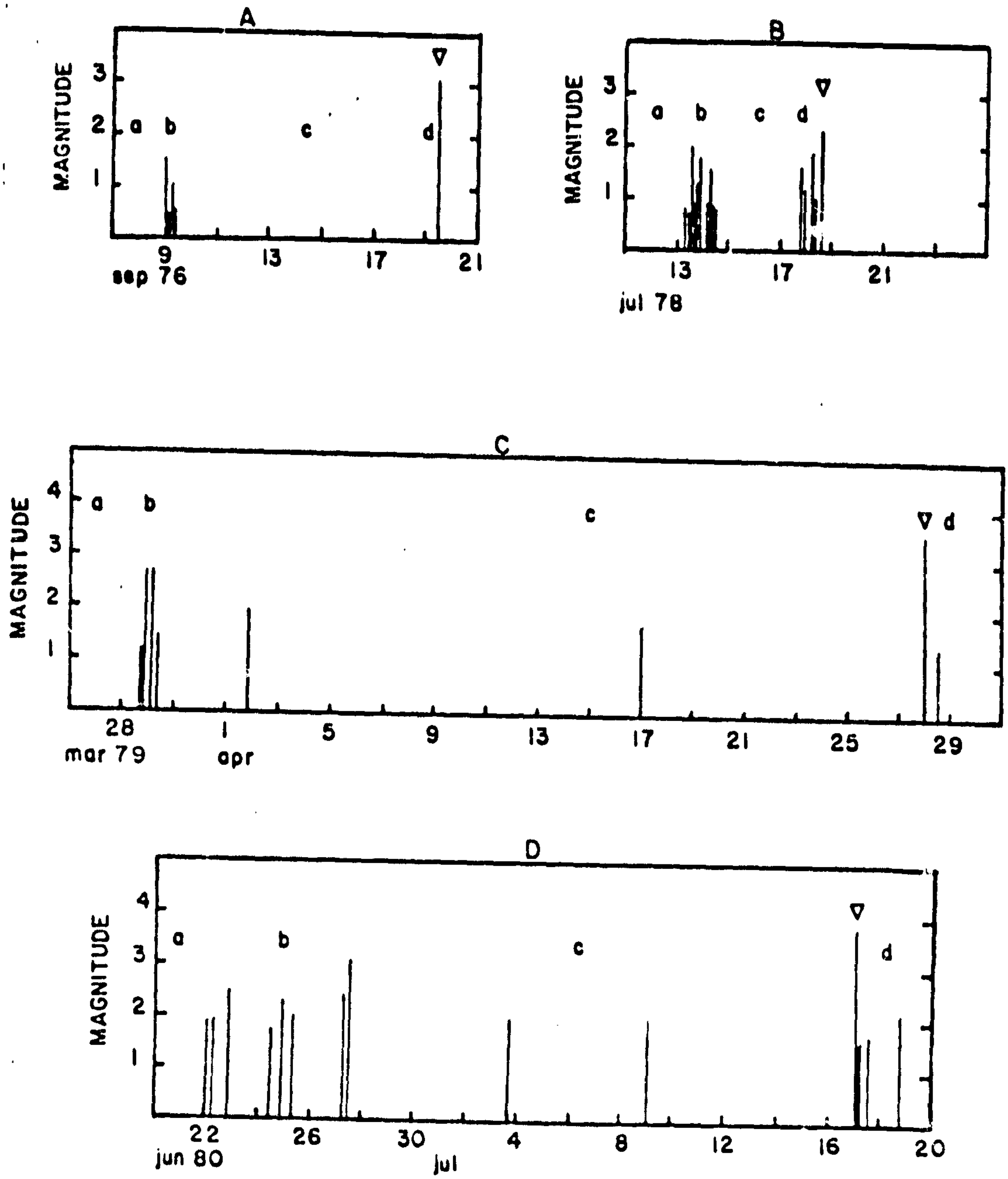
A
MAGNITUDE
3
2
1
a
b
c
d
9
13
17
21
sep 76
B
MAGNITUDE
3
2
1
a
b
c
d
13
17
21
jul 78
C
MAGNITUDE
4
3
2
1
a
b
c
d
28
mar 79
1
apr
5
9
13
17
21
25
29
D
MAGNITUDE
4
3
2
1
a
b
c
d
22
jun 80
26
30
jul
4
8
12
16
20

the first report of temporal variations in foreshock activity preceeding small shocks ($m_{\ell} < 3.7$). The low-level of background seismicity in the B&R makes small sequences more conspicuous than in more active areas where they may be masked by the higher background seismicity.

If we assume that earthquakes are completely independent from each other then the probability that r earthquake(s) will occur in time T is given by a Poisson's distribution (Sacuiu and Zorilescu, 1970)

$$P(r,T) = \frac{(\bar{N}T)^r e^{-\bar{N}T}}{r!}$$

where $\bar{N}$ is the mean number of earthquakes per unit time. A property of the Poisson process is that the expected number of earthquakes in the time interval T is $\bar{N}T$. The mean number of earthquakes at MOT (S-P<8.5) is 2.42 events/ 30 days. The minimum number of events in Figure 16 (part b) for a 3 day interval is 4 events. The expected number of events for a 3 day interval is .242 and the probability of a swarm of this size occurring within a radius of S-P<8.5 sec of MOT is 1.12×10^{-4}. The probability of all events having the same epicenters is even lower. This suggests that based on a Poisson's distribution the events in Figure 16 are not spatially and temporally independent.

Evison (1977) also found a linear relationship between the magnitudes of the largest foreshock and the main event. In this study, no correlation was found between the magnitudes of the largest foreshock and main event. This is not unique for the small shocks observed here; Papozachos (1975) also found that for Greek earthquakes the magnitude of the main shock ($m_b > 4.7$) to be independent of the largest foreshock for events. It thus appears that the relationship between magnitudes of foreshocks and main shock is dependent on the locale. There were however, six other events occurring in the Marfa Basin with local magnitudes greater than 2.5m_ℓ that were not preceded by foreshock activity. Therefore, in terms of prediciting the size of an earthquake for the B&R, the magnitude of the largest foreshock in the swarm (if a swarm does occur) will give no indication of the size of the main shock.

The seismicity on the western side of the Marfa Basin is lower than on the eastern side. Five events located south of station MR and BR are probably associated with the southern section of Rim Rock fault system (Figure 13).

Four events larger than 1.5 were located along the eastern boundary of the Salt Basin Graben (Figure 13). Figure 12 indicate that small events (<1.5m_ℓ) on the western side of the SBG are below the location capabilities of the network. By comparing the total number of recorded earthquakes to the total number of located earthquakes, it is estimated that the number of earthquakes occurring in the SBG is 1.0 to 1.5 orders of magnitude higher than Figure 13 indicates.

Approximately 10 earthquakes with S-P times between 1 and 3 sec, and magnitudes less than 0.3 were detected only at station BR. These events are located between 8 and 25 km from station BR and may be associated with the Rim Rock fault system. Numerous small events with S-P times less than 2.5 sec (epicentral distance less than 20 km) were also detected at stations MOT and EM; however, because of the numerous faults in the Davis and Eagle Mountains, these events cannot be assigned to a particular fault.

Seismcity along the Texas-Mexico Border

The epicenters located in the study and plotted in Figure 13 for this area are accurate within 8 km, even though they lie outside the array. Most of them fall on a north-south line coinciding with the Sierra Pilares and Pinosa Ranges. Pre-1975 events located by the U.S.G.S. appear to form a trend striking in a northeasterly direction, approximately prependicular to the local structural trend. The locations of these pre-1975 events (Figure 13) may not be reliable, because of the sparse seismograph coverage in the area at the time.

One of the largest earthquakes ($3.6m_\ell$) located instrumentally by the UT/NASA array occurred on February 18, 1978 approximately 50 km SSW of Van Horn, Texas and was followed by 23 aftershocks (1.3 to 2.9 m_ℓ) within two days. The main event was located at 105.10°W, 30.67°N, origin time was $14^h22^m22.10^s$. A few WWSSN stations recorded weak emergent P phases of the main shock and therefore, the hypocenter obtained from these readings had very large solution errors. The inability of the WWSSN network to detect and locate small events in northern Mexico implies that this region may be more seismically active than previously observed. The 'b' (LS) value of 0.59 ± .36 for the frequency-magnitude curve of the aftershock sequence (Figure 14b) is less than that for the regional seismicity (Figure 7). The flatting of the curve at lower magnitudes indicates that many of the smaller events of the sequence may have gone undetected.

Close examination of Figure 17 shows that a foreshock preceded the main s ck by 12.5 sec. This is seen from the consistent time difference in the two P-arrivals (foreshock and main shock) at all stations, regardless of epicentral distance, which implies that phase 'a' (Figure 17) is associated with a different event and is not a later arrival of the same event. Figure 18 shows the close waveform similarities between seismograms for five events including the foreshock (*) at station EM. Similar seismograms are also found at the other recording stations as well. Figure 19 shows the ratios of S/P amplitudes are approximately constant for six events recorded at

Figure 17: Seismograms of the foreshock (P-arrival indicated by 'p') and the main shock (P-arrival indicated by 'a') for the February 18, 1978 Texas-Mexico sequence. The arrival times for all high speed playouts are delayed 40 sec.

Figure 17

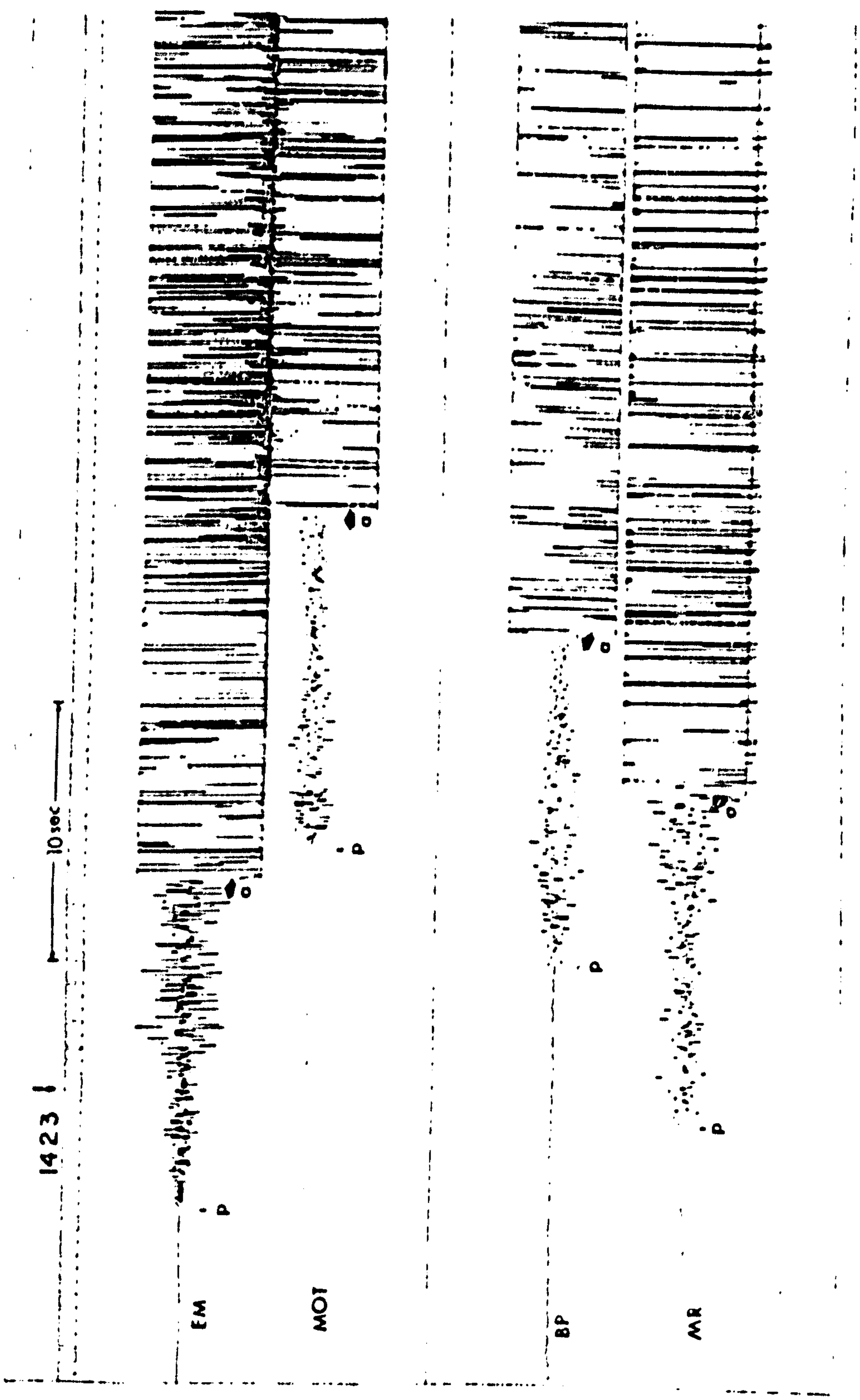

61

Figure 18: Seismograms of five events from the Texas-Mexico sequence recorded at station EM illustrating the close similarties in waveforms. The (*) indicates the one foreshock and the other seismograms are aftershocks.

Figure 18

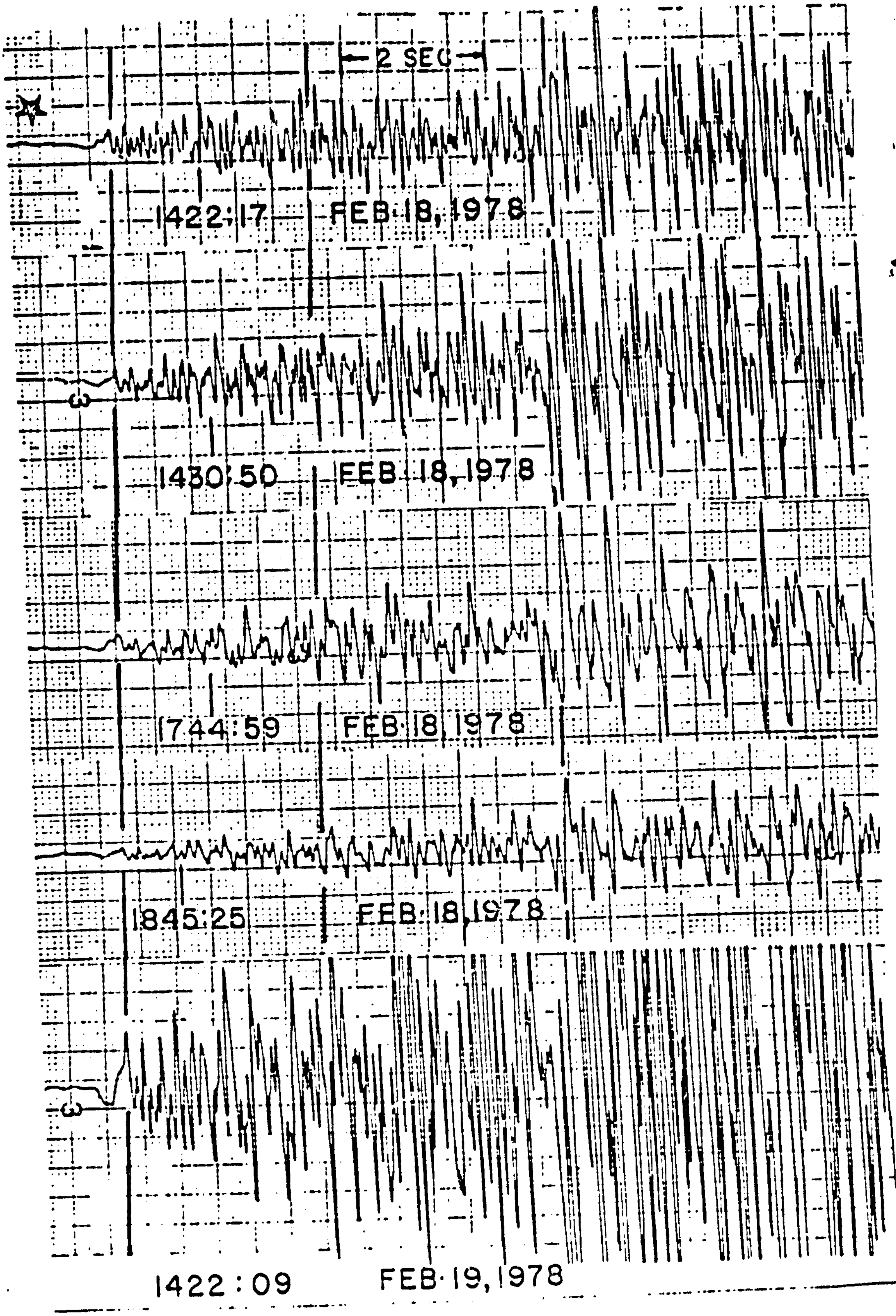
2 SEC
1422:17 FEB 18, 1978
1430:50 FEB 18, 1978
1744:59 FEB 18 1978
1845:25 FEB 18 1978
1422:09 FEB 19, 1978

Figure 19: Ratios of S-wave to P-wave amplitudes (S/P) versus the S-wave amplitudes at station EM for the Texas-Mexico 1978 sequence. The open circle represents the foreshock and the circles represent aftershocks. The S/P ratios remained constant for all events that did not exceed the dynamic range of the recorder.

Figure 19

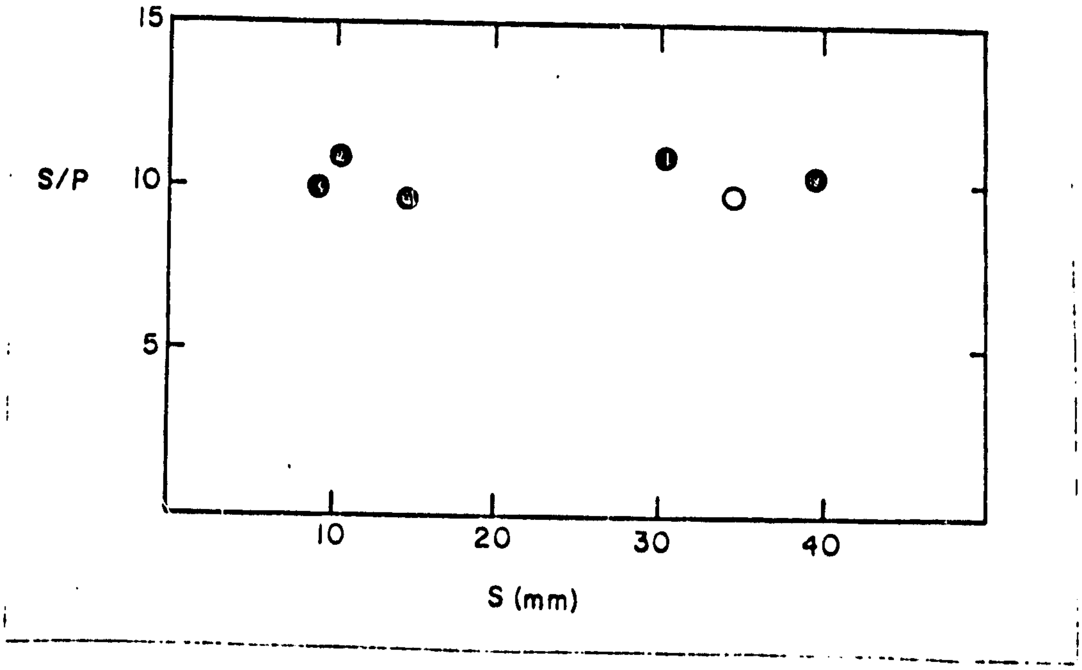

station EM that did not exceed the dynamic range of the recorder. Thus, all the data suggest that the same focal mechanism is responsible for all events and that their epicenters must lie within a fraction of a wave length of each other. Reexamining the MOT helicorder records for the month preceding the main shock revealed no other foreshocks.

Another Chihuahua sequence began on June 22, 1980. It was located approximately 100 km south of the above mentioned sequence and 103 km southwest of BR, along the southern section of the Sierra Pinoza Range. The main shock ($3.8m_\ell$) occurred on July 17, 1980 at 29.50°N and 105.18°W, and the origin time was $3^h41^m31.3^s$. Unlike the previous Mexican sequence this one contained 10 foreshocks and 4 aftershocks. The temporal variation in seismicity preceding the main shock is similar to that of the Marfa Basin sequences (Figure 16D). The 'b' values for the foreshocks and aftershocks are .51 ± .38 and 1.08 ± 1.7, respectively (Figure 20). The large uncertainity in the 'b' value for the aftershocks is attributed to the small amount of data available and not to the quality of the data itself which was quite good. The higher 'b' value for aftershocks relative to the foreshocks has been noted by Rikitake (1976). The S/P amplitude ratios for 6 foreshocks (Figure 21) that did not exceed the dynamic range of the recorder and with readable P-arrivals are approximately constant with one exception (P~19.3 mm). The latter suggests that the focal mechanism did not remain constant during the entire foreshock sequence.

Numerous Mexican events outside the area of Figure 13 were also recorded. The larger events had magnitudes between 3.0 and 3.5 (m_ℓ) with clear P and S-wave arrivals. Location errors for these events are large due to the poor station distribution. None of these Mexican events were located or detected by local or regional WWSSN stations. Smaller events inside the area of Figure 13 had emergent P and S arrivals and could not be located.

Figure 20: Frequency-magnitude curve for foreshocks (x) and aftershocks (0) for the June, 1980 Chihuahua sequence.

Figure 21: S/P amplitude ratios for the Chihuahua, Mexico 1980 sequence. With the exception of the P-wave data point near 19 mm, S/P ratios are almost constant.

Figure 20

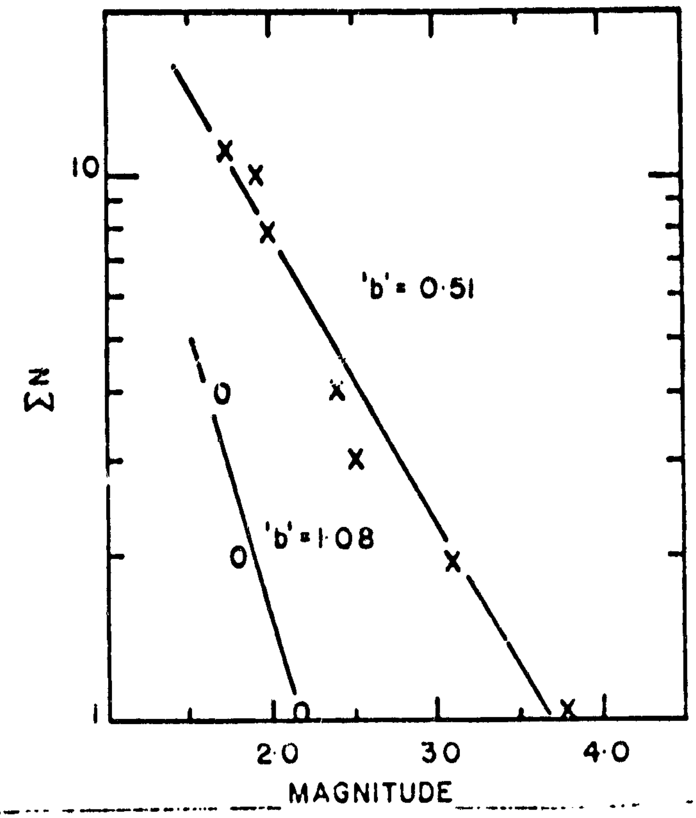

Figure 21

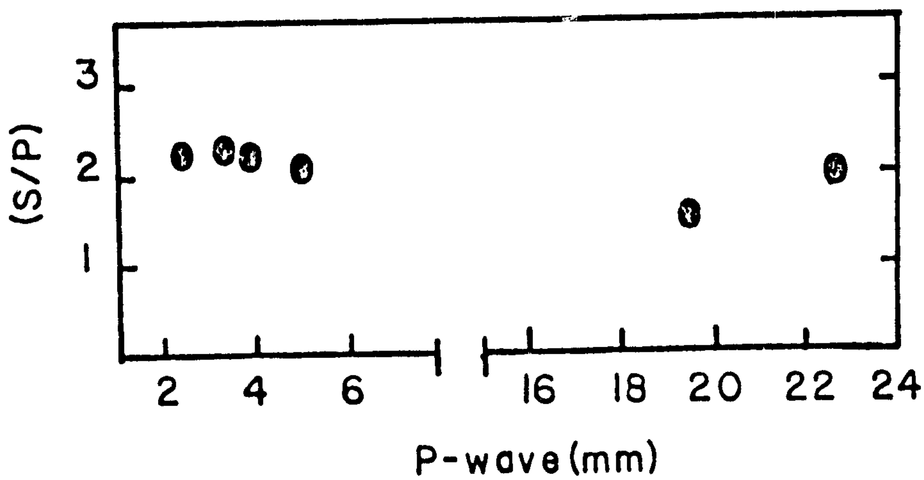

FOCAL MECHANISMS

Focal mechanisms were determined from fault-plane and composite fault-plane solutions (Figures 23, 24, and 25, Table 5) based on first motion data. Since the point at which the ray emerges from the focal sphere depends on the crustal model, inaccuracies of the model distort the fault-plane solution. Also, the quality of the fault-plane solution reflects the number and distribution of recording stations with respect to the hypocenter. The nodal plane selected as the fault-plane is the one that agrees with: 1) the strike of the local geology, and/or 2) the direction of the seismic trend. Because of the limited number of stations and the limited crustal information the solutions are only rough approximations of the focal mechanisms.

The Valentine Fault Zone

The composite first motion plot of impulsive first arrivals from 15 events located in the Valentine Fault Zone is shown in Figure 22. Attempts were made to plot the first arrivals by varying the hypocenter depths, since the uncertainity in hypocenter depths allows some flexibility in changing the angle at which the ray emerges from the focal sphere. Thus by increasing or decreasing the hypocenter depths, the data outside the inner cricle of points will move inwards or outwards on radii of the focal sphere projections, respectively. Varying detphs did not however, remove the inconsistences in Figure 22. The composite fault-plane solution for the Valentine Fault zone (Figure 23) was obtained subjectively by small adjustments of the nodal planes of the 1931 Texas earthquake on Figure 22 (See Part I) and by removing earthquakes for which the number of inconsistent points

Figure 22: Composite first motion plot of all events located on the Valentine Fault. See Figure 23 for explanation.

Figure 23: Fault-plane solution (equal-area, lower hemisphere projection) for the Valentine Fault zone. Closed cricles indicate compression and open circles indicate dilatation. The projection of the tensional and compressional axes are indicated by T and P, respectively. Dashed lines represent the 1931 fault-plane solution (Part I, Figure 3). The fault-plane is indicated by α. Hatched area indicates the range of uncertainity in the fault plane solution.

Figure 22

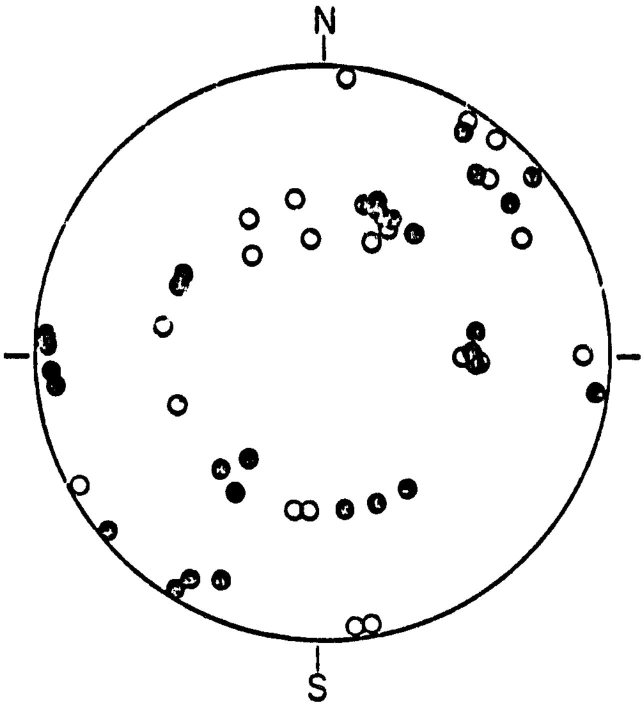

Figure 23

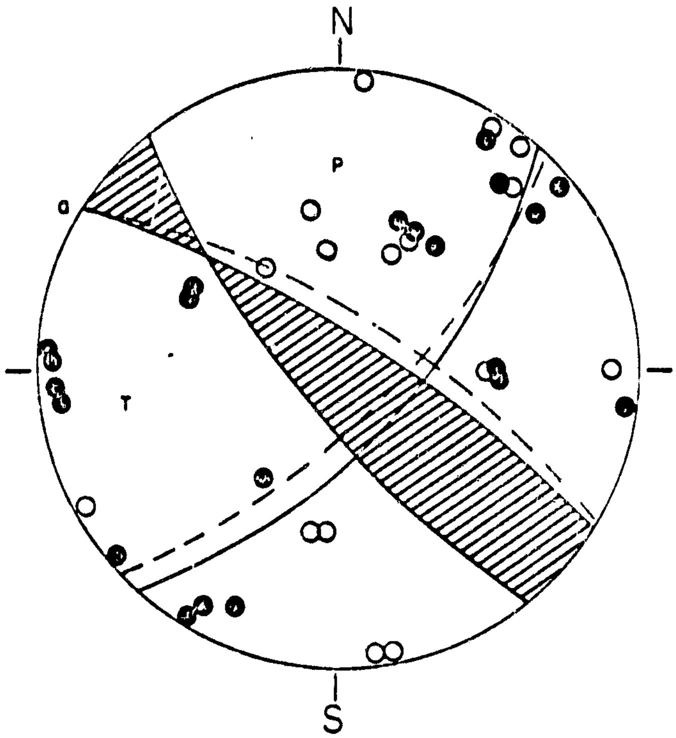

Table 5

Fault Plane Solutions

Figure	Location N. Lat.	W. Long.	Nodal Plane α Strike Dip	Nodal Plane β Strike Dip	P axis Strike Plunge	T axis Strike Plunge
23[a]	30.69°	104.57°	N 59°W 70°NE	N 36°E 70°SE	S 16°E 14°	S 74°W 14°
24[b]	30.67°	105.10°	N 45°E 30°NW	N 70°E 65°SE	N 05°E 67°	S 35°E 22°
25	30.40°	104.64°	N 10°W 45°W	N 03°E 45°E	N 05°W 80°	S 85°W 05°
23	~30.50°	~104.40°	N 57°W 75°SE	N 41°E 60°E	N 05°W 20°	S 80°W 20°

[a]Solution of the 1931 earthquake

[b]Either nodal plane can be selected as the fault plane.

exceeds the number of consistent points with respect to a final adjusted solution. By this criterion a population of 10 events remained to fit to a single solution. It appears several other orientations are needed to fit all the data for the 5 events removed. The nodal planes of the 1931 earthquake and of the composite solution, which includes inconsistent points, strike in northwesterly and northeasterly directions. The strike of two northwesterly planes of the composite solution is approximately equal to that of the 1931 fault plane. However, the 1931 fault plane dips towards the NE (Figure 3), whereas the dip of the composite solution nodal planes range between 75°NE to 75°SW. Considering the available data, any nodal plane in the hatched area of Figure 23 that strikes in the NW direction could be selected as the fault-plane. The differences in the two solutions are attributed to the uncertainities in the crustal model used in this study.

Texas-Mexico Border Area

A composite first motion plot (Figure 24) combines data from four pre-1975 earthquakes located in the northeasterly striking zone that was mentioned in the seismicity section and the main shock of the February 18, 1978, sequence. Stations BP and MR had impulsive dilatational and compressional arrivals respectively, whereas MOT and EM had emergent compressional arrivals. The strike of the left hand nodal plane ranged between N 12°E and N 64°E with dips of 40°NW and 20°NW, respectively. The southeastward dipping nodal plane is poorly constrained by compressional and dilatational points in the eastern part of the projection and was drawn to coincide with the southwesterly line of earthquakes which provided the first motion data. Although numerous nodal planes are possible, especially

73

Figure 24: Composite fault-plane solution for the February 18, 1978 sequence and four events located in northern Mexico by the USGS (Earthquake File Tape). The first-motion data for the four pre-1975 events are from Tucson, Albuquerque, and Junction (USGS, micro-film library). See Figure 23 for explanation.

Figure 25: First motion plot of the event of June 3, 1978 that occurred on the Rim Rock Fault. See Figure 23 for explanation.

Figure 24

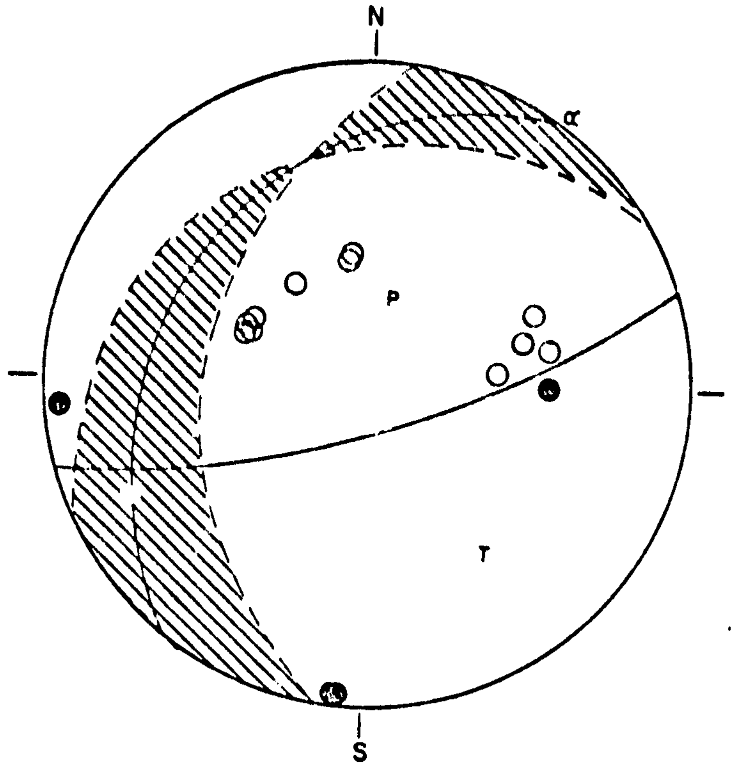

Figure 25

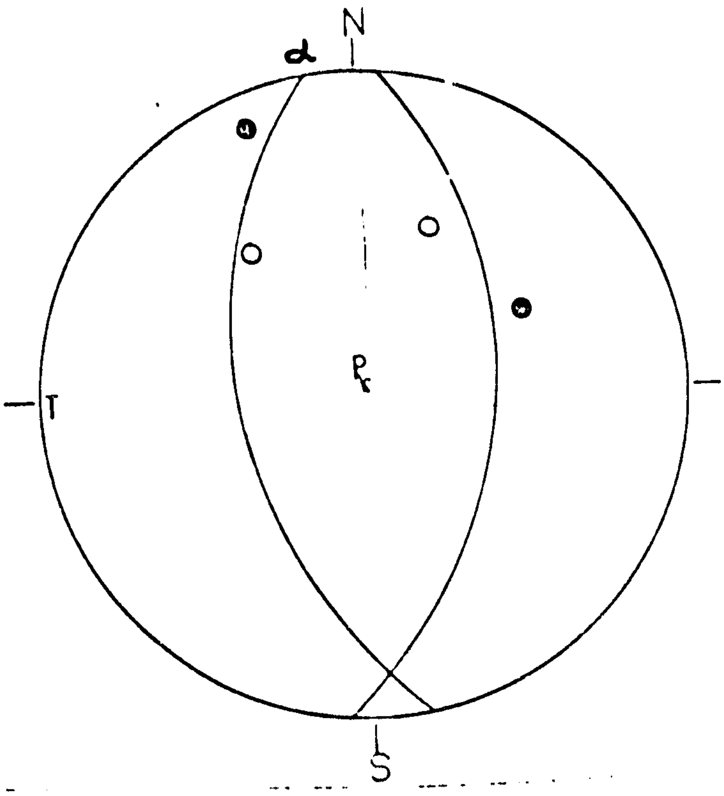

nodal planes dipping towards the NW (hatched area indicates the range of acceptable solutions), the solid lines represent the most favorable solution. Regardless of the nodal plane chosen as the fault-plane, Figure 24 indicates northeasterly striking normal faulting. The fault-plane solution implies, at least locally, extension in a NW-SE direction. Except for the February 18, 1978 event, which lies at the intersection of two trends, none of the earthquakes located on the north-south line had clear impulsive first arrivals needed to obtain a fault-plane solution.

The Rim Rock Fault

Only one event located on the Rim Rock fault had sufficiently large P-wave amplitudes to determine a fault-plane solution (Figure 25). Although the solution is poorly constrained, it is consistent with the local geology. Figure 25 indicates a normal fault striking N 10°W and dipping 45°W and the tension axis is oriented S 85°W. Except for the Texas-Mexico solution, the other three solutions indicate the tension axes are oriented in a SW-NE direction.

TECTONICS

Fault-plane solutions of Figures 23, 24, and 25 (Table 5) indicate that strike-slip faulting and normal faulting are occurring in the eastern and western sides of the Marfa Basin, respectively. These solutions indicate that the B&R is undergoing extension in a west-southwest and east-northeast direction. In Chihuahua (Figure 26), the tension axis is oriented in a southeasterly-northwesterly direction. The strike of the tension axis in that area (Figure 26) is almost orthogonal to the strike of the tension axes for the previously mentioned solutions. Thus, it appears that all obtainable fault plane solutions represent tensional fracturing or crustal spreading, though the

Figure 26: Map of study area showing fault-plane solutions. Large arrow heads indicate the direction of the tension axes. The number by each solution corresponds to the figure numbered in Table 5. See Figure 13 for meaning of initials. Solid triangles indicate seismic stations.

Figure 26

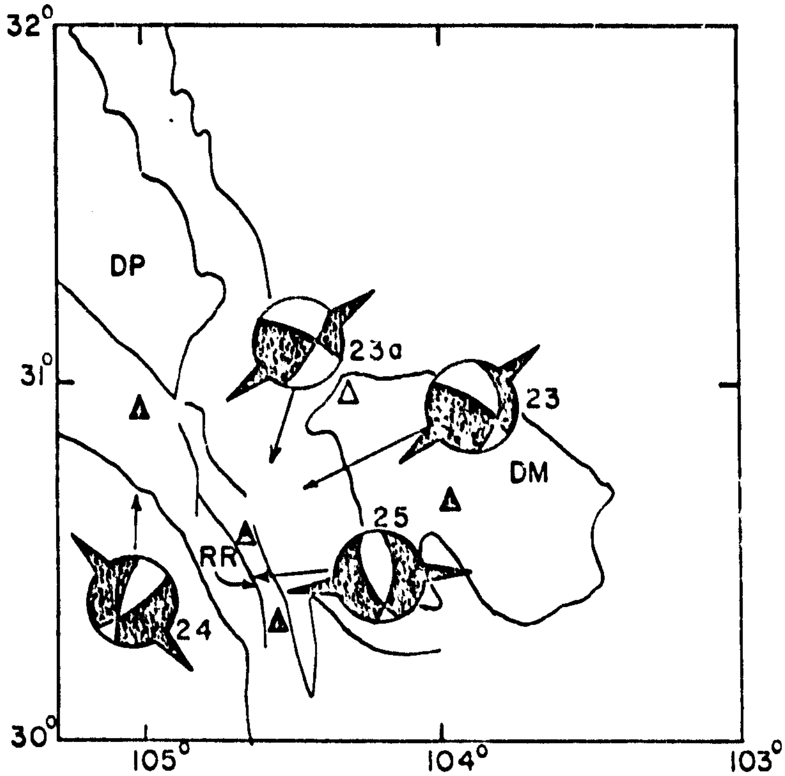

direction of the tension axes differ in different parts of the region.

DISCUSSION AND CONCLUSIONS

The seismicity map in Figure 13 indicates that earthquakes in the B&R of Texas and Chihuahua, Mexico, occur along linear trends. Some of these trends appear to be associated with previously mapped faults which have been thought to be inactive, while others cannot be correlated with any visible structural features. In this section each seismic trend will be discussed separately as it relates to the immediate area in which it occurred. The data are insufficient to support a statement concerning the overall relation between the trends. At this time each trend appears to be independent of the others.

The seismic patterns in northern Chihuahua are oriented in a north-south and northeast-southwest direction. The seismic events, located by the UT/NASA array in the Chihuahua Trough, appear to be associated with the Sierra Pilares and Pinosa Ranges. Gries and Haenggi (1970), suggested that the tilting of the evaporites to the east during the time of Laramide deformation produced the thrust faults in the Chihuahua Trough. They also suggested that tilting was caused by broad arching from the center of the Chihuahua Trough and perhaps some minor basement deformation.

Gries and Haenggi (1970), showed that most of the tear faults in the Chihuahua Trough extend to a depth of less than 3.0 km. Therefore, these earthquakes are probably shallower than 3.0 km. The seismic activity we observe today along the Sierra Pilares and Pinosa Ranges may reflect continuing arching or basement deformation.

Figure 27 is a regional seismicity map for eastern Arizona, New Mexico, west Texas and northern Mexico for the time interval between 1960 and 1978. The seismicity associated with the Rio Grande Rift system in New Mexico appears to terminate at the United States/Mexico border. Activity is again observed in the Chihuahua Trough approximately 200 km southeast of where the Rio Grande Rift seismicity terminates and this appears to be the most active area in northern Mexico outside the Gulf of California. Figure 27 indicates no discernable seismic patterns for events occurring in the region, furthermore the events cannot be correlated with any structural surface features in the area.

The seismicity data from Mexico reveal little about a possible extension of the Rio Grande Rift system in Chihuahua. Only through detailed geophysical investigations in Mexico will this problem be solved.

In discussing the structural and tectonic implications of the B&R we begin by examining the section north of Interstate 10. Seismicity in the northern section, as mentioned earlier, is observed on the eastern side of the SBG and the area west to southwest of Van Horn. We cannot report that the western side of the SBG north of Van Horn is inactive but that the network is incapable of locating any small events which may have occurred in the area. Because of the confusion about natural and artifical sources near Van Horn we could only speculate on possible tectonic implications of these events.

Repeated leveling traverses examined by Brown et al. (1978), indicate the Diablo Plateau (which forms the western boundary of the SBG) is presently undergoing uplifting at a constant rate of 5±1 mm/yr, relative to the surrounding areas. This seems tectonically compatible with the SBG seismic activity reported in this study.

The SBG has the morphology of an active rift. However, Decker and Smithson (1975) reported normal heat flow (1 HFU) in the graben. Therefore,

Figure 27: Regional seismicity map (redrawn from Stover, 1977) for a portion of the southwestern United States and northern Mexico between 1960 and 1978. Epicenter locations are from the U.S.G.S., I.S.C., Sanford and Toppozada, (1976), and events located during the study with magnitudes greater than 2.5 m_ℓ. The rectangle indicates the area enclosed by Figure 13.

Figure 27

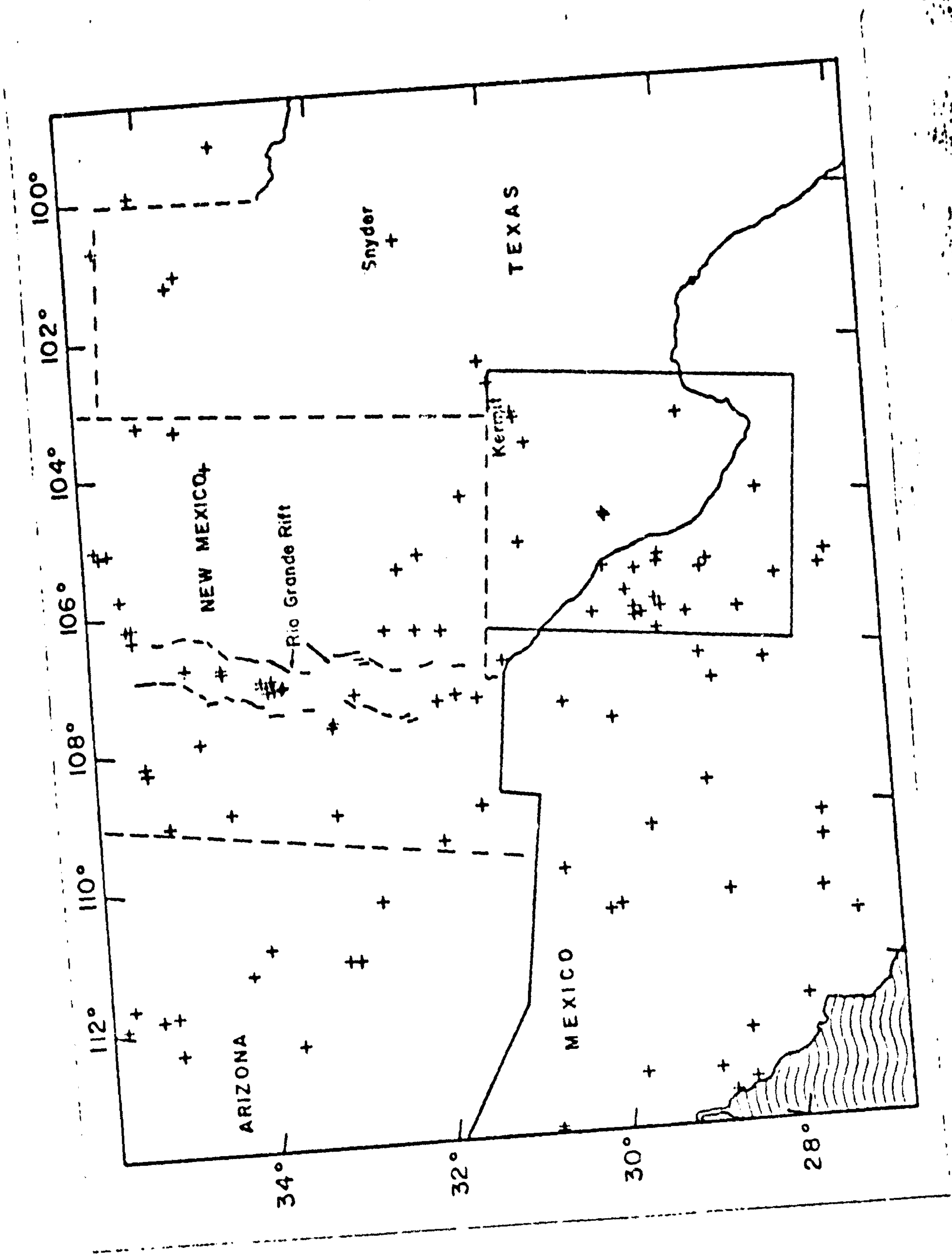
100°
102°
104°
106°
108°
110°
112°
34°
32°
30°
28°
TEXAS
Snyder
Kermit
NEW MEXICO
Rio Grande Rift
ARIZONA
MEXICO

a feature of rifts such as the Rio Grande and East African rifts is lacking in the SBG.

South of the SBG (south of Interstate 10), the seismicity along the eastern side of the graben terminates. Activity is again observed immediately south of the Wylie Mountains in the eastern side of the Marfa Basin along the Valentine Fault zone. The importance of this active zone derives from the revised epicenter of the 1931 earthquake which lies at its northwestern end. Also, the zone coincides closely with part of the proposed eastern boundary of B&R faulting (Muehlberger, 1978). Thus, this zone may be the site of future earthquakes similar to the 1931 event.

Muehlberger's (1978) proposed eastern limit of B&R faulting extends from the Black Gap area, northwest through the Marfa Basin, past Valentine where it turns northwards and forms the eastern boundary of the SBG (See broken line Figure 13). However, field evidence of surface breakage is not visible in the alluvium in this section of the Marfa Basin. The northwest trending portion of the fault zone corresponds to the fault-plane solutions in Figure 23.

Hae-Roe (1975) and Muehlberger et al., (1978) have mapped a fault striking approximately N 15°W, and dipping 72°E just east of the Wylie Mountains (East Wylie Fault). This fault may continue southward to join the Valentine Fault zone in the area of greatest seismic activity, just north of Valentine. This area also coincides with the locus of maximum seismic intensity for the 1931 earthquake.

Based on the pattern of Quaternary fault scarps, Muehlberger et al., (1978) suggest the B&R of west Texas is undergoing extension in a S 80°W direction. This is in agreement with the orientation of maximum extension from the seismic data in this study and by Dumas et al., (1980).

The new findings about the 1931 earthquake (Dumas et al., 1980) and the nature of active seismicity in the eastern side of the Marfa Basin suggest the possibility of forecasting/predicting an earthquake from short term precursor (foreshocks). In the 1931 earthquake sequence and in several small earthquake sequences reported above, the main shocks were preceded by foreshocks. We have an eyewitness report that foreshocks of the 1931 earthquake were felt just hours before the main shock. Thus it seems probable that imperceptiable foreshocks occurred for days, weeks, or even months before the main event. Contemporary reports do not provide a detailed history of foreshocks activity for the 1931 event, but data on temporal behavior of the Marfa Basin foreshocks sequences derived from Figure 16 may be combined with the precursory time data taken from Evison, (1977) and Ohtake et al., (1977) as in Figure 28. Here the precursor time measured from the start of the anomalous foreshock activity to the main event is plotted against the magnitude of the main shock. The anomalous foreshock period from Evison (1977) and Figure 16 begins with the precursor swarm (Figure 16, part b), whereas the anomalous foreshock period from Ohtake et al., (1977) begins with a decline in activity before the main shock. The data in Figure 28 are approximated by the line

$$\log T = 0.56M - 0.60 \qquad (8)$$

This investigation indicates the B&R is a very complex area. On a broad scale, the B&R consists of four crustal layers, having seismic velocities of 3.60, 4.93, 6.11 and 6.60 km/sec, overlying a possible 8.37 km/sec mantle velocity. Except for the uncertainity about the presence of a 7.1 km/sec layer in the B&R, we are unable to identify a gross difference in layering between the Great Plains and the B&R in west Texas. Thus, it appears that the B&R crust is simply an area of Great Plains crust disrupted by volcanism and young faults, some presently active. The data support

83

Figure 28: Time intervals between the beginning of anomalous foreshock activity and main events plotted against the main shocks magnitudes. Crosses and circles from Evison (1977) and Ohtake et al. (1977), respectively. Δ's are from Figure 16.

Figure 28

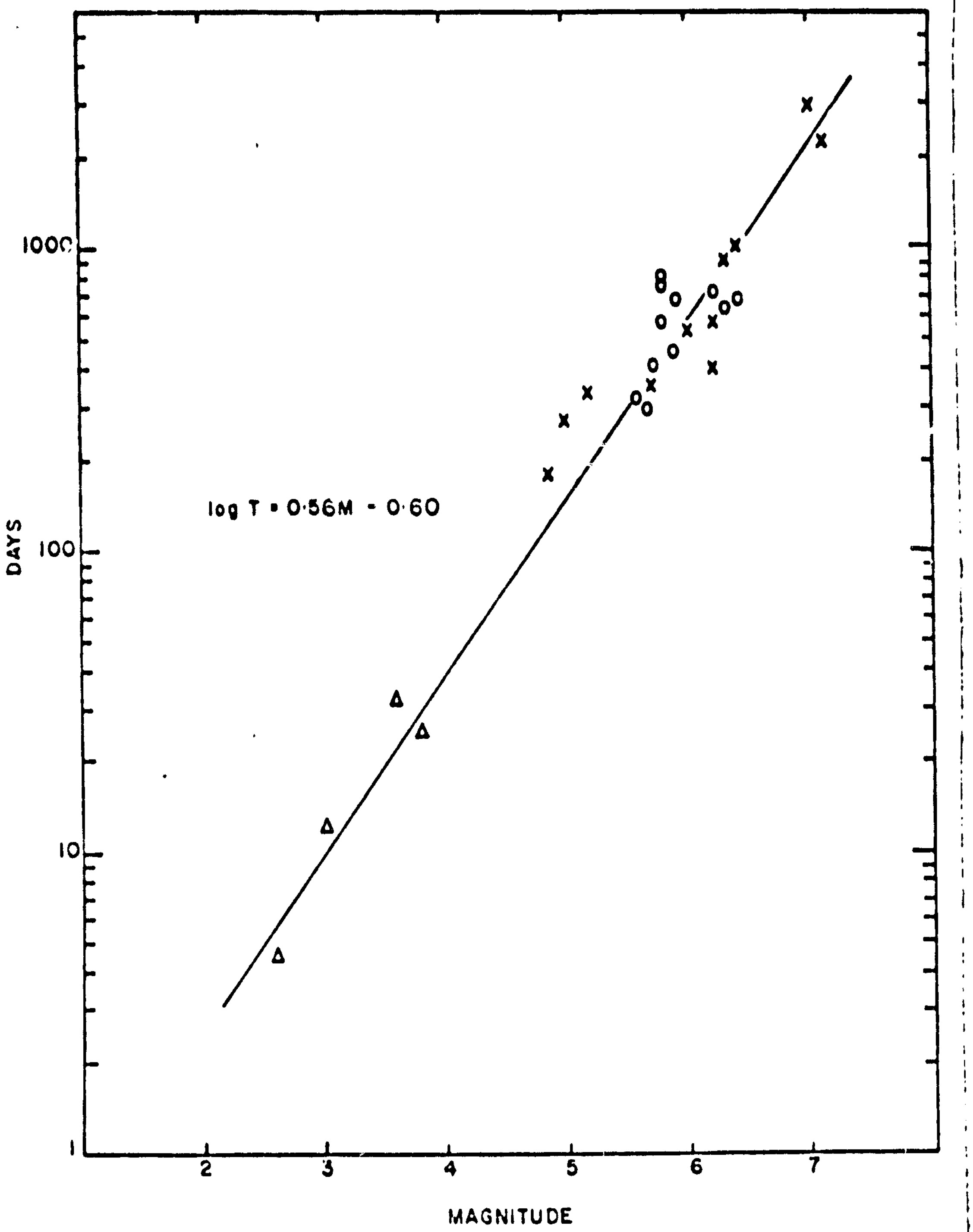

Muehlberger's (1978) proposed eastern boundary of Basin and Range faulting which coincides with an active fault zone in the eastern side of the Marfa Basin. The 1931 earthquake occurred along this zone and only a few of our localized epicenters are east of this line. It appears that this active trend consists of a possible spreading axis in the SBG which bends sharply into a right lateral transform fault along the active Valentine trend.

Appendix

Instrumental locations for earthquakes in the Basin and Range province of Texas and the adjacent area of Mexico. Locations were determined by the use of HYPO-71 (Lee and Lahr, 1975). The column headings are as follows:

Date - Year/month/day

Origin Time - This is universal time (UT) and is given to the nearest tenth of a second.

Lat N - Latitude (North) given to the nearest hundredth of a minute.

Long W - Longitude (West) given to the nearest hundredth of a minute.

Depth - Depth is given in km. (*) indicates depth is constrained to 4 km.

Mag - The magnitudes listed are local magnitudes determined from signal durations and are obtained from the following formula

$$m_\ell = 2 . \log \tau - 2.51$$

MOT, BP, EM, MR, and BR - These are the UT/NASA stations used in the location scheme. The numbers in the columns indicate the number of readings per station used to locate each event. One (1) indicates P-wave arrival only and two (2) indicate both P and S wave arrivals were used.

Dmin - Distance to nearest station in km.

Gap - Largest azimuthal separation in degrees between stations.

RMS - Root mean square error of time residuals in sec.

ERH - Estimated standard error of the epicenter in km. If ERH is blank this means ERH cannot be computed because of insufficient data.

ERZ - Estimated standard error of the focal depth. If ERZ is blank this means that ERZ cannot be computed because either the focal depth was fixed in the solution or because of insufficient data.

Q - Quality of the hypocenter solution. This measure is intended to indicate the general reliability of the solution (Lee and Lahr, 1975).

Comments - The three (3) letter codes indicate additional station(s) used in the epicenter locations.

DATE	ORIGIN TIME	LAT N	LONG W	DEPTH	MAG	MOT	BP	EM	MP	BF	DMIN	GAP	RMS	ERH	ERZ	Q	COMMENTS
77/ 7/11	1219 37.6	30-59.90	104-53.00	4.00*	2.3	1	2	2	2	1	22	213	0.37	13.7	15.2	D	
77/ 7/11	2015 26.5	31- 4.22	105- 0.64	3.64	1.3	2	1	2	1	1	20	265	0.73	14.9	12.9	D	
77/ 7/13	1514 24.1	31- 1.00	105- 1.00	20.45	1.5	2	2	1	0	0	14	254	0.22	7.0	5.3	D	
77/ 7/16	1747 31.3	29-44.74	105-33.78	1.44	1.9	2	2	2	1	2	112	321	0.51	14.2	9.7	D	
77/ 7/25	1217 17.8	31- 6.00	105- 1.02	4.00*	1.9	2	1	2	1	2	23	274	0.54	21.[illegible]	14.3	D	
77/ 7/29	2335 43.1	31- 0.27	104-54.55	4.00*	1.8	1	2	2	1	1	20	225	0.21	15.5	15.6	D	
77/ 7/30	1617 16.2	31- 1.00	104-54.60	2.00	1.5	2	2	2	1	1	21	239	1.28	70.3	72.5	D	
77/ 8/ 1	1644 51.1	30-55.00	104-55.29	4.00*	1.8	0	2	1	2	2	17	210	1.23	44.0	52.2	D	
77/ 8/ 3	1622 47.2	30-53.03	104-54.91	4.00*	1.6	2	2	2	1	1	15	167	1.57	26.2	41.5	D	
77/ 8/ 6	2043 53.7	31- 2.15	104-57.05	9.75	2.2	2	2	2	2	1	19	246	0.62	13.6	8.7	D	
77/ 8/ 7	1909 42.0	31- 4.58	105- 3.22	13.00	1.5	1	1	2	2	1	20	276	0.51	6.5	15.2	D	
77/ 8/ 9	1637 2.3	31- 2.52	104-39.12	4.00*	1.9	2	0	0	2	2	57	301	0.15	12.0	11.5	D	
77/ 8/21	391 0.2	30-33.07	105- 5.67	21.56	3.3	1	1	0	1	1	41	272	0.59	24.7	11.2	D	KTX,KT4,CLN
77/10/29	49 11.6	30-32.00	104-11.26	4.00*	1.9	2	2	2	2	2	27	155	0.77	8.6	9.8	D	
77/11/ 5	1229 53.7	31- 5.29	104-58.15	0.20	1.9	1	1	1	1	1	23	260	0.75			D	
78/ 1/21	117 2.4	31-32.26	104-39.15	2.46	3.2	1	1	1	0	0	69	150	0.23			C	CLN
78/ 1/24	1406 22.4	30-41.06	104-35.14	14.98	1.9	2	2	2	2	0	19	115	0.63	4.0	15.1	C	
78/ 2/ 5	1419 55.0	31-32.41	104-39.15		2.7												MOT,BP,CLN
78/ 2/15	1433 0.2	30-37.15	105-11.66	2.00	2.0	1	1	2	2	0	33	279	0.32	3.4	3.0	D	
78/ 2/18	1400 22.1	30-39.43	105- 6.00	1.12	3.6	1	1	1	1	0	27	255	0.24			C	
78/ 2/18	1429 22.3	30-37.35	105- 9.72	2.52	2.5	2	2	2	2	0	32	272	0.26	3.0	1.4	D	
78/ 2/18	1529 37.0	30-36.00	105-10.02	2.00	1.5	1	1	2	2	0	35	277	0.37	6.7	5.5	D	
78/ 2/19	1544 4.7	30-36.35	105-11.46	2.00	1.0	1	1	2	2	0	33	278	0.32	5.6	4.5	D	
78/ 2/15	1730 6.5	30-36.84	105-11.49	0.42	2.9	2	2	2	2	0	33	278	0.31	3.2	1.6	D	
78/ 2/16	1754 9.8	30-36.74	105-11.45	0.32	2.3	2	2	2	2	0	34	278	0.28	2.9	1.4	D	
78/ 2/16	1645 16.5	30-37.45	105-11.52	2.00	2.1	2	2	2	2	0	33	279	0.34	6.0	5.4	D	
78/ 2/19	725 18.7	30-36.69	105-11.00	2.00	1.9	2	1	2	2	0	33	277	0.32	10.2	0.9	D	
78/ 2/19	1212 0.2	30-36.65	105-11.69	0.69	2.5	2	2	2	2	0	34	273	0.35	3.6	1.7	D	
78/ 2/22	252 55.4	30-37.33	105-11.65	2.00	1.9	2	2	2	2	0	33	279	0.32	5.5	4.3	D	
78/ 3/20	14 12.6	30-26.00	104-16.00	2.00	1.7	2	1	0	2	0	37	241	0.45	0.2	0.1	D	
78/ 4/ 6	913 27.4	30-5. 58	104-51.75	4.00*	2.0	2	2	0	2	0	41	287	0.15	7.1	5.3	D	
78/ 4/12	2325 0.0	30-39.52	104-29.07	2.27	1.9	1	2	0	2	0	23	145	0.55	0.3	4.6	D	
78/ 5/30	1315 31.7	30-39.14	104-33.77	12.70	2.2	2	0	2	2	2	35	117	0.69	3.0		D	
78/ 6/ 3	1142 10.2	30-24.23	104-38.63	2.73	2.4	1	1	1	0	1	16	165	0.22	4.0	5.3	C	CLN
78/ 6/ 6	2225 2.1	30-10.00	104-35.00	16.94	2.2	1	1	1	0	1	3	153	1.02			D	
78/ 7/19		30-30.00	104-33.00		2.6	1											
78/ 8/29	2033 38.3	31- 1.81	104-56.74	9.26	1.7	1	2	2	1	1	19	249	0.38	11.7	7.4	D	
78/ 9/ 2	716 45.3	30-42.46	104-31.65	12.52	1.2	2	2	1	2	1	21	97	0.62	3.6	27.6	C	
78/ 9/29	1753 41.4	30-15.10	104-33.41	2.00	2.2	1	1	0	1	1	9	231	0.95			D	
78/12/20	131 21.9	30-37.97	104-28.69	6.35	1.0	2	2	0	2	0	22	155	0.52	6.8	6.6	D	
79/ 1/11	319 5.9	30-32.44	104-24.62	5.97	1.2	2	2	0	2	0	25	152	0.29	1.9	2.4	C	
79/ 1/15	36 35.8	30-35.81	105-21.04	6.26	1.5	2	2	2	2	1	42	282	0.31	9.6	11.3	D	
79/ 1/19	907 55.1	30-32.00	105- 7.14	2.40	1.8	2	1	1	2	2	43	249	0.29	3.2	1.6	D	
79/ 2/13	1522 13.4	30-12.29	104-21.47	1.02	1.6	2	2	0	2	0	50	292	0.61	7.4	7.2	D	
79/ 2/16	2352 32.5	31- 1.56	104-54.00	7.77	2.0	2	2	0	2	0	50	325	0.16	17.4	16.5	D	
79/ 3/17	1949 2.4	30-39.54	104-35.02	16.53	1.1	1	1	0	2	2	17	162	0.52	9.5	16.8	D	
79/ 3/24	1455 35.5	30-31.07	104-19.92	6.40	1.1	1	2	0	2	2	32	161	0.49	0.9	1.7	C	
79/ 3/[illegible]	551 35.4	29-41.64	104- 2.[illegible]	2.00	1.0	2	2	0	2	1	03	319	0.15	15.5	20.3	D	
79/ 3/28	1457 10.5	30-35.76	104-32.22	0.64	1.3	2	2	0	2	2	20	149	0.59	4.2	3.4	D	
79/ 3/29	935 42.9	29-35.47	102-55.85	4.00*	2.5	2	2	0	2	2	16[illegible]	336	0.54			D	KTX,KT4
79/ 3/29	1352 29.2	30-42.04	104-32.25	5.03	1.3	2	2	0	2	2	21	170	0.54	4.0	3.5	D	
79/ 6/ 9	129 55.1	30-39.12	104-30.14	9.30	1.5	2	2	1	0	2	21	149	0.36	3.6	2.8	C	

79/ 6/10	1847	45.5	30-32.00	104-10.28	4.00*	1.7	2	2	0	2	2	35	171	0.64	3.7	4.4	D
79/ 6/17	1736	30.3	30-42.48	104-31.71	11.31	1.7	2	2	0	2	2	31	159	0.13	1.2	36.4	D
79/ 6/21	1032	3.5	30-36.06	104-26.68	0.48	1.2	2	2	0	2	2	23	121	0.62	1.1		D
79/ 6/22	559	16.0	30-34.66	104-28.06	5.43	1.7	2	2	0	1	2	22	122	0.35	2.6	3.0	C
79/ 6/25	1723	36.8	30-34.41	104-10.54	7.18	1.1	2	2	0	2	2	20	175	0.43	6.6	6.9	D
79/ 6/28	337	9.4	31-11.41	104-33.10	20.67	1.5	2	2	0	0	2	33	316	0.27	1.5	1.7	C
79/ 6/28	1923	45.4	30-23.06	105- 6.64	2.00	1.9	1	1	0	2	1	56	307	0.25	2.4		D
79/ 7/10	2132	27.2	30-48.40	104-29.53	10.59	0.9	2	2	0	0	2	30	188	0.25	2.4		D
79/ 7/10	2145	15.8	30-42.48	104-31.52	11.99	0.5	2	2	0	0	2	20	203	0.65	1.8	32.5	D
79/ 7/10	2202	22.4	30-42.10	104-29.83	6.03	0.9	2	2	0	0	2	31	189	0.53	0.5	0.6	D
79/ 7/10	2229	15.8	30-41.02	104-30.13	9.33	0.5	2	2	0	0	2	29	192	0.45	0.8	1.3	D
79/ 7/24	327	56.0	30-37.37	104-25.16	2.35	0.7	2	2	0	6	2	34	163	0.95	0.5	15.2	D
79/ 8/ 4	2131	8.2	30-52.13	104-13.51	4.00*	1.0	2	2	0	2	2	10	184	1.07	40.5	31.7	D
79/ 8/ 9	1257	55.2	31- 0.77	104-55.64	5.84	1.2	1	1	2	2	2	19	231	0.34	27.0	23.1	D
79/ 8/ 9	1443	40.3	30-32.71	105- 3.48	9.89	1.4	1	0	2	2	2	37	233	0.19	2.5	2.6	D
79/ 8/10	1804	42.5	31- 0.01	104-56.64	7.23	0.9	1	2	2	2	1	17	223	0.20	12.2	9.9	D
80/ 2/ 5	2356	54.7	29-55.46	104-26.50	3.22	1.2	2	2	0	2	2	41	304	0.42	3.0	1.4	D
80/ 6/22	302	8.2	29-23.89	105-11.79	2.00	1.5	2	0	2	2	2	104	323	0.35	31.5	26.6	D
80/ 6/22	1210	14.7	29-27.10	105- 5.38	6.01	1.9	2	1	2	2	2	105	323	0.27	8.8	7.7	D
80/ 6/22	2135	53.6	29-30.03	105-10.25	2.71	2.5	2	1	2	2	2	103	323	0.30	35.0	23.9	D
80/ 6/24	1146	19.4	29-29.99	105- 7.93	2.02	1.7	1	1	1	2	2	101	322	0.08	13.0	11.5	D
80/ 6/24	2323	0.6	29-28.28	105-10.63	4.00*	2.6	1	1	2	2	2	105	323	0.33	30.1	26.7	D
80/ 6/25	623	17.6	29-31.24	105-10.76	2.00	2.0	2	2	2	2	2	101	322	0.19	16.9	14.9	D
80/ 6/27	722	26.1	29-30.43	105-12.25	2.02	2.4	2	1	2	2	2	104	323	0.16	17.5	15.3	D
80/ 6/27	1159	41.9	30-37.16	104-39.64	19.62	0.7	1	1	1	2	2	10	123	0.72	6.6	7.3	C
80/ 6/27	1204	36.9	30-41.57	104-35.32	11.02	1.3	2	2	2	2	2	20	122	0.52	2.3		C
80/ 6/27	1227	52.6	30-42.42	104-35.17	7.81	0.7	1	1	1	2	2	21	123	0.47	3.3	2.3	C
80/ 7/ 3	353	36.0	30-42.17	104-35.54	6.22	0.4	1	1	1	2	2	21	122	0.41	2.9	2.1	C
80/ 7/30	0	29.3	30-31.72	104-27.28	1.00	0.7	2	2	1	2	2	22	134	0.42	1.1	2.4	C

BIBLIOGRAPHY

Aggarwal, Y., L. Sykes, D. Simpson, and P. Richards, (1975). Spatial and temporal variations in t_s/t_p and in P wave residuals at Blue Mountain Lake, New York: Application to earthquake prediction, J. Geophys. Res. 80: 718-732.

Aki, K., (1965). Maximum likelihood estimate of b in the formula log N=a-bm and it's confidence limits, Bull. Earthquake Res. Inst., Toyko, Univ., 43: 237-239

Barker, D., and F. Hodges, (1977). Minerology of intrusions in the Diablo Plateau, northern Trans-Pecos magmatic province, Texas and New Mexico, Geol. Soc. Am. Bull. 88: 1428-1436.

Brown, L., R. Reilinger, and J.R. Hagstrum, (1978). Contemporary uplift of the Diablo Plateau, west Texas, from leveling measurements, J. Geophys. Res. 83: 5465-5471.

Byerly, P., (1934a). The Texas Earthquake of August 16, 1931, Bull. Seism. Soc. Am. 24: 81-99.

Byerly, P., (1934b). The Texas Earthquake of August 16, 1931, Bull. Seism. Soc. Am. 24: 303-325.

Chan, K.N., (1977). Modeling of west Texas crustal structure from earthquake data, The University of Texas, MS Thesis, 38p.

Decker, E.R., and S.B. Smithson, (1975). Heat flow and gravity interpretation across the Rio Grande Rift in southern New Mexico and west Texas, J. Geophys. Res. 80: 2542-2552.

Dumas, D., (1979). Active seismic focus near Snyder, Texas, Bull. Seism. Soc. Am. 69: 1295-1299.

Dumas, D.B., H.J. Dorman, and G.V. Latham, (1980). A reevaluation of August 16, 1931 Texas Earthquake, Bull. Seism. Soc. Am. 70: 1171-1180.

Earthquake File Tape, National Earthquake Information Service (NEIS).

Evison, F., (1977). The precursory earthquake swarm, Phys. Earth and Plan. Int. 15: P19-P23.

Gawthrop, W., (1978). The 1927 Lompoc, California earthquake, Bull. Seism. Soc. Am. 68: 1705-1716.

Gries, J., and W. Haenggi, (1970). Structural evolution of the eastern Chihuahua tectonic belt: Symposium in honor of Professor R.K. DeFord. West Texas Geological Society, Ken Seewald and Dan Sundeen, Editors, 119-137.

Gutenberg, B. and C.F. Richter, (1949). Seismicity of the earth and associated phenomena, Princeton University Press, Princeton, N.J.

Hae-Roe, H., (1957). Geology of the Wylie Mountains and vicinity, Culberson and Jeff Davis Counties, Texas; The University of Texas, Bureau of Economics Geology, Geologic Quadrangle, Map 21.

Herrin, E. and J. Taggart, (1962). Regional variation in Pn velocity and their effect on the location of epicenters, Bull. Seism. Soc. Am. 52: 1037-1046.

Herrin, E., E.P. Arnold, B.A. Bolt, G.E. Clawson, E.R. Engdahl, H.W. Freedman, D.W. Gordon, A.L. Hales, J.L. Lobdell, O. Nuttli, C. Romney, J. Taggart, and W. Tucker, (1968). Seismological tables for P phases, Bull. Seism. Soc. Am. 58: 1196-1220.

King, P., (1935). Outline of structural development of Trans-Pecos Texas, Am. Assoc. Pet. Geol. 19: 221-261.

Kodama, K.P., and C.G. Bufe, (1979). Foreshock occurrence in Central California, Eq. Notes. 50: 9-20.

Lee, W. and J. Lahr, (1975). Hypo-71 (revised), a computer program for determining hypocenter, magnitude, and first motion pattern of local earthquakes, U.S. Geol. Surv., Open File Rpt., 75-311.

Muehlberger, W., R. Belcher, and L. Goetz, (1978). Quaternary faulting in Trans-Pecos Texas, Geology 6: 337-340.

Muehlberger, W., (1978). The areal extent of Cenozoic faulting in Trans-Pecos Texas, Bureau of Economic Geology, Guidebook 19, A. Walter and C. Henry, Editors, 19-21.

Nakamura, Y., (1978). A_1 moonquakes: Source distribution and mechanism, Proc. Lunar Sci. Conf. 9th: 3589-3607.

Nuttli, O.W., (1973). Seismic wave attenuation and magnitude relations for eastern North America, J. Geophys. Res. 78: 876-885.

Nuttli, O.W., (1976). Comments on "Seismic intensity, 'size' of earthquakes, and related parameters", by Jack F. Evernden, Bull. Seism. Soc. Am. 66: 331-338.

Nuttli, O.W., G.A. Bollinger, and D.W. Griffiths, (1979). On the relation between Modified Mercalli intensity and body-wave magnitude, Bull. Seism. Soc. Am. 69: 893-909.

Ohtake, M., T. Matumoto, and G. Latham, (1977). Temporal changes in seismicity preceding some shallow earthquakes in Mexico and Central America, Bull. Inter. Inst. Seis. Eq. Eng., 15: 105-123.

Papozachos, B.C., (1975). Foreshock and earthquake prediction, Tectonophysics 28: 218-226.

Richter, C., (1958). Elementary Seismology, W.H. Freedman and Co., New York, 786p.

Rikitake, T., (1976). Earthquake Prediction, Elseviser Scientific Pub. Co., New York, 357p.

Rogers, A., (1979). A study of earthquakes in the Permian Basin of Texas-New Mexico, Bull. Seism. Soc. Am. 69: 843-865.

Romney, C., B.G. Brooks, R.H. Mansfield, D.S. Carder, J.N. Jordan, and D.W. Gordon, (1962). Traveltimes and amplitudes of principal body phases recorded from Gnome, Bull. Seism. Soc. Am. 52: 1057-1074.

Sacuiu, I. and D. Zorilescu, (1970). Statistical analysis of seismic data on earthquakes in the area of the Vrancea focus, Bull. Seism. Soc. Am. 60: 1089-1099.

Sanford, A., and T. Toppozada, (1974). Seismicity of proposed radioactive waste disposal site in southeastern New Mexico, New Mexico Bureau of Mines and Mineral Resources, Cir. 143.

Sekiya, H., (1977). Anomalous Seismic Activity and Earthquake Prediction, J. Geophys. Res. (Supplement) 25: 85-93.

Sellards, E.H., (1932). The Valentine, Texas earthquake. In contribution to Geology, University of Texas Bull., 3201: 113-138.

Shurbet, D.H., and C.C. Reeves Jr., (1977). The fill in the Marfa Basin, Texas, Am. Assoc. Pet. Geol., 61: 612-615.

Stewart, S., and L. Pakiser, (1962). Crustal structure in eastern New Mexico interpreted from the Gnome explosion, Bull. Seism. Soc. Am. 52: 1017-1030.

Stover, C., (1977). Seisimicity map of the conterminous United States and adjacent areas, 1965-1974, United States Geol. Survey.

United States Earthquakes (1931). Coast and Geodetic Survey, U.S. Department of Commerce, 10-13.

von Hake, C., (1977). Earthquake history of Texas, Eq. Info. Bull. 9: 30-32.

VITA

David B. Dumas was born [redacted] the second son of Mr. and Mrs. Dumas. After completing his work at Central High School, Galveston, Texas, in 1965, he entered Texas Southern University, Houston, Texas. He then entered active duty with the Navy in 1967, serving two years in and out of Vietnam. He returned to Texas Southern University in 1969 and received the degree of Bachelor of Science with a major in physics in May 1973. He then entered the Graduate School of Rice University, Houston, Texas. He was awarded the degree of Masters of Arts for Geophysics in May 1976. While working towards the degree of Doctor of Philosphy from the University of Texas at Dallas he has author or co-authored the following articles:

Geophysical Investigation of Salt at the University of Texas Geophysical Laboratory, Salt Dome Symposium, Louisiana State University, 1976 (Coauthor).

Seismicity in and around west Texas, Presented at the Conference of Cenozoic Geology of the Trans-Pecos Volcanic Field, 1979.

Active Seismic Focus near Snyder, Texas, Bull. Seis. Soc. Am., 1979.

The Seismicity of the Gulf of Mexico, EOS, vol. 61, no. 17, 1980 (Coauthor).

A reevaluation of the August 16, 1931 Texas Earthquake, Bull. Seis. Soc. Am., 1980 (Coauthor)

Seismicity in the Basin and Range province of Texas and northeastern Chihuahua, Mexico, New Mexico Geological Society Guidebook, 31st Field Conference, Trans-Pecos Texas, 1980.

Summary of local and regional earthquakes (S-P<30 sec) recorded at the University of Texas/National Aeronautics and Space Administration (UT/NASA) seismic network, UT Marine Science Institute, Contribution No. 465, 1981.

Permanent address: 3918 M½
Galveston, Texas 77550

This dissertation was typed by Jennifer Jackson.